INVESTIGATION OF THERMAL ASPECTS OF BUILDING INTEGRATED PHOTOVOLTAIC/THERMAL SOLAR COLLECTORS

A thesis

submitted in partial fulfilment

of the requirements for the degree

of

Doctor of Philosophy

at

The University of Waikato

by

TIMOTHY NICHOLAS ANDERSON

The University of Waikato

2009

ABSTRACT

In this study a novel building integrated photovoltaic/thermal (BIPVT) solar collector was developed, tested, modelled and optimised both experimentally and theoretically. Experimental testing found that glazing the prototype collector improved the maximum thermal efficiency by approximately 25% and decreased heat loss, by a factor of two, relative to an unglazed collector. Additionally, the spectral absorptance of a photovoltaic (PV) cell and several coloured absorber samples were characterised.

The experimental data was subsequently used in the development and validation of an optimisation model for BIPVT style collectors. Numerical optimisation showed that the collector thermal efficiency could be improved by maximising the geometric fin efficiency, reducing the thermal resistance between the PV cells and the absorber, and by increasing the transmittance-absorptance product of the PV cells and/or the absorber. The results showed that low cost materials, such as mild steel, could be used without significantly affecting the BIPVTs thermal efficiency. It was also shown that there was potential to develop coloured BIPVT collectors with acceptable thermal efficiencies. Finally, the model showed that potentially the air space in an attic could be used rather than “traditional” insulating materials.

Subsequent computational and experimental fluid dynamics studies found that the heat transfer coefficients in a scale-model attic would result in R-values similar to

mineral wool type insulation and therefore may provide sufficient insulation of a BIPVT in a cold roof building. In these studies the validity of an existing correlation for natural convection in an attic-shaped enclosure was extended to Grashof numbers in the range 10^7 to 10^9 from its previous range, 2.9 x 10^6 to 9 x 10^6.

The use of a single vertically mounted baffle was also found to reduce the natural convection heat transfer coefficients in attic-shaped enclosures. This led to the development of a new generalised correlation that can be used to determine the Nusselt number in an attic-shaped enclosure with regard to the proportions of the baffle.

This work has shown that it is possible to achieve satisfactory thermal performance from BIPVT style collectors fabricated from low cost materials such as colour coated mild steel. Further it has demonstrated that there is potential to reduce the cost of such systems by integrating them *into* a building rather than *onto* a building.

ACKNOWLEDGEMENTS

Obviously in a project such as this, there are a number of people who deserve credit. Firstly, I would like to thank my supervisor Dr Mike Duke for letting me undertake this work. Also I'd like to thank my co-supervisor Dr James Carson for his thoughts on all things thermal. A very big thank you must also go to my industry mentor, Ian McClew at Dimond, for supporting this project and arranging all the prototypes.

Thanks must also go to Prof. Janis Swan for her support during the troubled times that can plague a PhD. Thanks to Em Prof. Graham Morrison at UNSW, for setting me up with a desk and computer when I was in Sydney, and for his input on the thermal modelling.

Thanks also to Rob, Luis and Justin for the relaxing board game evenings and Mark for the afternoon runs. And, to the IBN boys: Lars, Dave, Mike, Brendan, Kyle, Adam and Anand, I'm sure all those stimulating conversations will come in handy some time. I'm not sure if they've made me smarter, in fact I'm not sure how many of them I can actually remember….

Finally, to Arwen, Luke, Mum and the rest of my family thanks for your love and support. I couldn't have done this without you.

LIST OF PUBLICATIONS

The following publications have been derived in whole or in part from the work contained within this manuscript. They form the basis of each chapter in this thesis as well as a body of complimentary work to which the reader may also wish to refer.

Book Chapters:

Anderson, T.N., Duke, M. and Carson, J.K., 2008, "Chapter 12: Designing Photovoltaic/Thermal Solar Collectors for Building Integration", *Solar Energy: Research, Technology and Applications*, Nova Science Publishers, New York

Journal Papers:

Anderson, T.N., Duke, M., Morrison G.L. and Carson, J.K., 2009, "Performance of a Building Integrated Photovoltaic/Thermal (BIPVT) Solar Collector", *Solar Energy*, Vol. 83, No. 4, pp. 445-455

Anderson, T.N., Duke, M. and Carson, J.K., 2009, "Convection suppression in a triangular shaped enclosure", *Computational Thermal Sciences*, (In Press)

Anderson, T.N., Duke, M. and Carson, J.K., 2008, "A Design Method for Building Integration of Photovoltaic/Thermal Solar Collectors", *International Journal of Energy, Environment and Economics*, Vol. 16 No. 2/3

Anderson, T.N. and Duke, M., 2008, "Solar Energy Use for Energy Savings in Dairy Processing Plants", *Transactions of Engineers New Zealand, Engineering TreNZ,* 2008-001

Anderson, T.N., Duke, M. and Carson, J.K., 2007, "A Typical Meteorological Year for Energy Simulations in Hamilton, New Zealand", *Transactions of Engineers New Zealand, Engineering TreNZ,* 2007-003

Conference Papers:

Anderson, T.N., Duke, M. and Carson, J.K., 2009, "Performance of coloured solar collectors", *Proceedings of ICAE'09 International Conference on Applied Energy*, Hong Kong, January 2009

Anderson, T.N., Bura, S., Duke, M., Carson, J.K. and Lay, M., 2008, "Development of a Building Integrated Photovoltaic/Thermal Solar Energy Cogeneration System", *Proceedings of 3rd International Conference on Sustainability Engineering and Science,* Auckland, December 2008

Anderson, T.N., Duke, M. and Carson, J.K., 2008, "Experimental performance of water cooled building integrated photovoltaic/thermal solar collectors", *Proceedings of 3rd International Solar Energy Society Asia-Pacific Congress*, Sydney, November 2008

Anderson, T.N., Duke, M. and Carson, J.K., 2008, "Measurement of natural convection heat transfer in an attic shaped enclosure", *Proceedings of 3rd International Solar Energy Society Asia-Pacific Congress*, Sydney, November 2008

Anderson, T.N., Duke, M. and Carson, J.K., 2008, "Designing a Low Cost Solar Collector System for Process Industry Applications", *Proceedings of Society of Chemical Engineers NZ Annual Conference*, Hamilton, October 2008

Anderson, T.N., Bura, S., Duke, M., Carson, J.K. and Lay, M, 2008, "Development of a Building Integrated Photovoltaic/Thermal Solar Collector Based on Steel Roofing", *Proceedings of 4th New Zealand Metals Industry Conference*, Auckland, October 2008

Anderson, T.N., Duke, M. and Carson, J.K., 2008, "Convection suppression in an attic shaped enclosure", *Proceedings of CHT08: 4th International Symposium on Advances in Computational Heat Transfer*, Marrakech, May 2008

Anderson, T.N., Duke, M. and Carson, J.K., 2007, "Improved Electrical Efficiency by Active Cooling of Building Integrated Photovoltaic Panels", *Proceedings of ENZCon'07, 14th Electronics New Zealand Conference*, Wellington, November 2007, pp. 31-36

Anderson, T.N. and Duke, M., 2007, "Analysis of a Photovoltaic/Thermal Solar Collector for Building Integration", *Proceedings of SB07, New Zealand Sustainable Building Conference*, Auckland, November 2007

Bura, S., Duke, M., Lay, M. and Anderson, T., 2007, "Investigation of Production Systems for a BIPVT Product", *Proceedings of SB07, New Zealand Sustainable Building Conference*, Auckland, November 2007

Anderson, T.N. and Duke, M., 2007, "Photovoltaic/Thermal Solar Collectors – An Introduction", *Proceedings of IRHACE Technical Conference*, Napier, May 2007

TABLE OF CONTENTS

LIST OF FIGURES

LIST OF TABLES

NOMENCLATURE

A	Enclosure aspect ratio
$A_{collector}$	BIPVT gross collector area (m^2)
A_h	Heater area (m^2)
a	Panel length (m)
b	Trough width (m)
b	Collector breadth (m)
C_p	Specific heat (J/kgK)
d	Rectangular tube width (m)
d_h	Hydraulic diameter (m)
E	Young's modulus (Pa)
E_{g0}	Linearly interpolated zero temperature band gap
F	Fin efficiency
F	View factor
F'	Corrected fin efficiency
F_r	Collector heat removal factor
G	Incident radiation (W/m^2)
$G"$	Global irradiance (W/m^2)
Gr	Grashof number
h_c	Convection heat transfer coefficient (W/m^2K)
h_{fluid}	Collector fluid internal heat transfer coefficient (W/m^2K)
h_{nat}	Natural convection heat transfer coefficient (W/m^2K)

h_{PVA}	Heat transfer coefficient from PV cells to absorber plate (quasi bond resistance) (W/m^2K)
h_w	Wind induced heat transfer coefficient (W/m^2K)
I_λ	Monochromatic incident energy (J)
I_0	Diode saturation current (A)
I_{sc}	Short circuit current (A)
k	Boltzmann constant (J/K)
k	Insulation conductivity (W/mK)
k_{abs}	Absorber conductivity (W/mK)
k_{PV}	PV thermal conductivity (W/mK)
L	Collector length (m)
L_b	Backing insulation thickness (m)
L_{edge}	Edge insulation thickness (m)
L_{PV}	PV thickness (m)
L/H	Blockage ratio (ratio of baffle length to enclosure height)
m	Mass flow rate (kg/s)
N	Number of glazing layers or covers
n	Number of tubes
Nu	Nusselt number
p	Collector perimeter (m)
Q	Collector heat transfer (W)
Q_e	Electrical power (W)
Q_{cond}	Conduction heat loss (W)
Q_{rad}	Radiation heat loss (W)

$Q_{convection}$	Convection heat loss (W)
q	Elemental charge
q	Maximum working pressure (Pa)
Ra	Rayleigh number
S	Packing factor
T	Temperature (K)
T_h	Hot wall temperature (K)
T_c	Cold wall temperature (K)
T_{out}	Collector outlet temperature (K)
T_i	Collector inlet temperature (K)
T_s	Sky temperature (K)
T_{pm}	Mean plate temperature (K)
T_p	Mean heater plate temperature (K)
T_e	Mean enclosure temperature (K)
t	Absorber thickness (m)
t	Material thickness (m)
U	Overall enclosure heat transfer coefficient (W/m^2K)
U_L	Collector heat loss coefficient (W/m^2K)
U_{top}	Overall top heat transfer coefficient (W/m^2K)
V_{oc}	Open circuit voltage (V)
V_{g0}	E_{g0}/q
v	Wind velocity (m/s)
W	Tube spacing (m)

α	Absorptance
α_λ	Monochromatic absorptance
β	Collector mounting angle (degrees)
γ	Parameter for temperature dependencies in PV cells
ε_p	BIPVT collector plate emittance
ε_c	BIPVT glazing emittance
η	Collector efficiency
η_G	Instantaneous collector efficiency
η_{0A}	Collector optical efficiency
$\eta_{thermal}$	BIPVT thermal efficiency
ρ	Reflectance
λ	Wavelength (m)
σ	Stefan-Boltzmann constant (W/m^2K^4)
σ	Combined bending and membrane stress (Pa)
σ_m	Membrane stress (Pa)
τ	Transmittance
$\tau\alpha$	Transmittance-absorptance product
$\tau\alpha_{PV}$	Photovoltaic transmittance-absorptance product
$\tau\alpha_T$	Absorber transmittance-absorptance product

Chapter 1: Introduction

1.1 Overview

In recent times there has been a growing concern over the use and availability of energy sources. These concerns have been driven by a number of factors including ensuring security of supply, increasing costs and environmental issues. There has also been a widespread realisation that the rate at which existing fuel sources, in particular fossil fuels, are being consumed is unsustainable. The result has been an increasing amount of research directed towards renewable energy technologies such as wind power, biomass and tidal power. In particular, the use of solar energy has been widely suggested as a means of reducing dependence on energy derived from fossil fuel sources.

1.2 Solar Energy

In practical terms, the sun is the largest source of energy that is available to humanity. Each year it supplies in the order of 5.4 million EJ to earth of which 30% is reflected back into space. However, the remainder represents 10,000 times the world's consumption of fossil and nuclear fuel sources in the year 2002. Considering that in the same year, fossil and nuclear fuels provided over 80% of the world's energy consumption, there is significant potential to offset the use of these with solar energy (Boyle, 2004).

The utilisation of solar energy has traditionally been divided into two fields; solar thermal and photovoltaics. Solar thermal research is, as the name suggests, concerned with the utilisation of solar radiation to provide useful heating. Typical examples include passive solar heating of houses and solar water heating. Photovoltaics are concerned with the conversion of solar energy to electricity, mainly through the use of silicon based solar cells.

One of the key shortcomings of photovoltaics is their relatively low efficiency. Typically, commercially available PV modules convert only 6-18% of the incident radiation falling on them to electrical energy with the remainder lost by reflection or as heat (Bazilian et al. 2002). However, a small portion of the heat is "sunk" into the cells which results in a reduction in their efficiency.

Green (1998) noted that the short circuit current of PV cells is not strongly temperature dependent but tends to increase slightly due to increased light absorption. Green attributes the increased absorption to the temperature dependant decrease in band gap in the semiconductor materials used in the cells.

Moreover, using a simple diode model Green showed that the relationship between the short circuit current (I_{sc}) and open circuit voltage (V_{oc}) (Equation 1) can be reduced to an expression for the change in open circuit voltage with respect to temperature (T) (Equation 2) where I_0 is the diode saturation current, k is the Boltzmann constant, q is the element charge and γ is a parameter used to

accommodate other temperature dependencies. This he notes leads to a decrease in efficiency of approximately 0.5%/°C for typical silicon based PV cells.

$$I_{SC} = I_0\left(e^{qV_{oc}/kT} - 1\right) \tag{1}$$

$$\frac{dV_{oc}}{dT} = -\frac{V_{g0} - V_{oc} + \gamma\left(\frac{kT}{q}\right)}{T} \tag{2}$$

In order to reduce the impact of temperature on PV cells, a cooling system can be implemented to remove heat. However rather than just losing this heat to the environment, it is possible to capture and store it. Based on this premise, a number of studies in the late 1970's, investigated the use of the heat generated by photovoltaics in what have become known as Photovoltaic/Thermal (PVT) solar collectors. These studies were largely shelved during the 1980's but with growing concern over energy sources, and their usage, PVTs have started receiving more attention (Zondag, 2008).

1.3 PVT Solar Collectors

The attraction of PVT style collectors is due to three main benefits: firstly, the efficiency of PV cells under high radiation and ambient temperature levels can be improved by actively cooling them using a solar thermal system, secondly, they offer by their nature the opportunity to generate both electrical and thermal energy

and finally, by incorporating both systems into a single unit, a larger portion of the incident radiation on a unit area can be captured.

In their 2004 study Van Helden et al. noted that PV collectors absorb up to 80% of the incident solar radiation but convert only a small portion of this to electrical energy, the remainder being dissipated as thermal energy. They noted that the temperatures reached by PV laminates can be much higher than the ambient temperature (>30K) and that the efficiency of PVTs is greater than the combined sum of separate PV and thermal collectors. In light of this, they suggest that PVT systems could offer a cost effective solution for applications where roof area is limited.

1.3.1 PVT Air Heating Collectors

Arguably, the simplest, and cheapest, configuration for a PVT collector is as an air heating device. A cavity is formed behind a PV panel (module) where air is circulated; this cools the panel and heats the air as shown in Figure 1.

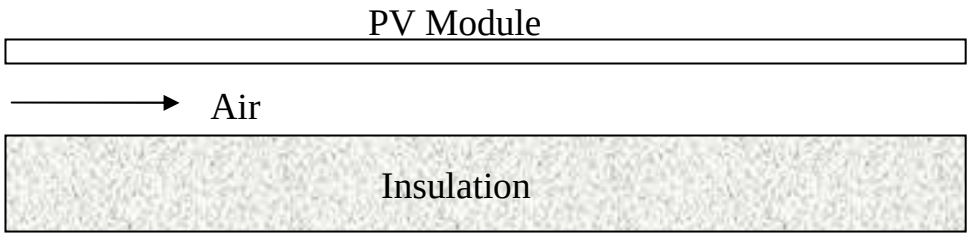

Figure 1: PVT Air Heater

Tiwari and Sodha (2007) examined a PVT air heater, shown in Figure 2, in which air was circulated along the rear surface of a PV module. They found that the maximum thermal efficiency of this system was in the order of 25%, however they found that by adding an air gap and glazing layer above the collector, the thermal efficiency was almost doubled.

Figure 2: PVT Air Heater (adapted from Raman and Tiwari, 2008)

Hegazy (2000) examined four types of PVT air heating solar collectors using a numerical model. Unlike the collector shown in Figure 1, the systems in the study utilised a glass cover mounted above the PV module thus forming a second air gap. This is commonly used on collectors for solar water heating to reduce convection heat losses from the top surface of the collector plate.

Hegazy found that a system where air was circulated along the back surface of the module between it and the insulation layer, as well as along the top surface

between the module and the glass cover, gave the best compromise between electrical and thermal performance.

Tripanagnotopoulos et al. (2002) also demonstrated the use of a PVT air heating system similar to those of Hegazy. In addition they studied a system that utilised a static reflector plate that directed solar radiation from an area of similar size to their PVT, onto their collector, thus giving a concentration ratio of approximately 1.3. They found that an unglazed PVT collector, similar to that shown in Figure 1, had a maximum thermal efficiency of 38%. They also found that by glazing the system, or adding a static reflector, this efficiency could be increased to approximately 60%, and that by glazing and adding the reflector 75% was possible. Tripanagnotopoulos et al. noted however, that although glazing improved the thermal efficiency it tended to increase optical losses, resulting in a decreased electrical efficiency.

Although the previously discussed studies examined cooling of flat-plate PV modules, Tonui and Tripanagnotopoulos (2007, a and b) showed that a number of simple low cost alterations could be made to PVT air heaters to improve their performance. They showed that by adding fins to the rear of the PV module they could improve the electrical and thermal efficiency of their PVT systems. They also found that, using a system like Hegazy's (2000), by adding a thin metal sheet in the air passage behind the PV module the electrical and thermal efficiency were improved.

1.3.2 PVT Water Heating Collectors

Another application that has been proposed for PVT collectors is as water heating devices. In its simplest form a PVT could look very similar to a "standard" solar thermal collector with the PV module taking the place of the collector plate, as shown in Figure 3. Florschuetz (1979) provided perhaps the earliest theoretical analysis of a PVT solar collector through the use of a modified version of the Hottel-Whillier model, developed for predicting the performance of solar thermal collectors.

An early study by Andrews (1981) showed that PVT collectors were, at the time, marginally suitable for low temperature heating operations such as pool heating. However, Andrews suggested that PVT were not suitable for medium temperature operation due to the relatively low cost of energy at that time.

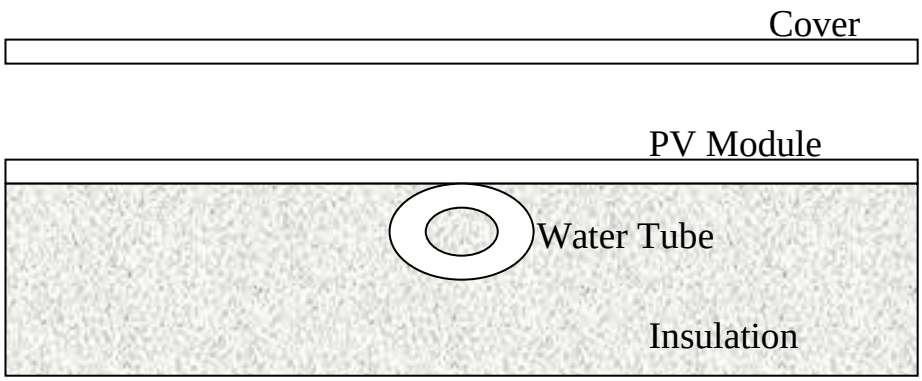

Figure 3: PVT Water Heater

With increases in the cost of energy, and improvements to photovoltaic technology, interest has been renewed in the use of PVT for water heating. Recently Bergene and Lovvik (1995) conducted a theoretical examination of a flat

plate solar collector with integrated solar cells. They developed a series of algorithms which they utilized in calculating both the thermal and electrical efficiency of a PVT system. They suggested that such systems might be useful as pre-heaters for domestic hot water services. Garg and Agarwal (1995) also demonstrated the ability of a 2 m^2 domestic solar water heater to generate a useful amount of electricity when integrated with a series of PV cells.

Tripanagnostopoulos et al. (2002) conducted tests on hybrid PVT systems using polycrystalline-Silicon (pc-Si) and amorphous-Silicon (a-Si) PV cells. They found that the cooling provided by the thermal integration assisted in improving the efficiency of the pc-Si PV cells by approximately 10% for a back insulated PV module and 3% for a free standing PV module. They also found that water cooling provided better cooling than air circulation. Finally, they suggested that the performance of these systems could be further improved through the use of diffuse reflectors or glazing. However, as they found with their air heating collectors, glazing the collectors would improve thermal performance to the detriment of the electrical efficiency.

Despite the effects of glazing on electrical efficiency, Kalogirou and Tripanagnostopoulos (2007) showed that PVT was economically viable in industrial applications in a Mediterranean environment and had positive life cycle savings for medium temperature applications. They suggested that PVT systems based on amorphous silicon technology, although having lower electrical efficiencies, would have shorter payback times.

He et al. (2006) studied a hybrid PVT system which used natural convection to circulate the cooling water. They found that their system showed a combined efficiency in the order of 50%, with the thermal efficiency contributing approximately 40%. Although they found that the thermal efficiency was less than a conventional thermosyphon solar water heater they noted that the energy saving efficiency was greater.

Chow et al. (2006) also examined the hybrid PVT system of He et al. (2006), shown in Figure 4, and developed a dynamic thermal model to describe its performance. They suggested that this system could be improved by placing the PV cells on the lower portion of their collector. They noted that there was a larger temperature gradient between the water entering the thermosyphon tubes and the PV cells in this region and so the electrical and thermal efficiency could be improved by placing the cells there.

Zondag et al. (2003) examined the performance of nine variations of PVT water heaters including glazed and unglazed systems. They found that an unglazed sheet and tube collector, as shown in Figure 5, had the lowest thermal but highest electrical efficiency. They also showed that their glazed PVT collectors had a maximum thermal efficiency of approximately 65%.

Figure 4: Thermosyphon PVT water heater

(adapted from Chow et al., 2006)

Figure 5: Unglazed PVT water heater

(adapted from Zondag et al., 2004)

1.3.3 Concentrating PVT Collectors

Another less common variation on the PVT collector is the concentrating PVT. As the name suggests, this involves the concentration of solar radiation onto a PVT collector.

The static reflector system of Tripanagnostopoulos et al. (2002), discussed previously, is perhaps the simplest incarnation of a concentrating PVT collector. A reflector plate of the same area as the collector was used to direct extra solar radiation onto a PVT collector giving a concentration ratio of 1.3. However, concentration of solar radiation can also be achieved with compound parabolic concentrators (CPC), Fresnel lenses and parabolic dishes. A typical arrangement of a CPC PVT collector is shown in Figure 6.

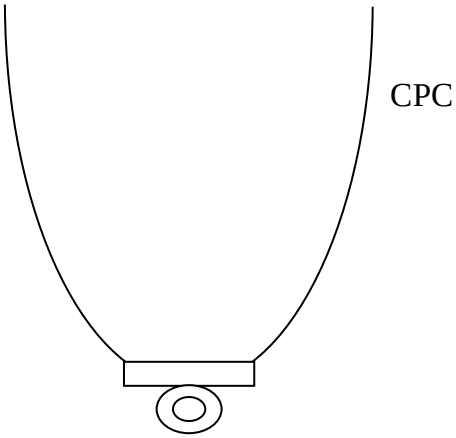

Figure 6: CPC PVT Collector

Garg and Adhikari (1999) demonstrated the use of several truncated CPCs in a single PVT module. They theoretically demonstrated that their collector for air heating, with a concentration ratio of 2.88, resulted in an electrical and thermal

output approximately 2.5 times higher than a system with no concentration. However the maximum thermal efficiency of a collector without concentration was actually higher, but so too was the heat loss.

A similar system was also demonstrated by Othman et al. (2005), where Garg and Adhikari used a single pass to heat air, they utilised a double pass with a rear finned surface in their system, as shown in Figure 7. The aim of the finned surface was to improve heat transfer on the rear face of the PV module. They found, experimentally and theoretically, that increased mass flowrates through their system improved the thermal efficiency significantly but had little influence on the electrical efficiency.

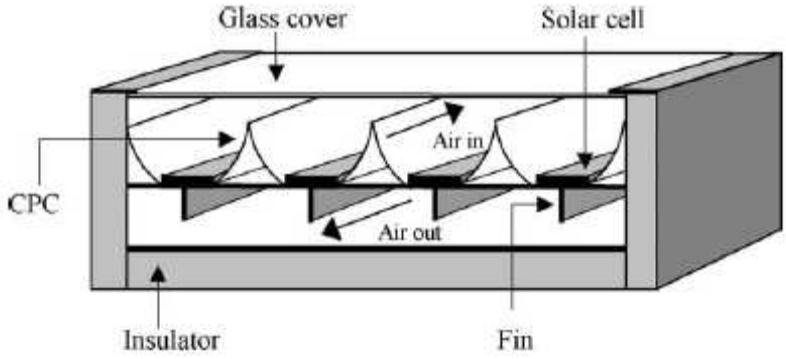

Figure 7: Double pass air cooled CPC PVT collector

(adapted from Othman et al., 2005)

Rosell et al. (2005) demonstrated a linear Fresnel reflector that had a concentrating ratio of 11. They were able to obtain a maximum thermal efficiency of approximately 60% from their system with no electrical load. They identified the fact that one of the main thermal resistances in their PVT was that between the

PV cell and the absorber plate to which it was bonded, thus suggesting efficiency could be improved by reducing this resistance.

Another variation on line focusing PVT collectors is the CHAPS (combined heat and power system); currently in use at one of the residential colleges at the Australian National University (ANU). This system, discussed by Coventry (2005), uses a parabolic trough reflector with a PVT module mounted at its focus, as shown in Figure 8.

The system has a concentration ratio of 37 and has a maximum reported combined efficiency of 69%. Coventry noted that although the system had a lower thermal efficiency than those reported in other studies, the heat losses from the CHAPS system where much lower, due to its smaller heated area. Coventry also noted that imperfections in the concentrator shape resulted in non-uniform illumination thus affecting the electrical performance.

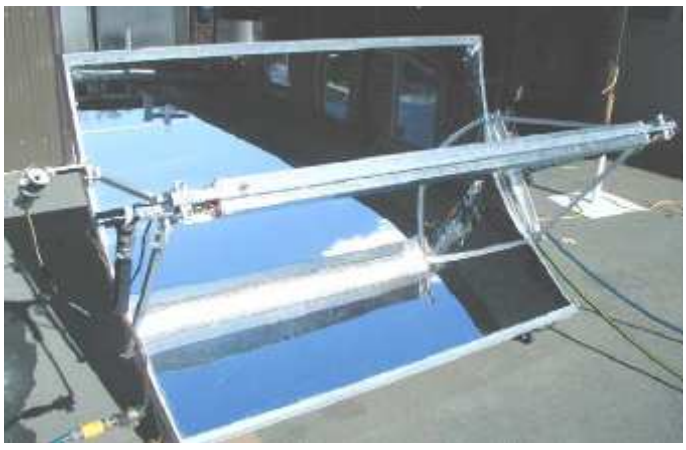

Figure 8: CHAPS concentrating PVT

(adapted from Coventry, 2005)

Kribus et al. (2006) discussed the design of a PVT system using a small-scale parabolic dish concentrator, with a concentration ratio of approximately 500. Unlike the systems discussed earlier, their system design was able to provide very high temperature heating (>450K). They suggest that such system could be used in residential applications for driving absorption cooling systems.

1.3.4 Market Potential for PVT Solar Collectors

As can be seen from the preceding examination of the research literature, a significant amount of research has been conducted into PVT collectors in recent years. This research has also been complemented by rapid growth in both photovoltaic and solar thermal markets. A survey by the International Energy Agency Solar Heating and Cooling programme (IEA SHC, 2006) found that, in 2004, there was approximately 141 million m^2 of solar thermal collectors in its 41 member countries. It was also found that the solar thermal collector market in Australia and New Zealand was growing at a rate of 19% per annum. Furthermore it showed that the use of solar thermal energy made significant reductions in the use of energy from other sources. In addition, the market for photovoltaic solar collectors has experienced high growth during the last decade as can be seen in Figure 9. This has been made with the majority of growth in grid connected systems (IEA PVPS, 2005).

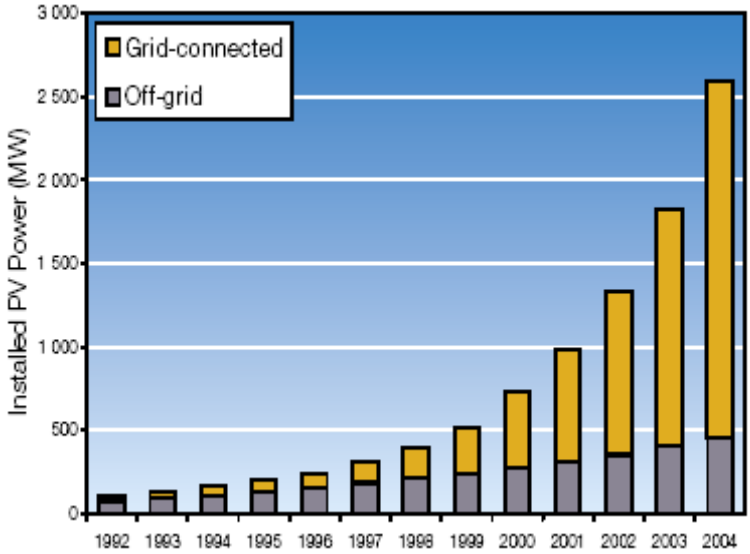

Figure 9: Cumulative installed PV capacity in IEA PVPS member nations

(adapted from IEA PVPS, 2005)

By spanning both the PV and solar thermal markets, it is possible that PVT systems could draw from both these existing markets. Zondag et al. (2005) noted that based on European targets for the installation of PV and solar thermal collectors, the use of PVT systems could meet the entire PV quota while also providing 30% of the solar thermal target.

More specifically, the EU-supported Coordination Action "PV Catapult" (2005) suggested that the market for PVT collectors could be divided into several smaller markets. Of these the largest is the domestic sector, where there is a need for low to medium temperature heating and power generation. In the short to medium term they suggested PVT would find "niche market" applications such as pool heating and hospitals.

PV Catapult noted that for PVT collectors to become accepted in the market there are a number of issues to be addressed. Aside from the technical issues with regard to stagnation temperatures, which can be overcome through the use of silicone encapsulants, they highlight the need to reduce the capital cost of these systems, possibly through subsidies, and for better building integration and aesthetics. In particular they call for the development of prefabricated PVT building elements, as well as PVT modules that offer flexibility in terms of both colour and size.

1.3.5 Building Integrated Solar Collectors

A significant portion of studies into PVT systems have been aimed at producing "standalone" collectors similar to those already used for water heating, rather than producing truly building integrated solar collectors. The downside of this approach is that aesthetics may be compromised, an area that was noted by PV Catapult (2005).

Bazilian et al. (2001) noted that the integration of PV systems into the built environment can achieve "a cohesive design, construction and energy solution". By capturing the "waste" heat from a building integrated photovoltaic (BIPV) system it is possible to create a building integrated PVT (BIPVT) that is architecturally acceptable. In essence, BIPVT is the use of PVT as building elements such as roofing or façade.

To date the majority of studies on BIPVT style collectors have examined the use of air cooling of PV panels similar to the PVT air heaters discussed in Section 1.3.1. In this regard, studies such as those of Mosfegh and Sandberg (1998) and Brinkworth (2006) have concentrated on using natural convection to cool the rear surface of vertically mounted BIPV panels. These studies have paralleled, and in some respects led to, the development of dual façade and ventilated wall buildings.

The use of water cooled solar collectors as building elements has, until recently, been largely ignored. Ji et al. (2006) and Chow et al. (2007) both examined a PVT system for integration into building walls in Hong Kong. They showed that these systems could make useful heat gains while also acting to reduce thermal load on the building. However, as can be seen in Figure 10, these systems were essentially PVT panels integrated *onto* a building rather than *into* the building (i.e. individual PVT collectors are used as the material for the wall, rather than using the wall as the material for a PVT collector).

Figure 10: BIPVT solar collector (adapted from Chow et al. 2007)

Similarly, Kang et al. (2006) discussed the performance of a roof integrated solar collector which again consisted of a series of "standalone" collectors used as a roof, as shown in Figure 11.

Figure 11: Roof integrated solar collector (adapted from Kang et al. 2006)

Again, this system although integrated *onto* the building is not integrated *into* the building. In a study by Probst and Roecker (2007) this method of integrating solar collectors was considered to be “acceptable” to architects. However they note that in the future, building integrated solar collectors “should be conceived as part of a construction system”, thus strengthening the views expressed by PV Catapult (2005).

Although somewhat self-evident the comments of Probst and Roecker appear to have been overlooked by the research community. Medved et al. (2003) however examined an unglazed solar thermal system that could be truly integrated into a building as shown in Figure 12. In their system they utilised a standard metal roofing system as a solar collector for water heating. They found that in a swimming pool heating system, that they were able to achieve payback periods of less than 2 years. This translated to a reduction of 75% in the time taken to pay for a glazed solar collector system. Similar systems to that of Medved et al. have been developed and discussed by Bartelsen et al. (1999), Colon and Merrigan (2001) and Anderson et al. (2009) (Appendix B).

Figure 12: Unglazed building integrated solar collector (adapted from Medved et al. 2003)

Similarly, Assoa et al. (2007) presented a concept for a BIPVT water and air heater in which a water tube was placed in the trough of a troughed-roof system while PV cells were added to the ridges, as shown in Figure 13. They theoretically demonstrated that combined efficiencies in excess of 80% could be achieved by their system.

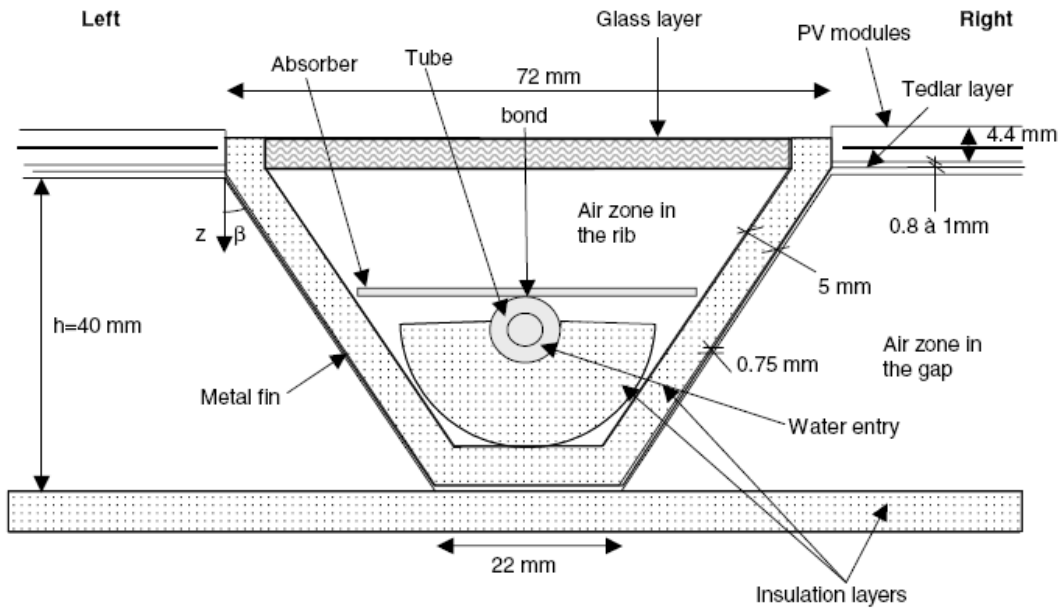

Figure 13: Water and air heating building integrated photovoltaic/thermal collector (adapted from Assoa et al. 2007)

However, despite the recent research and the recognition of the market for building integration of solar collectors, the work undertaken in the field is relatively small in comparison to work on stand-alone collectors. Although stand-alone collectors can successfully be integrated *onto* buildings it has been suggested that this does not necessarily result in an attractive finish. Recent initiatives in the field of photovoltaic/thermal collectors have identified the need for "plug and play" style collectors that can also be integrated with buildings (PV Catapult, 2005). On this basis it can be said that there is a need for "attractive" building integrated photovoltaic/thermal solar collectors to be developed that satisfy most if not all the points that have been raised.

1.4 Thesis Objective

Recently, Duke (2006) proposed a concept for a BIPVT style collector based on sheet metal roofing that displays a greater level of integration, and satisfies more of the requirements identified in the literature than many of the previous systems.

The aims of this thesis are to:

- develop the BIPVT collector proposed by Duke (2006)
- experimentally characterise the thermal efficiency and performance of the collector
- identify ways in which the collector can be optimised to result in improved performance
- identify modifications that could be made to the collector that would reduce its cost without unduly affecting its performance.

Chapter 2: Development and Testing of a Prototype BIPVT Solar Collector

2.1 Introduction

The system developed in this study is unique in a number of ways. Unlike many of the systems that have been proposed, this system is directly integrated into the roof of a building, in this case a standing seam or troughed sheet metal roof. Standing seam and troughed sheet roofs are typically made from aluminium or coated steel, although copper or stainless steel could be used. They are rolled or pressed into a shape that gives the roof product stiffness and strength, and when assembled are weather proof. This system utilises the high thermal conductivity materials used in these roofing systems to form the BIPVT collector. During the manufacturing process in addition to the normal troughed shape, channels are added to the trough for the thermal cooling medium to travel through (Figure 14).

An absorber plate having pc-Si PV cells laminated to its surface is bonded into the trough. The channels formed in the trough are subsequently enclosed by the cover; thus forming a riser tube to which heat can be transferred. The flow ways have an inlet and outlet at opposite ends of the trough. In addition the design allows a glass or polymer glazing to be added to the collector to create an air gap between the outer surface of the PV module and laminate surface and the ambient air.

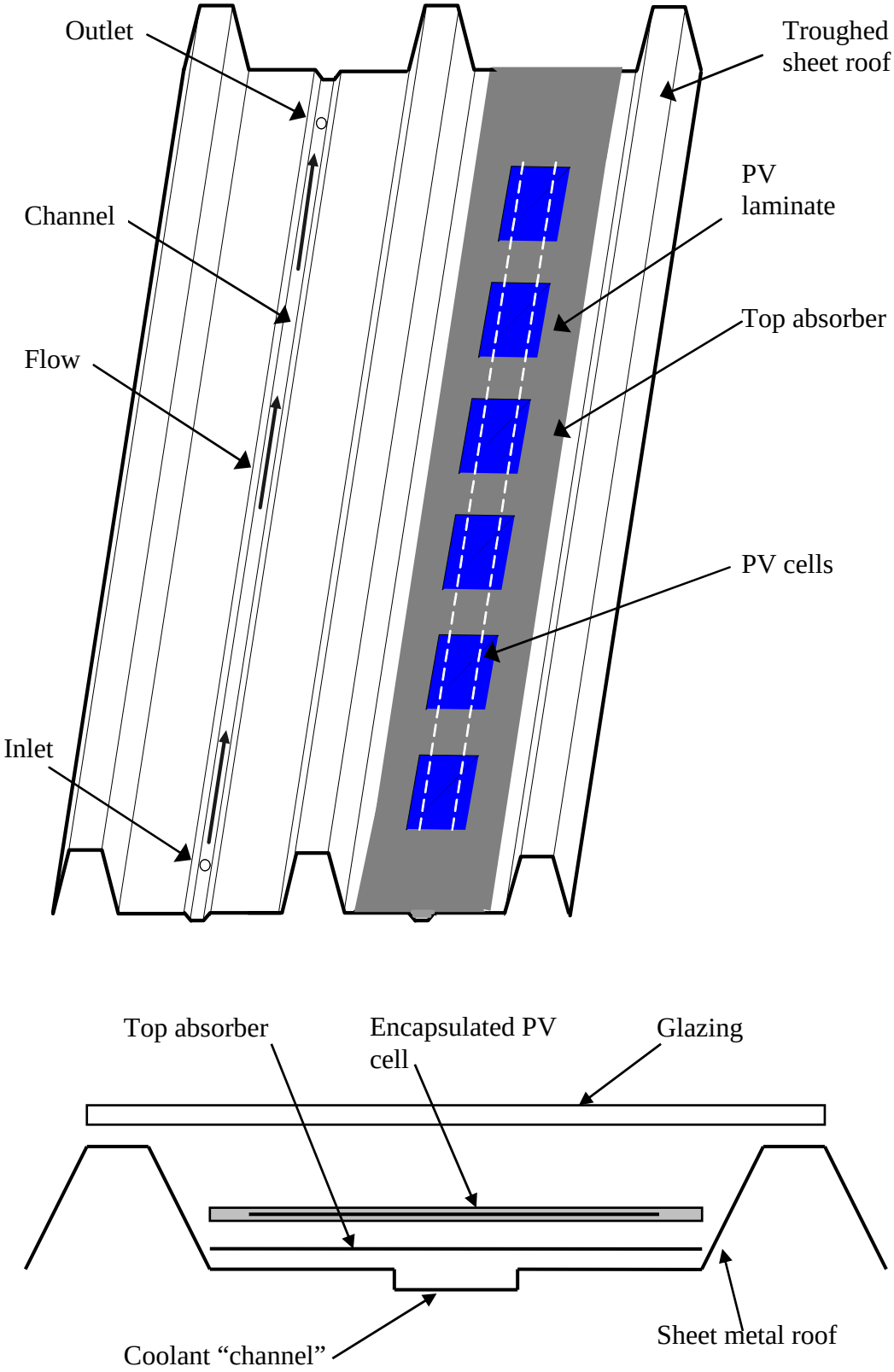

Figure 14: Assembled BIPVT collector (top), exploded assembly (bottom)

As the PV cells are exposed to sunlight they absorb radiation and generate electricity, however, silicon PV cells tend to convert only a small fraction of the radiation to electricity while the remainder results in heating of the laminate. In the BIPVT collector there is heat transfer from the cells through the laminate to the fluid passing underneath. The fluid is pumped along the flow paths and out through a manifold (header tube) and pipes and fed to a heat exchanger that removes the heat from the fluid. The heating of the fluid cools the PV cells, thereby increasing their efficiency under high temperature and radiation conditions.

2.2 BIPVT Prototype Fabrication

Although the fabrication of finned copper tube style collectors is well understood, the unconventional design of the BIPVT and some of the desired design goals, in particular that it be made from pre-coated steel, presented a number of challenges. This was mainly due to the fact that the material was galvanised and dip coated in black paint, so could not be easily welded without fully removing both these coatings.

Therefore, the roof profile was folded using a CNC folder, holes were drilled to allow fluid into the underside of the coolant channel and nipples were silver soldered to the rear surface to allow a manifold to be attached. The ends of the coolant trough and the top absorber sheet were glued and sealed to the profiled roof section using a high temperature silicone adhesive sealant. Once sealed and

watertight, PV cells were laminated to the top absorber sheet and encapsulated in a poly-vinyl resin.

This encapsulation method is significantly different from that used by previous researchers, who have utilised standard EVA or silicone encapsulated modules. It should be noted that this method of encapsulation would not be suitable for a commercial BIPVT due to the poor longevity of the resin under high temperature operation, but was considered adequate for research purposes. The ends of the roof profile were enclosed and a low-iron-glass cover was placed over the collector to prevent convection losses.

Finally, the rear surface of the collector panel was insulated with 100mm of mineral fibre insulation thereby forming a standalone collector with a roof profile, as shown in Figure 15. The design parameters of the prototype collector tested are shown in Table 1.

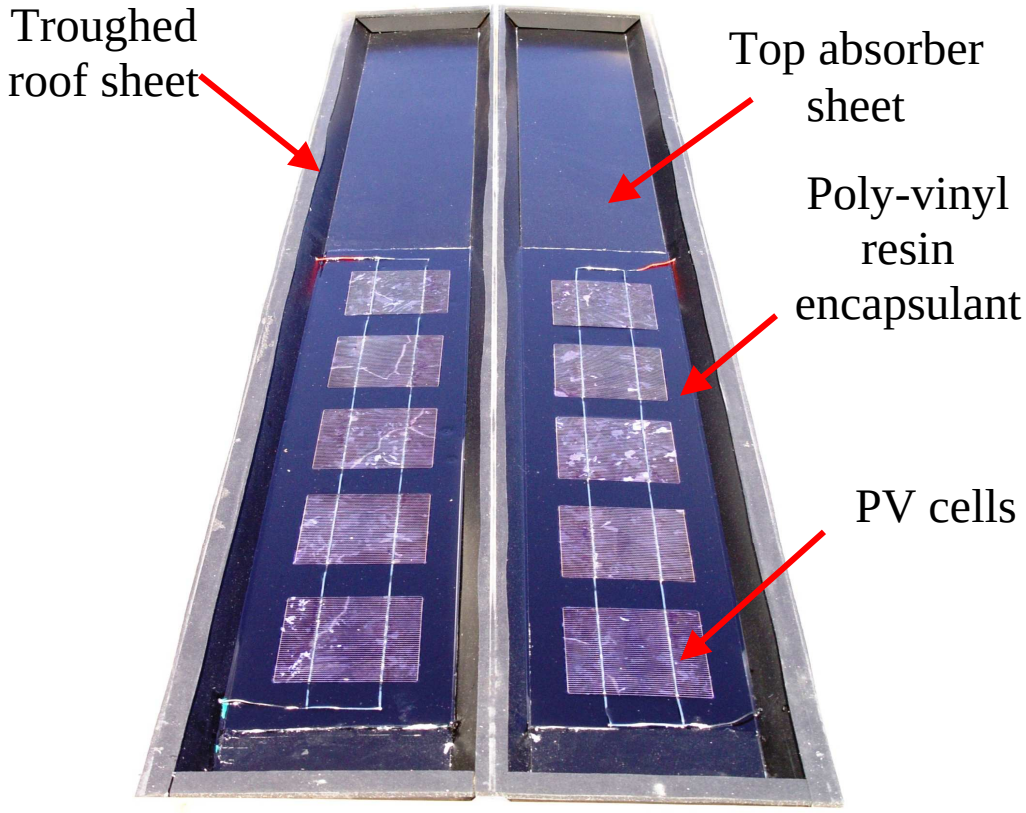

Figure 15: Proof-of-concept and test BIPVT collector

Table 1: Prototype experimental BIPVT physical characteristics

Parameter	Symbol	Value	Unit
Number of covers	N	1 or 0	
Emittance of plate	ε_p	0.95	
Emittance of cover	ε_c	0.88	
Number of tubes	n	2	
Collector Length	L	1.96	m
Collector Breadth	b	0.5	m
Collector Area	$A_{collector}$	0.98	m^2
Absorber thickness	t	0.5	mm
PV thickness	L_{PV}	0.4	mm
PV conductivity (Krauter, 2006)	k_{PV}	130	W/mK
Tube Hydraulic Diameter	d_h	8	mm
Tube Spacing	W	0.23	m
Ratio of Tube width to spacing	d/W	0.087	
Heat transfer coefficient from cell to absorber (de Vries, 1998)	h_{PVA}	45	W/m^2K
Insulation Conductivity	k	0.045	W/mK
Back Insulation Thickness	L_b	0.1	m
Edge Insulation Thickness	L_{edge}	0.025	m
Absorber Conductivity	k_{abs}	50	W/mK
Packing Factor	S	0.4	
Mounting Angle	β	37	Degrees

2.3 Experimental Setup

In order to test solar thermal collectors there are a number of standardised test methods that can be used, such as AS/NZS 2535.1-1999 and ISO 9806-3. For this study a steady state outdoor thermal test setup was used, similar to that recommended in AS/NZS 2535.1-1999 and shown in Figure 16.

The reason for choosing an outdoor test system lies in the fact that the results are based on energy provided by an actual solar spectrum. Though it is possible to test collectors indoors under controlled "weather" conditions, the replication of the solar spectrum and achieving a constant flux is extremely difficult. Studies by Adelhelm and Berger (2003), Tiedemann and Maytrott (1997) and Garg et al. (1985) regarding the use of indoor solar simulators showed either poor replication of the solar spectrum or non-uniform illumination, thus supporting the use of an outdoor system.

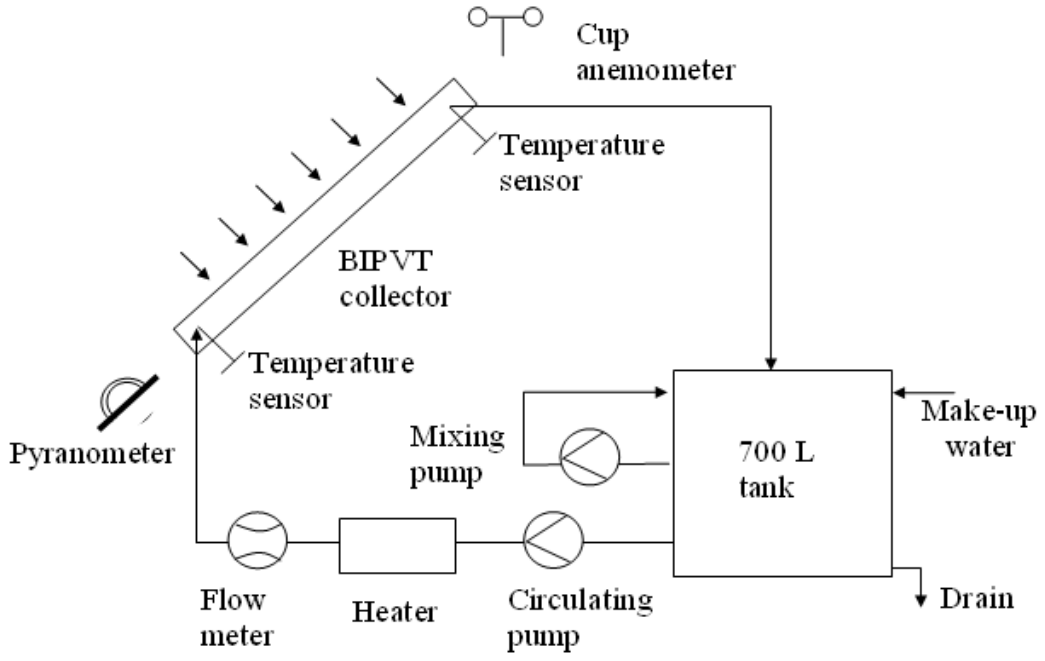

Figure 16: Steady state solar collector test system

In order to test the prototype collector, an unimpeded north facing test location on the University of Waikato library roof was chosen. To quantify the performance of the collector it was necessary to measure the global incident solar radiation to which the collectors were exposed. The measurement of the incoming radiation

was made using a calibrated WMO First Class pyranometer mounted inline with the collector at an angle of 38 degrees, equal to the local latitude.

T-type thermocouples, calibrated to ±0.3K against a platinum resistance thermometer, were used to measure the inlet and outlet temperatures to the collector and the local ambient air temperature. A cup anemometer was used to monitor the wind speed in the test area and was mounted adjacent to the test stand for the collector. The flow of water through the collector was set at a constant rate and monitored throughout the testing periods by manually measuring the time taken for a known mass to pass through the collector. The uncertainty associated with this technique and the data derived from it is outlined in greater detail in Appendix A.

In addition to the measurement apparatus, an instantaneous electric water heater with an inbuilt temperature controller was mounted on the inlet side of the collector so as to provide a controllable inlet water temperature. The outlet from the collector was returned to a 700 litre water tank where it was well mixed to ensure that large temperature spikes were not encountered by the heater.

2.4 Experimental Performance of BIPVT Prototype

The testing of the prototype BIVT was conducted in accordance with AS/NZS 2535.1-1999. This standard specifies a test method to determine the thermal efficiency of solar collectors. A prerequisite to accurately determining the performance of the collector is to conduct a number of outdoor tests under a range

of ambient conditions. In this case both a glazed and unglazed BIPVT collector were tested, and benchmarked against test results from a commercially available flat plate collector, and the published efficiency (SPF, 2007) of a commercially available high performance glazed flat plate collector.

For each test the temperatures, global radiation and wind speed were data-logged at 20 second intervals. The collector was given at least 15 minutes at the beginning of each test condition in which to reach a quasi-steady state. In analysing the data, only 5 minute periods in which the average global radiation exceeded 800W/m^2 and did not vary by more than 50W/m^2, the ambient temperature did not vary by more than 1K and the inlet temperature did not vary by more than 0.1K were taken to be steady-state. Additionally, any data points that satisfied these criteria but were more than 30 degrees either side of solar noon were also eliminated due to the possibility of including incident angle modifier terms.

When analysing the collectors, the instantaneous collector efficiency can be determined directly from the experimental results, as it is defined simply as the ratio of heat transfer in the collector (Equation 3) to the product of the collector area and the global solar irradiance, as shown in Equation 4.

$$\dot{Q} = \dot{m} C_p \left(T_{out} - T_i \right) \tag{3}$$

$$\eta_G = \frac{\dot{Q}}{A_{collector}\, G''} \tag{4}$$

However, further analysis of the raw data is needed to determine the efficiency equation of the BIPVT and solar collector. From the experimental data, the efficiency of a solar collector for all conditions can be represented by a linear equation of the form shown in Equation 5.

$$\eta = \eta_{0A} - a_1\left(\frac{T_i - T_a}{G''}\right) \tag{5}$$

To determine the efficiency of the BIPVT collectors a number of readings were taken when the collector was operating under steady state conditions. In Table 2 and Table 3 the data that was collected during the testing and the instantaneous heat gain and collector efficiency are shown for the glazed and unglazed BIPVT collectors.

Table 2: Glazed BIPVT test data

Outlet Temp	Inlet Temp	Global Radiation	Ambient Temp	Mass Flowrate	Instantaneous Efficiency	Heat Gain
°C	°C	W/m^2	°C	kg/s		W
28.2	25.5	999.8	28.2	0.05	0.59	582.8
28.3	25.7	1008.0	28.6	0.05	0.59	585.2
28.5	25.8	1018.8	30.1	0.05	0.60	601.0
28.5	25.8	1032.8	27.8	0.05	0.60	610.9
28.7	25.9	1037.2	28.1	0.05	0.59	600.4
29.1	26.3	1038.4	28.3	0.05	0.59	605.2
29.4	26.6	1042.6	27.4	0.05	0.61	623.5
54.7	52.6	995.3	29.8	0.05	0.46	446.2
54.6	52.7	952.3	29.9	0.05	0.47	436.7
54.3	52.3	931.6	30.1	0.05	0.49	446.2
55.0	53.0	971.3	29.5	0.05	0.46	441.8
54.1	52.2	1006.8	29.5	0.05	0.44	438.7
54.1	52.0	1015.9	29.2	0.05	0.46	455.8
54.0	52.0	1017.2	29.3	0.05	0.45	446.2
44.1	41.9	1022.0	29.0	0.05	0.49	491.7
44.4	42.1	1010.5	28.6	0.05	0.51	508.9
44.4	42.1	1008.8	29.5	0.05	0.52	509.7
44.6	42.3	994.7	30.4	0.05	0.52	503.1
44.5	42.2	1000.1	30.1	0.05	0.51	496.3
44.5	42.3	997.9	29.3	0.05	0.51	497.4

Table 3: Unglazed BIPVT test data

Outlet Temp	Inlet Temp	Global Radiation	Wind Speed	Ambient Temp	Mass Flowrate	Instantaneous Efficiency	Heat Gain
°C	°C	W/m^2	m/s	°C	kg/s		W
58.6	58.7	847.2	0.2	20.4	0.03	-0.03	-23.0
58.4	58.9	871.8	0.0	20.8	0.03	-0.09	-78.2
56.6	57.2	890.6	0.2	21.1	0.03	-0.09	-80.0
26.5	24.3	965.2	0.0	20.1	0.03	0.33	311.5
26.7	24.5	975.1	0.4	21.0	0.03	0.32	302.1
27.4	25.0	976.9	0.1	21.7	0.03	0.35	335.9
28.2	25.8	995.8	0.1	21.4	0.03	0.34	327.6
30.3	27.9	1009.1	0.0	20.9	0.03	0.33	330.1
37.0	35.3	1022.1	0.0	20.9	0.03	0.24	237.8
40.0	38.5	1021.6	0.1	21.1	0.03	0.21	206.1
40.5	38.9	1019.9	0.0	21.4	0.03	0.23	227.4
40.9	39.5	1020.0	0.1	21.0	0.03	0.20	199.1
41.2	39.7	1013.0	0.2	21.6	0.03	0.20	199.4
41.7	39.9	983.4	0.0	22.3	0.03	0.26	250.0
41.9	40.1	961.8	0.1	22.4	0.03	0.27	250.7
41.9	40.1	953.6	0.0	22.7	0.03	0.27	250.4
40.6	39.7	927.6	0.2	21.4	0.03	0.13	122.2
41.3	39.8	971.3	0.2	22.7	0.03	0.22	207.5
40.9	39.7	886.7	0.0	22.7	0.03	0.18	158.0
47.8	47.6	857.2	0.2	23.3	0.03	0.03	25.5
48.1	47.6	884.5	0.0	23.7	0.03	0.08	67.3
48.6	47.1	995.3	0.0	26.5	0.03	0.21	204.0
26.5	24.8	898.7	0.1	23.9	0.03	0.27	239.7
26.9	25.1	934.4	0.0	24.1	0.03	0.26	242.3
27.7	25.8	984.0	0.0	23.9	0.03	0.28	265.7
27.8	26.0	995.1	0.1	22.6	0.03	0.25	247.2
28.3	26.4	1009.7	0.0	24.1	0.03	0.26	258.5
29.1	27.0	1034.1	0.0	24.5	0.03	0.28	279.2
29.5	27.6	1087.7	0.0	23.7	0.03	0.24	258.5
30.9	28.6	1067.7	0.1	25.4	0.03	0.30	316.1
31.3	29.1	1061.8	0.0	25.9	0.03	0.29	303.1
31.2	29.1	1060.9	0.0	25.0	0.03	0.27	285.6

From the experimental data, it was possible to derive the performance of the collectors using a linear least squares regression analysis. The data shown in the tables yields two equations that describe the glazed and unglazed collector efficiencies, as shown in Equation 6 and 7 respectively.

$$\eta = 0.6 - 5.55\frac{T_i - T_a}{G''} \tag{6}$$

$$\eta = 0.36 - 9.22\frac{T_i - T_a}{G''} \tag{7}$$

The significance of the efficiency equations can be better understood from an inspection of Figure 17 and Figure 18. From these graphs it can be seen that as the difference in temperature between the collector inlet and the ambient increases, at constant radiation intensity, there is a decrease in collector efficiency. Moreover, the gradient of the curves is proportional to the heat loss from the collector. In this case it can be seen that the unglazed collector has higher heat loss and that there is significantly more scatter of the unglazed data. The scatter in the data is due to the increased influence of wind induced heat loss on unglazed collectors (Anderson, 2004).

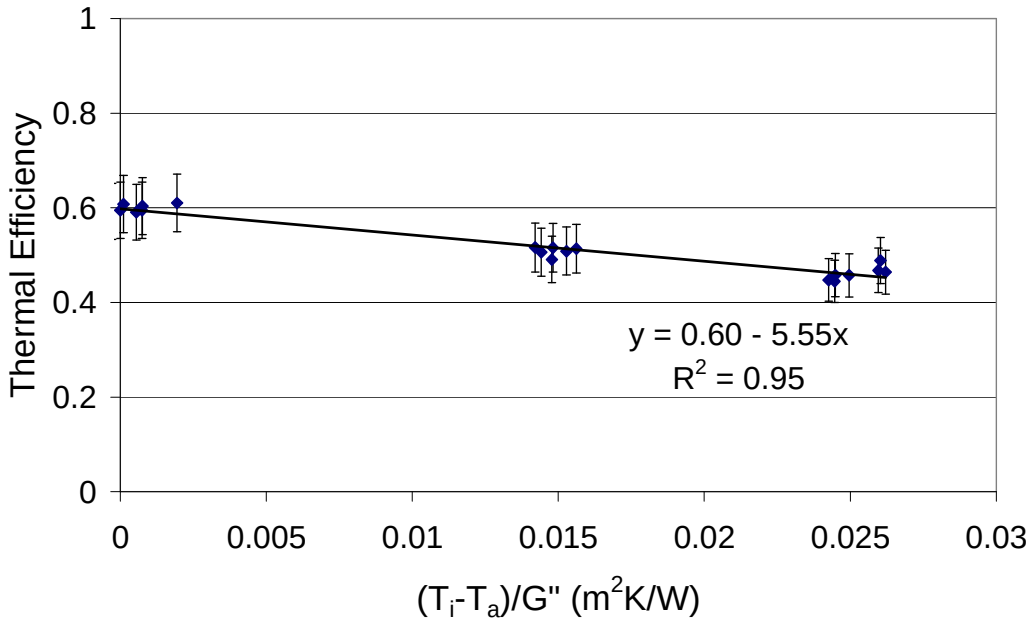

Figure 17: Thermal efficiency of prototype glazed BIPVT collector

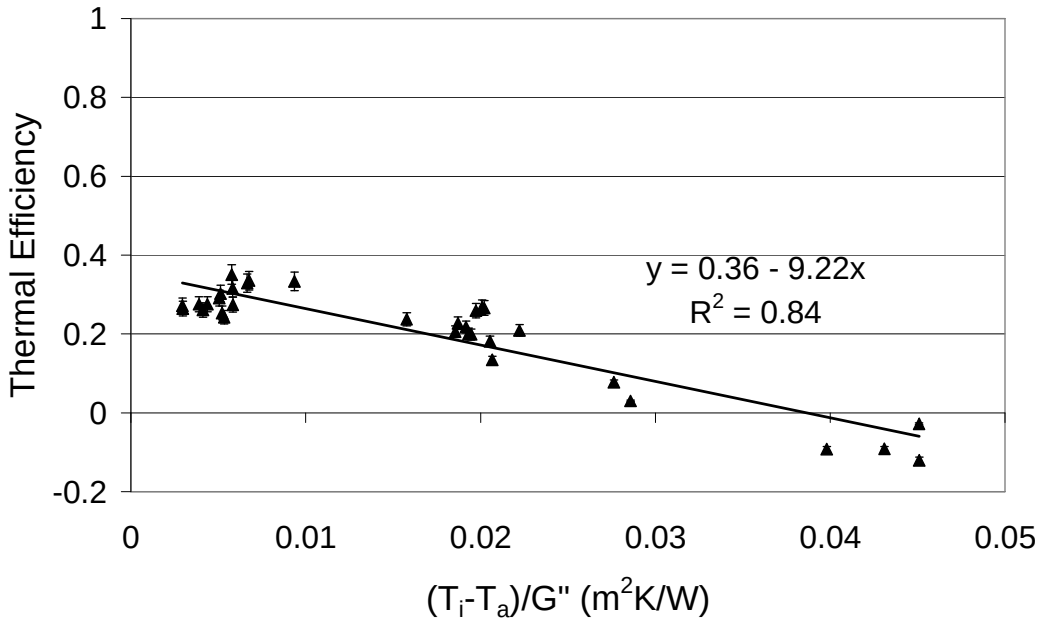

Figure 18: Thermal efficiency of prototype unglazed BIPVT collector

In the efficiency graphs the point at which the curve intersects the y-axis is commonly referred to as the optical efficiency (though it is actually a combination of the optical absorptance and collector fin efficiency) and in this case the unglazed collector is lower. This is the result of the collector's low geometric fin efficiency in combination with high radiative heat losses from the collector to the sky (due to the high emissivity of the collector and low sky temperature) and convective heat losses by natural convection and wind induced forced convection.

When the performance of the prototype BIPVT collectors is compared with test data of the commercially available glazed flat-plate collector, and the published data for a high performance glazed flat plate collector, it can be seen that there is not a significant difference in the heat loss, or slope, of the efficiency curves (Figure 19). However, there is a difference in the optical efficiency of the panels. In particular the high efficiency glazed flat plate collector has an optical efficiency of approximately 80%, whereas the BIPVT and tested glazed flat plate was closer to 65%. The reason for the low optical efficiency of the tested glazed flat plate was its use of a high-iron content glass cover. It has been shown, and is widely recognised, that the use of high-iron glazing tends to reduce the transmission of longer wavelength radiation (Dietz, 1954).

The glazed BIPVT used a low iron cover and so was almost comparable with the tested flat plate collector; however, the optical properties of silicon mean the PV cells tend to reflect a large portion of the solar spectrum (Green and Keevers, 1995). For this reason the BIPVT optical efficiency is lower than the flat plate

collectors. Furthermore, both the heat loss and optical efficiency are highlighted when considering the relative performance of the unglazed BIPVT. For all cases, there is significantly higher heat loss from the unglazed collector as well as a lower optical efficiency.

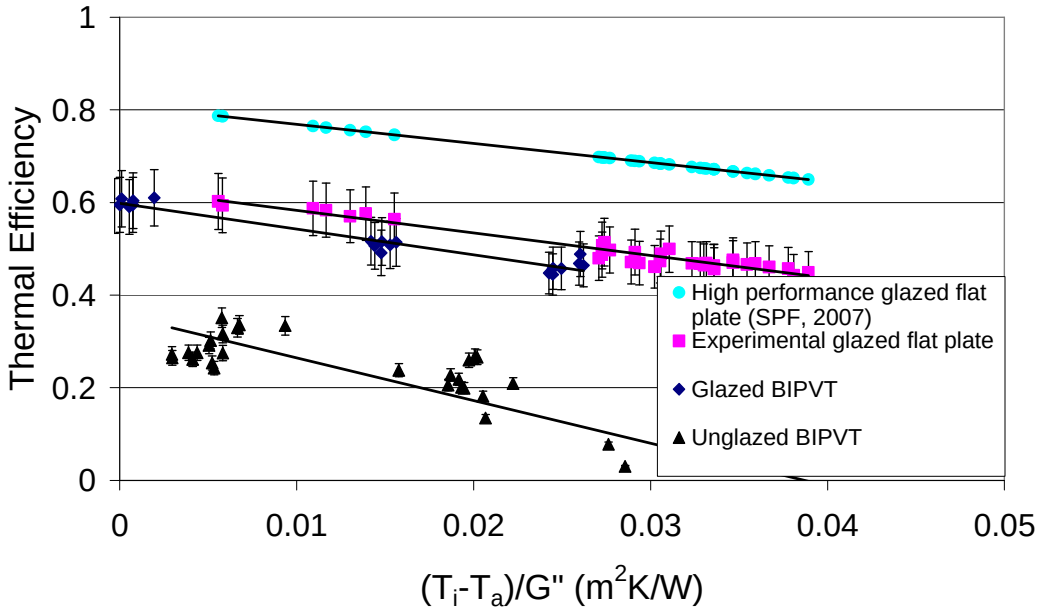

Figure 19: Comparative efficiency of glazed flat plate and BIPVT collectors

2.5 Measurement of BIPVT Absorptance and Transmittance-Absorptance Product

When comparing the efficiency of the BIPVT and glazed flat plate solar collectors, it was noted that there was a difference in the optical efficiencies. If the intention is to improve the performance of the BIPVT, it is logical that the parameters that affect its performance should be quantified. Previously it was noted that the efficiency of a solar collector could be represented by Equation 8.

$$\eta = \eta_{0A} - a_1\left(\frac{T_i - T_a}{G''}\right) \tag{8}$$

However, from a theoretical perspective the efficiency is represented by a relationship between the collectors heat removal factor (F_r), the collector heat loss coefficient (U_L), the inlet and ambient temperatures, solar radiation and the collector transmittance-absorptance product ($\tau\alpha$) as shown in Equation 9 (Duffie and Beckman, 2006).

$$\eta = F_r(\tau\alpha) - F_r U_L\left(\frac{T_i - T_a}{G''}\right) \tag{9}$$

Of these parameters, the transmittance-absorptance product is the only one that is based solely on a physical property of the collector materials. The absorptance provides a measurement of the optical properties of the radiation absorbing surface, in this case either the PV cells or the black steel roof, while the transmission component measures the portion of the radiation transmitted by any glazing layer. Therefore in order to understand the optical characteristics of the BIPVT it was decided to determine its absorptance properties over the solar radiation spectrum.

When radiation strikes a surface it can be transmitted, reflected or absorbed depending on the properties of the material. The non-dimensional sum of these components is unity, as shown in Equation 10.

$$\tau + \alpha + \rho = 1 \tag{10}$$

However of these three components only reflection needs to be physically measured to determine the optical absorption of the collector. This is because a solid steel collector is an opaque surface and so it is assumed that the BIPVT does not transmit radiation (Duffie and Beckman, 2006), as such Equation 10 reduces to Equation 11.

$$\alpha = 1 - \rho \tag{11}$$

To determine the absorption of the BIPVT, the diffuse reflectance of a resin encapsulated PV cell as used on the prototype collector, and a sample of the black coated steel were measured at 20 nm wavelength intervals for radiation in the range 300 nm to 2500 nm. These measurements were performed by Industrial Research Limited (Wellington, NZ) using a spectrophotometer and a 6° integrating sphere according to the Measurement Standards Laboratory of New Zealand Technical Procedure MSLT.O.024.005.

From the measurements of the reflectance shown in Figure 20 it can be seen that the black painted steel roofing material has relatively constant reflectance characteristics across the measured wavelengths of the Air Mass 1.5 (AM1.5) solar spectrum shown (NREL, 2008). The encapsulated PV cell however is far more sensitive to wavelength; in particular it absorbs a significant portion of the shorter wavelength radiation but reflects a large portion of the wavelengths above

1100 nm, this is due to the spectral characteristics of the silicon used in the PV cell, the back reflector behind the silicon and the anti-reflective coating on the cell.

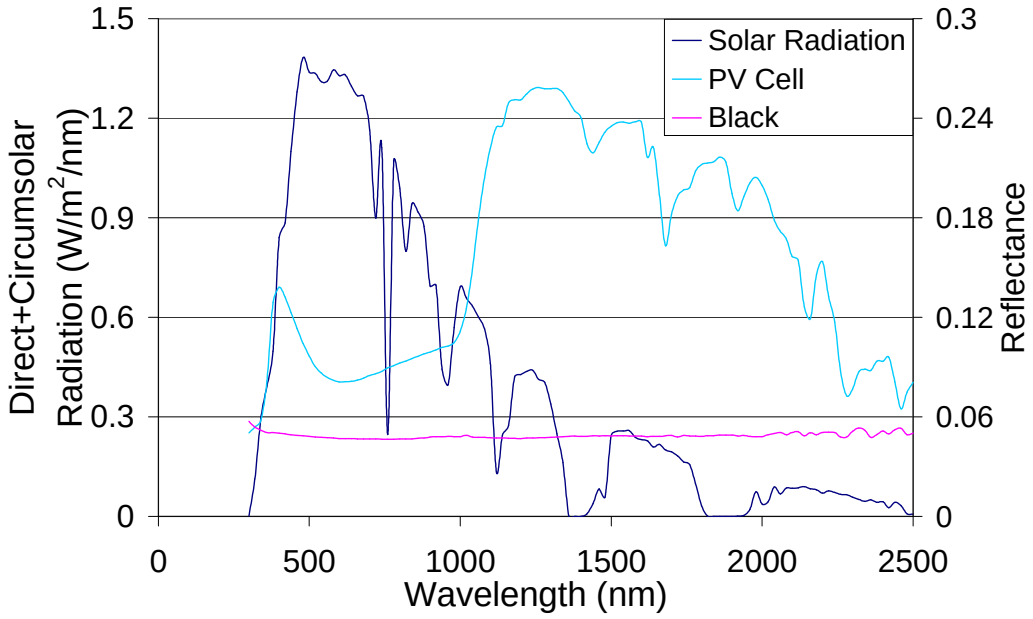

Figure 20: AM 1.5 spectrum and reflectance from PV cells and black coated steel

In the case of a black unglazed BIPVT it was possible to determine the absorptance of the panel by subtracting the reflected component from the unity sum, as discussed previously. By integrating the absorptance of the PV cell and the black coated steel samples over the tested wavelength of the AM1.5 solar spectrum, solving Equation 12 by the Trapezoidal Rule, the absorptances are found to be 0.88 and 0.95 respectively.

$$\alpha = \frac{\int_{\lambda_1}^{\lambda_2} \alpha_\lambda I_{\lambda,i} d\lambda}{\int_{\lambda_1}^{\lambda_2} I_{\lambda,i} d\lambda} \tag{12}$$

However for a black glazed panel, the presence of the glass cover must also be accounted for. Although glass is transparent, it absorbs a portion of the radiation and therefore its transmittance is not 100%. Dietz (1954) determined the spectral transmittance of the low iron glass used as the glazing of the BIPVT, and this is shown in Figure 21. Here it can be seen that the transmittance is relatively constant (~90%) across the AM1.5 spectrum for which the reflectance of the absorbing material were tested.

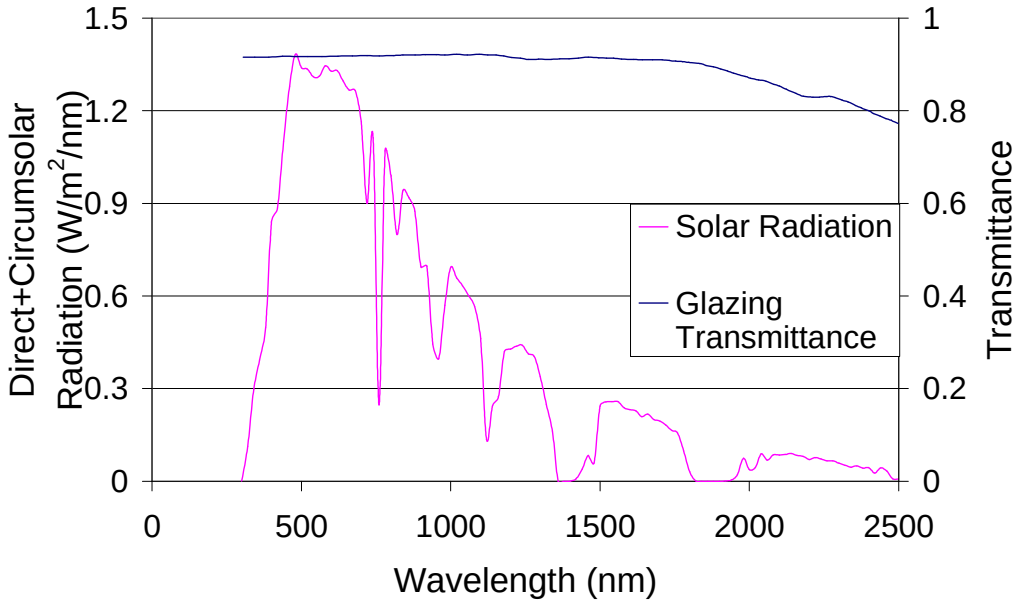

Figure 21: AM 1.5 spectrum and transmittance of low iron glass

To determine the transmittance-absoptance product for a glazed collector, the measured spectral absorption characteristics and the glass transmittance characteristics of Dietz (1954) were substituted into Equation 13 and integrated over the AM1.5 spectrum. By doing this it was found that the transmittance

absorptance product of the black steel surface and the PV cell in a glazed BIPVT collector were calculated to be 0.87 and 0.80 respectively.

$$\tau\alpha = \frac{\int_{\lambda_1}^{\lambda_2} \tau_\lambda \alpha_\lambda I_{\lambda,i} d\lambda}{\int_{\lambda_1}^{\lambda_2} I_{\lambda,i} d\lambda} \tag{13}$$

Similarly, it was recognised that both glazed and unglazed BIPVT collectors could be made in colours other than black. In fact, the work of PV Catapult (2005) and Weiss and Stadler (2001) suggested that the development of coloured collectors presented an unrealised opportunity.

Therefore, in addition to testing the black coated steel and the PV cell, six colour-coated steel samples (Titania, New Denim Blue, Pioneer Red, Lignite, Rivergum and Lichen, shown in Figure 22) were tested using spectrophotometry to determine their absorptance characteristics. In Figure 23 it can be seen that Titania and Pioneer Red have the highest reflectance while Lignite and New Denim Blue have the lowest. Although somewhat self-evident, the reason Pioneer Red has a high reflectance is that in order to appear “red” it must reflect wavelengths in the red portion of the solar spectrum.

Figure 22: Lignite, New Denim Blue, Titania, Lichen, Rivergum, Pioneer Red (from left to right)

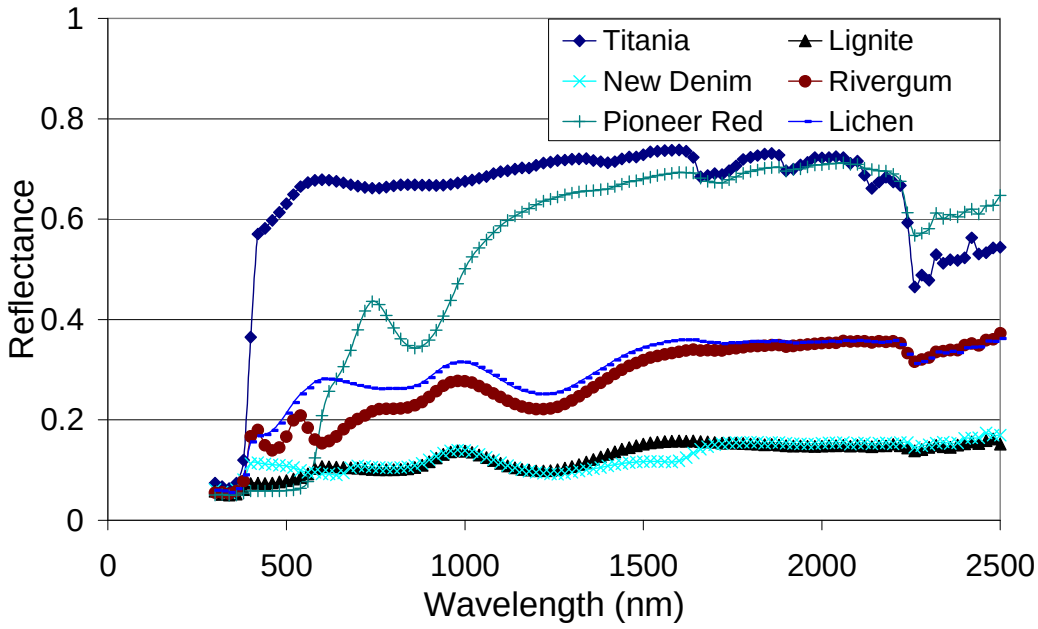

Figure 23: Reflectance of coloured steel samples

The absorptance characteristics of these samples were integrated over the AM1.5 spectrum, as discussed previously. The absorptance and transmittance-absorptance products for these samples in an unglazed or glazed BIPVT are given by the values shown in Table 4 and Table 5 respectively.

Table 4: Absorptance of coloured steel in an unglazed BIPVT

Colour	**Absorptance**
Lignite	0.89
New Denim Blue	0.89
Rivergum	0.78
Lichen	0.74
Pioneer Red	0.66
Titania	0.35

Table 5: Transmittance-absorptance product of coloured steel in a glazed BIPVT

Colour	**Transmittance-absorptance product**
Lignite	0.82
New Denim Blue	0.81
Rivergum	0.72
Lichen	0.67
Pioneer Red	0.60
Titania	0.32

Having obtained the optical characteristics for the materials used in the BIPVT, there was the opportunity to utilise these in optimising the BIPVT in terms of not only its thermal and electrical efficiency but also its aesthetics. Similarly, the optical properties could be used in the design of low cost coloured solar collectors for water heating (building integrated thermal) (Appendix B), or for the reflective colours, in low cost photovoltaic concentrators.

Although an optimisation of the collector could be achieved experimentally, this would be a time intensive process. Hence, in Chapter 3 a theoretical model of the BIPVT is presented and used to optimise its performance.

2.6 Experimental Summary

From the experimental testing, a novel method for the construction of BIPVT collectors was utilised in the development of a prototype collector. Furthermore, it was shown that the thermal efficiency of both the glazed and unglazed BIPVT collectors compared well with that of a commercial flat-plate solar water heater. However the heat loss from, and the low stagnation temperature of, the unglazed BIPVT collector would suggest that it is not well suited to higher temperature heating operations but may be well suited to operation as the heat source for heat pump water heaters.

The spectral reflectance characteristics of the materials used in the BIPVT absorber were measured and used to determine the absorptance. The results showed that one of the shortcomings of PV cells was their relatively high reflectance of long wavelength radiation (>1000nm). However, it was found that the black steel used in the prototype had very low reflectance across the AM1.5 visible spectrum. Furthermore, the properties of alternative steel colours were also determined to assess their suitability as absorbers for BIPVT collectors.

Chapter 3: Mathematical Modelling for Optimisation of BIPVT Collector Efficiency

3.1 Introduction

In Chapter 2 the design and development of a prototype BIPVT collector were examined. At the conclusion of this chapter it was noted that some of the experimental data could be used in optimising the performance and aesthetics of the BIPVT. This chapter describes the development of a mathematical model which was used to optimise the collector and to determine the effect of potential design parameters on the collector performance.

3.2 Modelling Methodology

In order to analyse the thermal and electrical performance of the BIPVT a one dimensional steady state thermal model was developed in which it was assumed that the collector could be represented as a flat plate thermal collector. For this study a modified form of the Hottel-Whillier-Bliss equations presented by Duffie and Beckman (2006) was used.

Under these conditions the useful heat gain can be calculated using Equation 14.

$$Q = AF_R\left[(\tau\alpha)_{PV}.G - U_L(T_i - T_a)\right] \tag{14}$$

In this equation the useful heat gain (Q) was represented by a function of the collector area (A), the heat removal efficiency factor (F_R), the transmittance-

absorptance product of the photovoltaic cells ($\tau\alpha_{PV}$), the solar radiation (G), the collector heat loss coefficient (U_L) and the temperature difference between the cooling medium inlet temperature (T_i) and the ambient temperature (T_a).

The heat removal efficiency factor (F_R) was calculated using Equation 15, which also accounted for the mass flow rate in the collector (m) and the specific heat of the collector cooling medium (C_p).

$$F_R = \frac{mC_P}{AU_L}\left[1 - e^{-\frac{AU_L F'}{mC_P}}\right] \tag{15}$$

In order to obtain the heat removal efficiency factor however, it was necessary to calculate a value for the corrected fin efficiency (F'). This was achieved by first calculating the fin efficiency (F) using Equation 16.

$$F = \frac{\tanh\left(M\frac{W-d}{2}\right)}{\left(M\frac{W-d}{2}\right)} \tag{16}$$

This equation determines the efficiency of the finned area between adjacent tubes by taking into account the influence of the tube pitch (W) and the tube width (d) of the rectangular cross-section tubes or channels formed in the fabrication of the BIPVT. As such all calculations related to flow in the tubes were based on the tubes' hydraulic diameter (d_h).

The coefficient (*M*) is a term which accounts for the thermal conductivity (bond resistance) of the absorber and PV cell and was represented by Equation 17 (Vokas et al. 2006).

$$M = \sqrt{\frac{U_L}{k_{abs}L_{abs} + k_{PV}L_{PV}}} \tag{17}$$

The corrected fin efficiency (*F'*) was calculated using Equation 18.

$$F' = \frac{\frac{1}{U_L}}{W\left[\frac{1}{U_L(d+(W-d)F}\right] + \frac{1}{Wh_{PVA}} + \frac{1}{\pi dh_{fluid}}} \tag{18}$$

In Equation 18, the overall heat loss coefficient (U_L) of the collector is the summation of the collector's edge (Equation 19), top and rear surface losses.

$$U_{edge} = \frac{K_{edge}pt}{L_{edge}A_{collector}} \tag{19}$$

Where *p* is the collector perimeter and *t* is the absorber thickness. It was assumed that the top loss coefficient, due to reflections and wind, could be calculated using Klein's empirical equation (Equation 20) as given by Duffie and Beckman (2006) and the rear loss coefficient could be given by the inverse of the insulations R-value (ie. K_b/L_b).

$$U_{top} = \left\{ \frac{N}{\frac{c}{T_{pm}}\left(\frac{T_{pm}-T_a}{N-f}\right)^e + \frac{1}{h_w}} \right\}^{-1} + \frac{\sigma\left(T_{pm}+T_a\right)\left(T_{pm}^2+T_a^2\right)}{\left(\varepsilon_p + 0.00591Nh_w\right)^{-1} + \frac{2N+f-1+0.133\varepsilon_p}{\varepsilon_g} - N} \quad (20)$$

Where:

$$c = (520 - 0.000051\beta^2) \qquad f = (1 + 0.089h_w - 0.1166h_w\varepsilon_p)(1 + 0.07866N)$$

$$e = 0.430(1 - \frac{100}{T_{pm}}) \qquad T_{pm} = T_i + \frac{Q/A_{collector}}{F_R U_L}\left(1 - F_R\right)$$

β is the collector mounting, σ is the Stefan-Boltzmann constant, N is the number of covers or glazing layers, ε_g the emittance of the cover or glazing, ε_p the emittance of the plate and h_w is the convection heat transfer coefficient due to the wind.

Furthermore, h_{PVA} is a "quasi" heat transfer coefficient to account for the bond resistance between the PV cell and the absorber (Zondag et al., 2002) and h_{fluid} is the forced convection heat transfer coefficient inside the cooling passage determined from the Dittus-Boulter equation (Cengel, 1998).

However, considering the case of an unglazed collector, in which there is no cover, Equation 20 can not be applied. Instead it was necessary to calculate the top loss coefficient by the individual contributions of radiation, natural and forced convection.

The heat loss due to radiation was expressed as a radiation heat transfer coefficient in terms of the sky temperature (T_s), the mean collector plate temperature (T_{pm}) and the plate emissivity (ε_p) as shown in Equation 21.

$$h_r = \sigma \varepsilon_p (T_{pm}^2 + T_s^2)(T_{pm} + T_s) \tag{21}$$

where the sky temperature is represented by the modified Swinbank equation of Fuentes (1987) as a function of the ambient temperature as shown in Equation 22.

$$T_s = 0.037536 T_a^{1.5} + 0.32 T_a \tag{22}$$

The losses due to natural and forced convection were also taken into account. The forced convection heat transfer coefficient (h_w) was calculated using the correlation of Watmuff et al. (1977) in terms of wind velocity (v), as shown in Equation 23, while the natural convection loss (h_{nat}) was represented by a function of the temperature difference between the mean collector temperature (T_{pm}) and the ambient temperature (T_a) as shown in Equation 24 (Eicker, 2003).

$$h_w = 2.8 + 3.0v \tag{23}$$

$$h_{nat} = 1.78(T_{pm} - T_a)^{1/3} \tag{24}$$

Using this method it was possible to determine an overall convection heat transfer coefficient (h_c) by combining both forced and natural convection heat transfer as

shown in Equation 25 (Eicker, 2003). Subsequently by taking the summation of the convection and radiation losses, it was possible to determine the overall top loss heat transfer coefficient (U_{top}) for the unglazed collector.

$$h_c = \sqrt[3]{h_w^3 + h_{nat}^3} \tag{25}$$

From these equations it was then possible to calculate the useful heat gain by the solar collector. Furthermore, by rearranging Equation 14, an equation for determining the thermal efficiency of the BIPVT was developed. This equation was expressed in the form shown in Equation 26.

$$\eta_{thermal} = F_R(\tau\alpha)_{PV} - F_R U_L \frac{T_i - T_a}{G} \tag{26}$$

Additionally, it was possible to analyse the thermal performance of the BIPVT collector by the inclusion of a packing factor. In practical terms, it is not always possible to have complete coverage of a panel with photovoltaic cells. As such Equation 14 was modified to account for this packing factor (S) and the transmittance-absorptance product of the absorber material ($\tau\alpha_T$) on to which the PV cells are laminated, as shown in Equation 27.

$$Q = S\left\{AF_R\left[(\tau\alpha)_{PV}.G - U_L(T_i - T_a)\right]\right\} + (1-S)\left\{AF_R\left[(\tau\alpha)_T.G - U_L(T_i - T_a)\right]\right\} \tag{27}$$

From these equations it was possible to calculate the useful heat gain by the solar collector and the mean temperature of the BIPVT (T_{pm}). Subsequently, the

electrical efficiency was calculated based on the difference between the mean temperature of the BIPVT and the Nominal Operating Cell Temperature (NOCT), taken as 298K. For this study it was assumed that the cell had an efficiency of 15% (typical of a crystalline silicon PV cell) at NOCT, and that the temperature dependent efficiency could be represented by Equation 28; where it was assumed that a 0.5%/°C decrease in electrical efficiency would occur (Green, 1998).

$$\eta_{electrical} = 0.15(1 - 0.005(T_{pm} - NOCT)) \tag{28}$$

Furthermore, an equation for determining the thermal efficiency of the BIPVT was developed based on the average transmittance-absorptance product of the BIPVT accounting for the packing factor. This equation was then expressed in the form shown in Equation 29.

$$\eta_{thermal} = F_R((S \times \tau\alpha_{PV}) + (1 - S) \times \tau\alpha_T) - F_R U_L \frac{T_i - T_a}{G} \tag{29}$$

3.3 Modelling Validation

To validate the model, the performance of the prototype BIPVT collectors in Chapter 2 was compared with the experimental data from the testing of the panel. In Figure 24 and Figure 25 it can be seen that the mathematical model, despite being a one-dimensional steady state model, was able to provide an accurate prediction of the heat gain by both an unglazed and glazed BIPVT panel over an extended testing period.

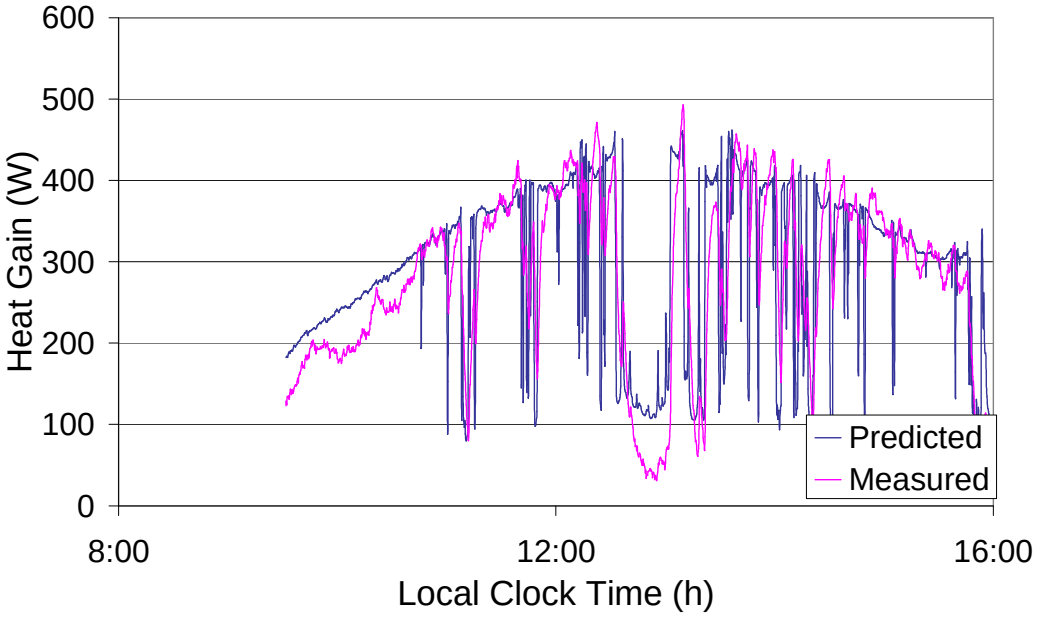

Figure 24: Predicted and measured heat gain by an unglazed BIPVT collector

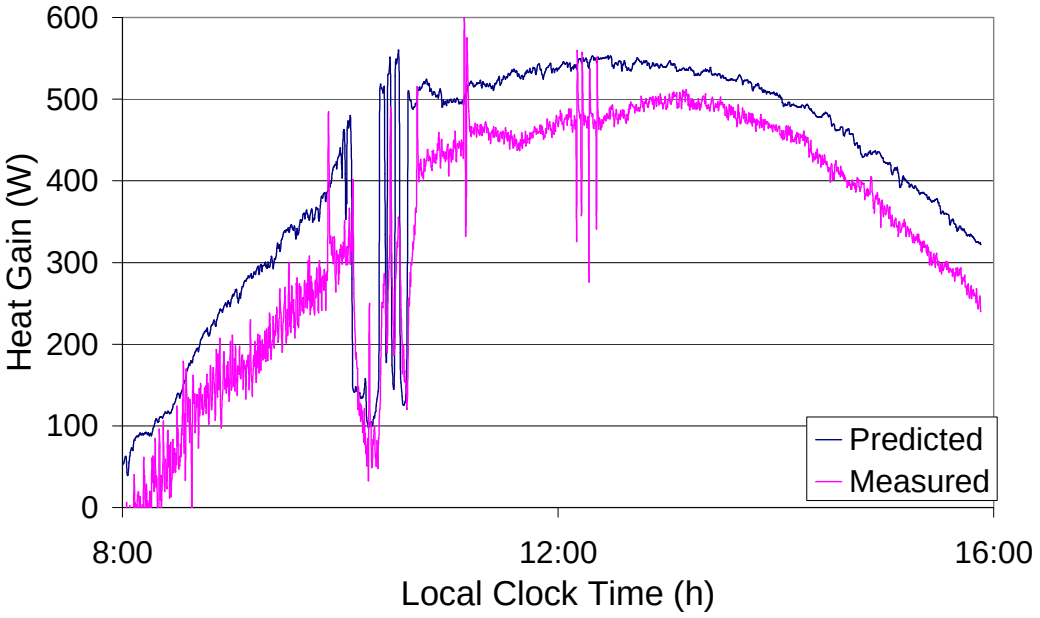

Figure 25: Predicted and measured heat gain by a glazed BIPVT collector

The validity of the model was also supported by Figure 26 and Figure 27 where it can be seen that there is quite good correlation between the predicted thermal

efficiencies for both the unglazed and glazed BIPVT and that from the experimental testing.

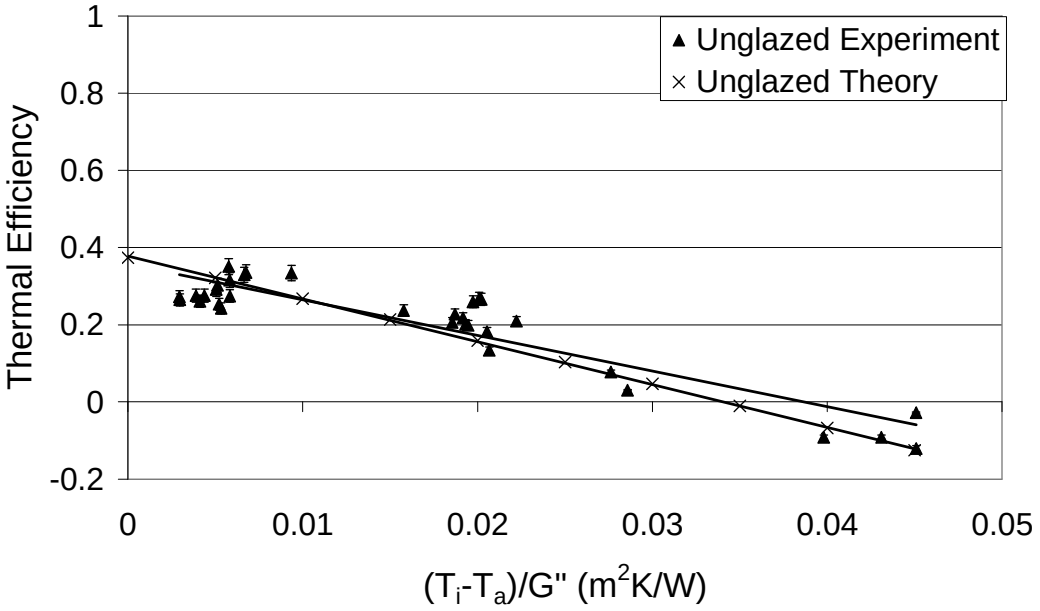

Figure 26: Experimental and theoretical thermal efficiency of an unglazed BIPVT collector

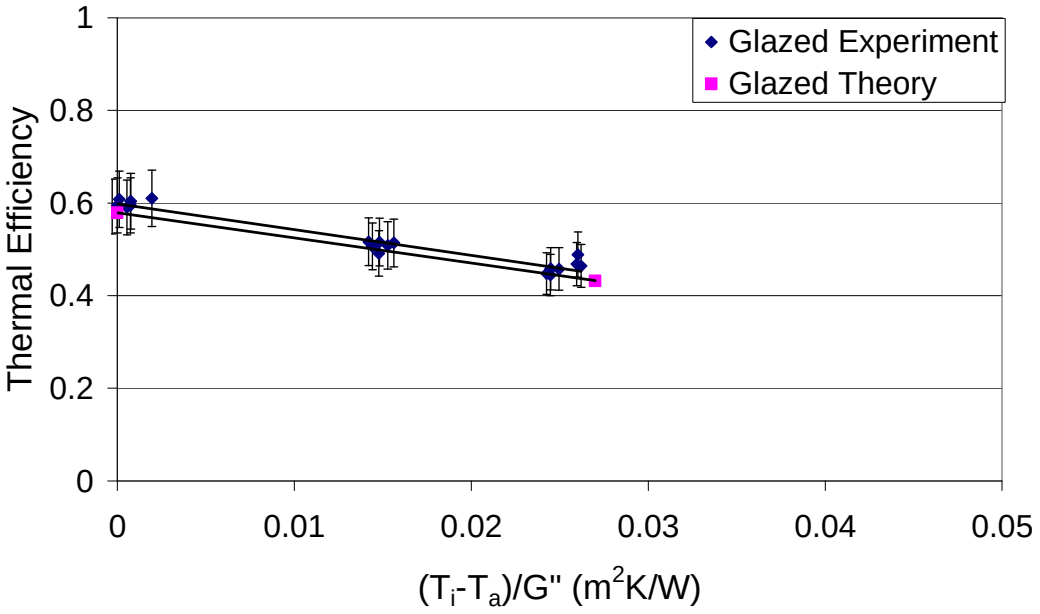

Figure 27: Experimental and theoretical thermal efficiency of a glazed BIPVT collector

3.4 Modelling Results

Having established the methodology for calculating the performance of a BIPVT solar collector, some hypothetical design values were chosen, as shown in Table 6. By varying these values the sensitivity of the design to various parameters can be examined.

Table 6: BIPVT physical characteristics

Parameter	Symbol	Value	Unit
Number of covers	N	1 or 0	
Ambient Temperature	T_a	298	K
Emittance of plate	ε_p	0.95	
Emittance of cover	ε_c	0.88	
Number of tubes	n	2	
System flow rate	m	2	l/min
Collector Length	L	1.96	m
Wind Speed	v	2	m/s
PV Trans/Abs (Chapter 3)	$\tau\alpha_{PV}$	0.80 (glazed) 0.88 (unglazed)	
Thermal Trans/Abs (Chapter 3)	$\tau\alpha_T$	0.87 (glazed) 0.95 (unglazed)	
Absorber thickness	t	0.5	mm
PV thickness	L_{PV}	0.4	mm
PV conductivity (Krauter, 2006)	k_{pv}	130	W/mK
Tube Hydraulic Diameter	d_h	9.7	mm
Tube Spacing	W	0.1	m
Ratio of Tube width to spacing	d/W	1.5	
Heat transfer coefficient from cell to absorber (de Vries, 1998)	h_{PVA}	45	W/m^2K
Insulation Conductivity	k	0.045	W/mK
Edge Insulation Thickness	L_{edge}	0.025	m
Absorber Conductivity	k_{abs}	50	W/mK
Heat Removal Efficiency Factor (typical)	F_R	~ 0.85	
Mounting Angle	β	37	degrees

From the physical characteristics given in Table 6 it was apparent that a number of variables could be modified in order to improve the thermal efficiency of the BIPVT system. As such a sensitivity analysis was conducted to determine how some of these variables would affect the thermal efficiency of the system relative to the ratio between the reduced temperature (T_i–T_a) and the global radiation incident on the collector surface (G"). In this sensitivity study, only a single design parameter was ever varied from the data given in Table 6 at any one time. This allows us to determine the parameters that have the greatest influence on the BIPVT performance, and to provide an insight into what gains could be made by changing them.

Typically, forced convection heat transfer is controlled by the Reynolds number which is a function of flow rate; as such the flow rate of the coolant through the BIPVT was varied to examine its effect on the thermal efficiency. In Figure 28 it can be seen that it has minimal effect on the thermal efficiency in this regard. However, the increase in the Reynolds number means that heat transfer from the PV cells is improved and the mean plate temperature is reduced. The reduction in the mean temperature, and therefore the PV cells temperature, means that the electrical efficiency increases marginally.

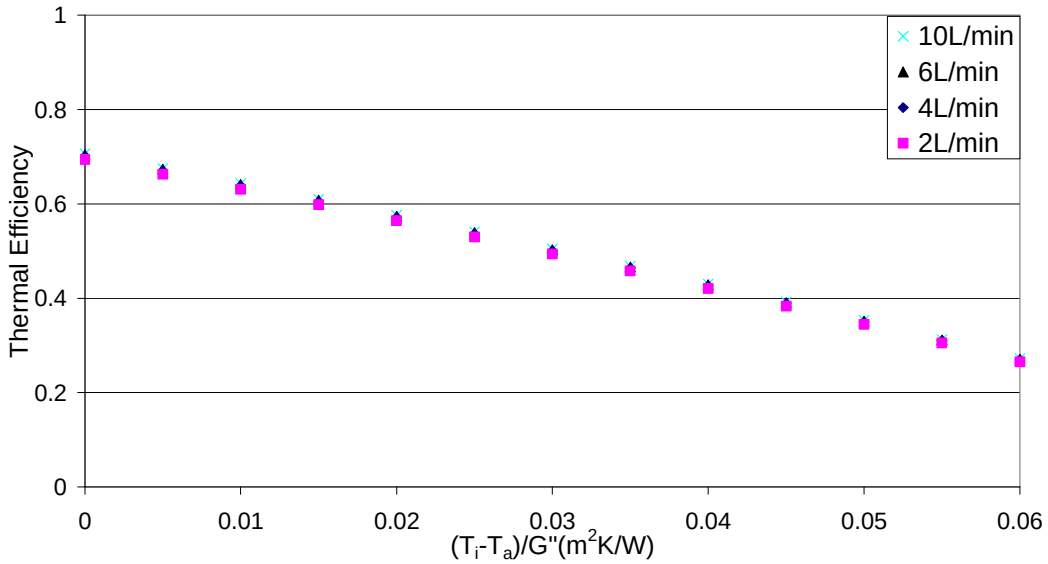

Figure 28: BIPVT thermal efficiency at varying flow rates

It may be possible to vary the material from which the collector is made. In Table 6 it was assumed that the collector was made from mild steel, however, by using aluminium or copper it is possible to increase the thermal conductivity and hence heat transfer within the panel. However, as shown in Figure 29, the material from which the collector is made does not significantly improve the thermal efficiency. This may appear to be a surprising result, as a solar collector for water heating would typically be constructed of copper to improve thermal conduction and maximise the fin efficiency, however according to the model the collector material appears to have negligible impact. As such, it suggests that lower cost materials such as mild steel could be used in their construction with negligible reduction in thermal performance, despite its relatively low thermal conductivity.

One reason for the lack of sensitivity to changes in the materials conductivity presented in Table 6 is the high geometric fin efficiency. As shown in Equation 16

the fin efficiency is a function of the rectangular tube width (*d*) used in the BIPVT and the spacing between adjacent tubes (*W*). For the results shown in Figure 29, it was assumed that the width of the tube extended almost the entire width of the trough between consecutive ridges and as such the fin efficiency begins to approach unity.

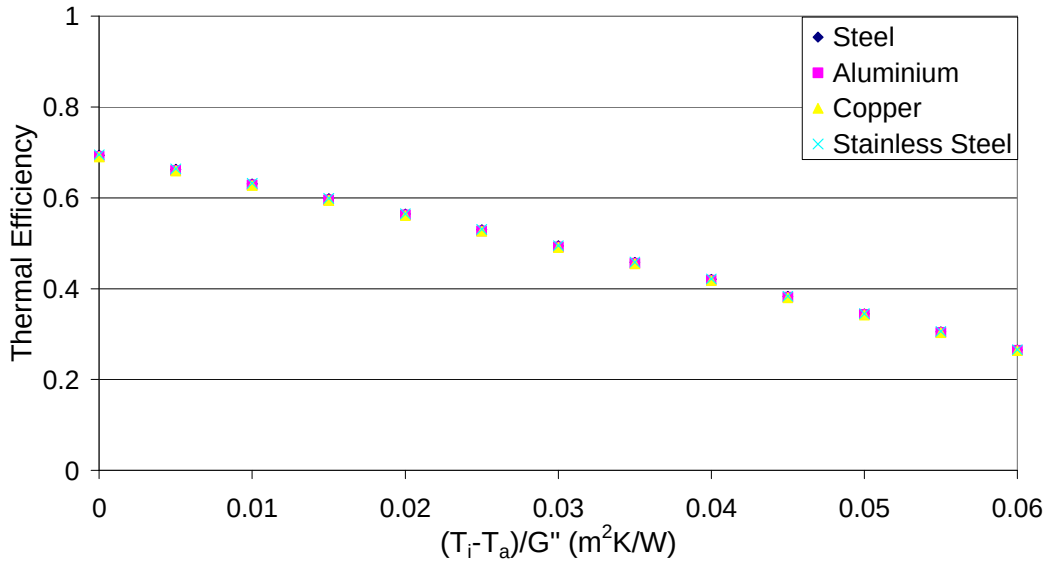

Figure 29: BIPVT thermal efficiency for varying collector materials

In Figure 30 it can be seen that by decreasing the ratio of tube width to spacing (*d/W*) the thermal efficiency of the collector is decreased for a constant hydraulic diameter. Similarly it can be seen in Figure 31 that having a large ratio *d/W* results in a significant improvement in the electrical efficiency. However it is clear that this relationship is asymptotic as shown in Figure 32.

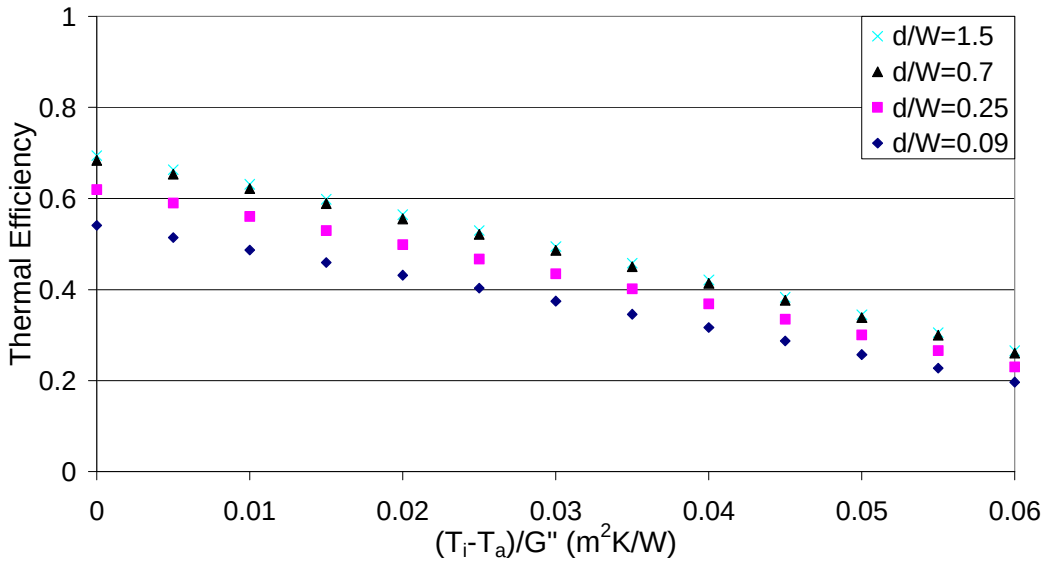

Figure 30: BIPVT thermal efficiency for varying tube width

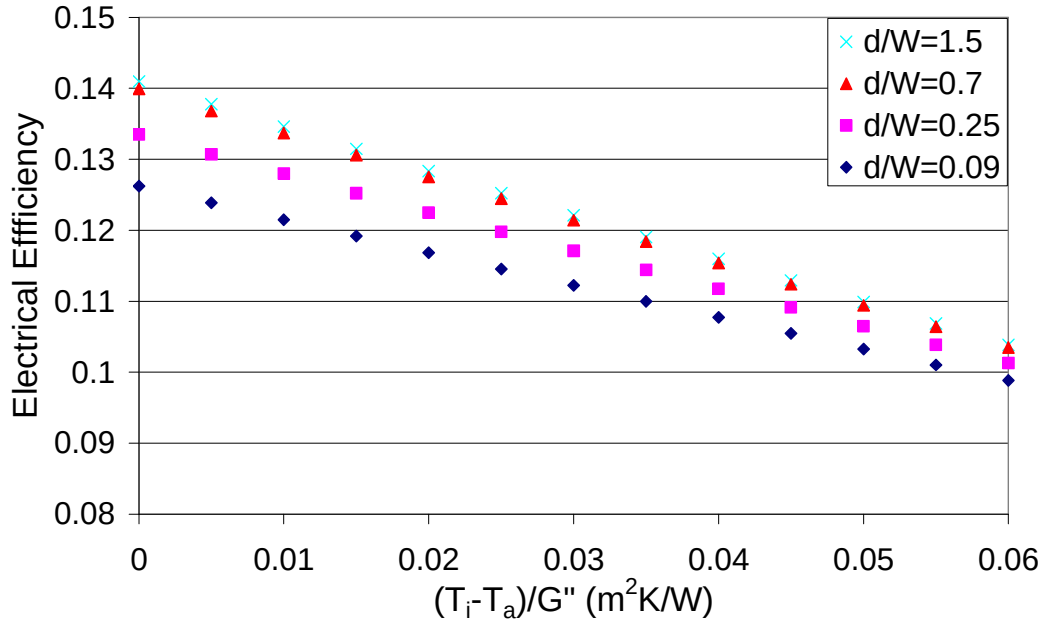

Figure 31: Electrical efficiency for varying tube width

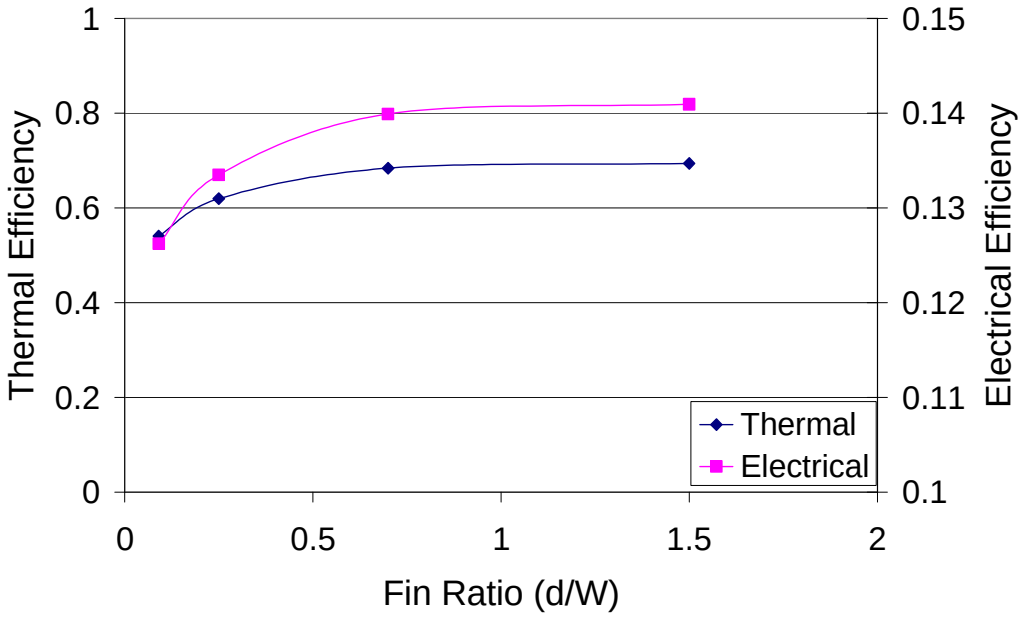

Figure 32: Effect of fin ratio on maximum thermal and electrical efficiency

However, it should be noted that increasing the geometric fin efficiency by increasing the channel width results in a higher bending stress in the absorber sheet to which the PV cells are laminated (Appendix C). This problem was noted by Bakker et al. (2002) who utilised an 8mm thick glass cover in their dual flow PVT panel to overcome the pressure loading. Rather than solely increasing the thickness of material, an alternative solution is to use multiple channels so the geometric fin efficiency is maintained but the unsupported area is smaller. This has been successfully demonstrated by Huang et al. (2001) and Chow et al. (2006) who both used multiple parallel rectangular riser tubes in their systems to achieve a geometric fin efficiency equal to unity.

Another way in which heat transfer can be improved is by increasing the thermal conductivity between the PV cells and the absorber plate. In Table 6 a value of 45

W/m^{2}K was used as a "quasi" heat transfer coefficient (h_{PVA}) between the PV cells and the absorber plate, rather than the bond resistance normally used in the Hottel-Whillier-Bliss equations (the experimental derivation of this value was reported and discussed by de Vries (1998) and Zondag et.al. (2002)). Furthermore, de Vries noted that this experimental value was low in comparison to the theoretical value of 450W/m^{2}K.

Based on the reported findings of de Vries (1998), it was assumed that thermal resistance between the PV cells and the absorber could be reduced through the use of thermally conductive adhesives. In Figure 33 it can be seen that by increasing the value of h_{PVA} to 135 W/m^{2}K, that the maximum thermal efficiency is improved by approximately 5%.

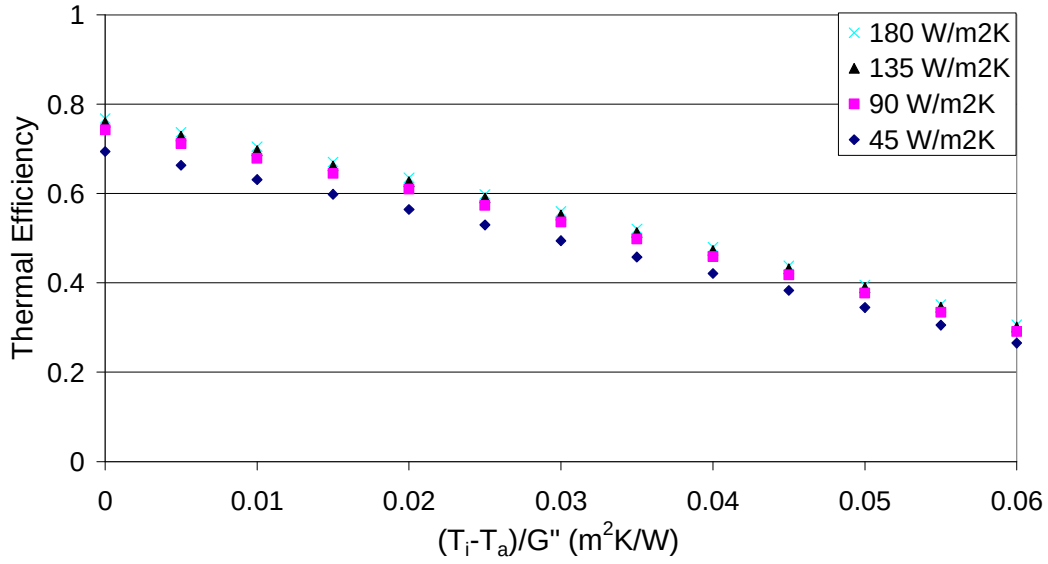

Figure 33: BIPVT thermal efficiency for varying PV to absorber conductivities

Given that high thermal conductivity adhesives are commonly used in attaching electrical components to heatsinks to improve cooling, it was evident that using

these to attach the PV cells in the BIPVT would also improve the electrical efficiency. In Figure 34 it can be seen that by reducing the thermal resistance, there is a marked increase in the electrical efficiency. Therefore, it would be beneficial to ensure that thermal conduction between these bodies is maximised.

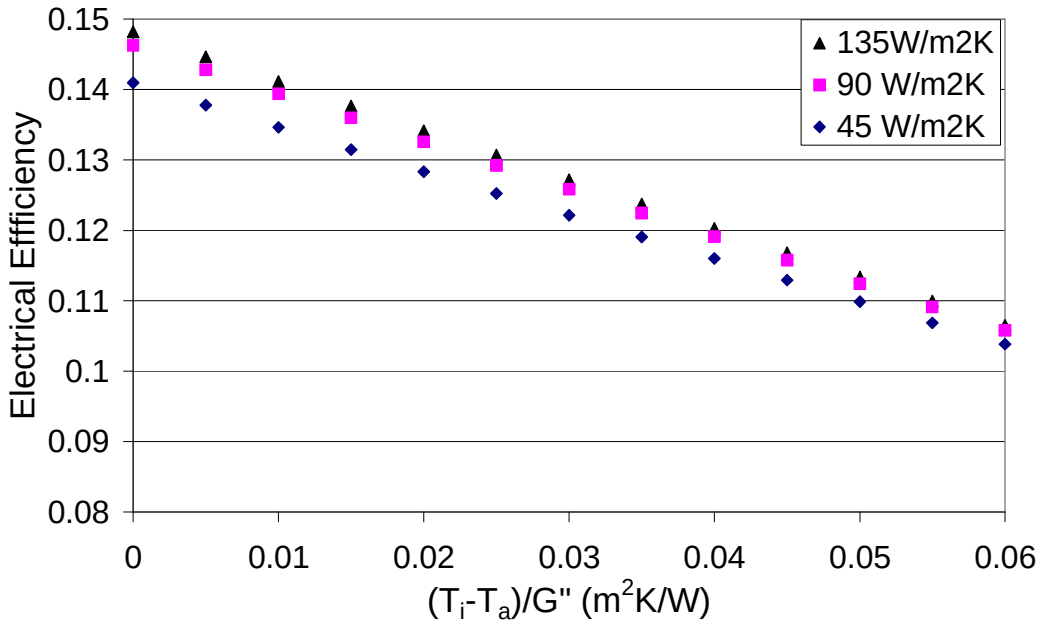

Figure 34: BIPVT electrical efficiency for varying PV to absorber conductivities

In addition to improving the heat transfer between the absorber and the PV cells, it may be possible to improve the optical efficiency of the BIPVT system by reducing the reflectance of the PV cells. In Table 6, a value of 0.80 was specified for the transmittance/absorptance product for the PV cells, based on the experimental measurements performed in Chapter 2. However, de Vries (1998) derived a value of 0.74 from a theoretical optical analysis of a photovoltaic laminate. It was found that this compared well with an experimentally determined value of 0.7 for a PVT collector.

Coventry (2004) found, using a spectrophotometer, that the cells in his concentrating PVT system had a transmittance/absorptance product of 0.82. The difference between Coventry and de Vries' values could be explained by the differing lamination methods, materials, and the method of practical implementation that were analysed by these authors. de Vries analysed a "typical" PV laminate using ethyl/vinyl acetate (EVA) encapsulation, whereas Coventry used silicone encapsulation. In a report from the Swiss Federal Office of Energy (2000), it was found that both encapsulation and cell type had an influence on the absorptance of PV modules, with transmittance/absorptance products between 0.73 and 0.9 being reported.

Moreover, Santbergen and van Zolingen (2006) suggested a number of modifications that could be made to PV cells, such as replacing the back contact with a material with a greater absorptance of long-wave radiation, in order to increase the transmittance/absorptance product for PVT collectors. The effect of varying this parameter is illustrated in Figure 35.

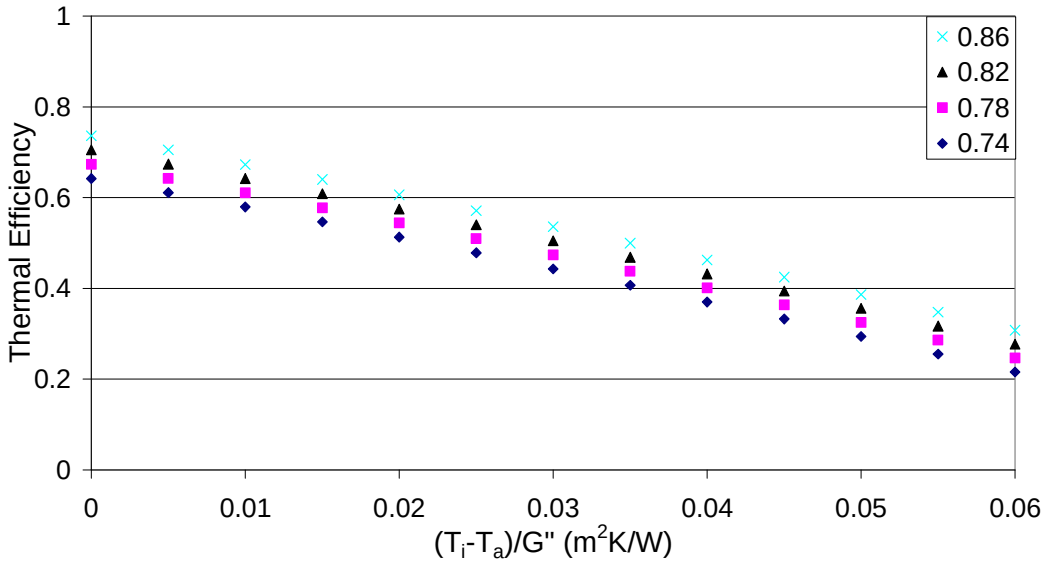

Figure 35: BIPVT thermal efficiency for varying transmittance/absorptance products

From Figure 35 it is clear that by increasing the transmittance/absorptance product, the thermal efficiency can be improved. The reason for this improved performance is related to the spectral absorption characteristics of PV cells. In the spectrophotometry measurements in Chapter 2 it was shown that the PV cells had a high absorption of short wavelength radiation, in the range from 400nm up to approximately 1200nm. The solar spectrum however continues to approximately 2500nm and these long wavelengths tend to be reflected from PV cells, whereas they are absorbed by solar thermal collectors.

The modifications suggested by Santbergen and van Zolingen (2006) were aimed at increasing the absorption of these longer wavelengths, while the use of a silicone encapsulant by Coventry (2004) meant that a greater portion of the longer wavelengths were absorbed by the silicone. One of the drawbacks of increasing

the absorption of longer wavelengths is that it tends to result in the PV cell temperature being increased. However, in Figure 36 it can be seen that the reduction in electrical efficiency is relatively minor.

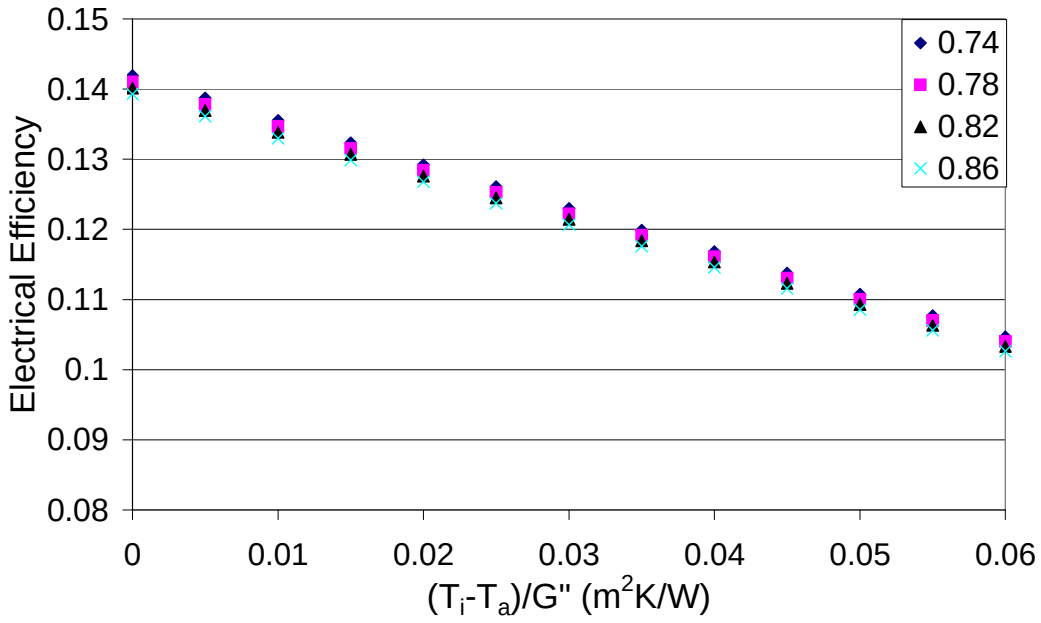

Figure 36: BIPVT electrical efficiency for varying transmittance/absorptance products

As an alternative method for improving the thermal efficiency it is possible to vary the area that is covered by PV cells. In Table 6 a value of 0.87 was specified as the transmittance/absorptance product for the absorber to which the PV cells were mounted. This is based on the assumption of the collector being made of the black colour coated steel used in the experimental analysis. As the absorptance of the black colour steel is higher than the unmodified PV cells with a transmittance/absorptance product of 0.80 it is apparent that by decreasing the area covered by PV cells the thermal efficiency increases. In Figure 37 it can be

seen that increasing the area covered by PV cells reduces the thermal efficiency. Obviously, however, increasing the area covered by PV cells also means that the overall electrical output, per unit area, is increased. Given that there is a significant mismatch between thermal and electrical efficiency consideration would need to be paid to ensuring that a reasonable compromise is made between the thermal and electrical loads that can be met.

The decrease in packing factor could be taken to its natural conclusion by removing the PV cells entirely, thereby forming a building integrated thermal collector (BIT). Although not the central focus of this thesis, such collectors were examined and the modelling and experimental testing of them is discussed in Appendix B.

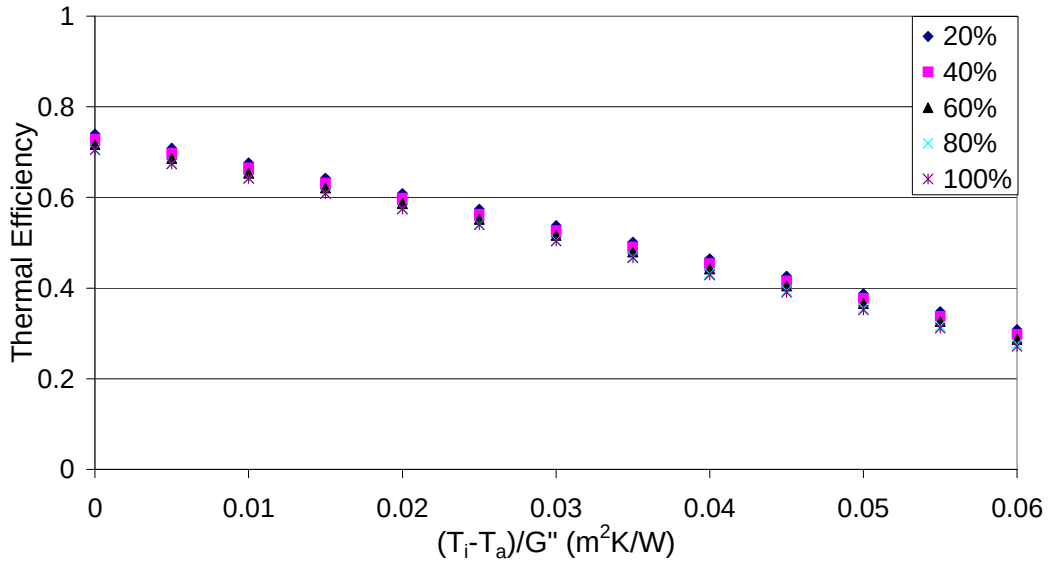

Figure 37: BIPVT thermal efficiency for varying PV area coverage

Decreasing the packing factor also allows the possibility of utilising an alternative colour as the absorber medium, as suggested by the PV Catapult (2005) program. Therefore, using the transmittance-absorptance products for glazed BIPVT collectors derived in Chapter 2, the performance of a BIPVT with 40% PV coverage and varying absorber colours was examined.

From this analysis, it can be seen that the thermal efficiency of the BIPVT is reduced by using a non-black absorber, as shown in Figure 38. This is to be expected, as it was shown experimentally that the reflectance of the alternate colours was greater than that of the black steel sample. However, the use of a coloured absorber with higher reflectance also means that the absorber is at a lower temperature. The by-product of a lower temperature absorber is improved electrical efficiency, which is clearly illustrated in Figure 39 where it can be seen that the Titania collector, with the highest reflectance, also has the highest electrical efficiency. This high reflectance suggested that this colour could be suitable for use in a low cost photovoltaic concentrator.

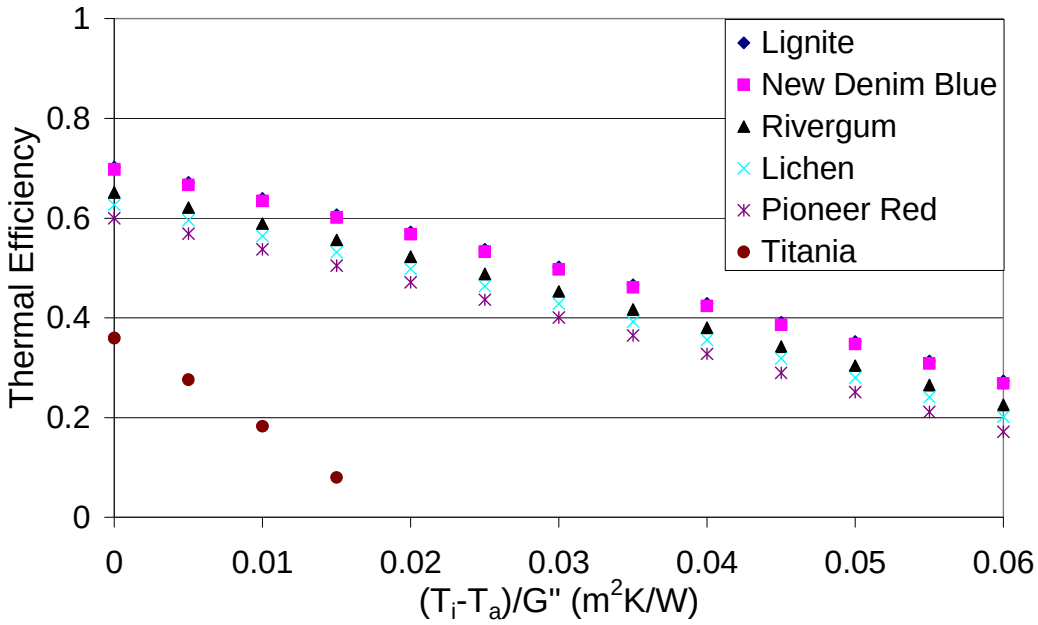

Figure 38: Thermal efficiency of coloured BIPVT collectors with 40% packing factor

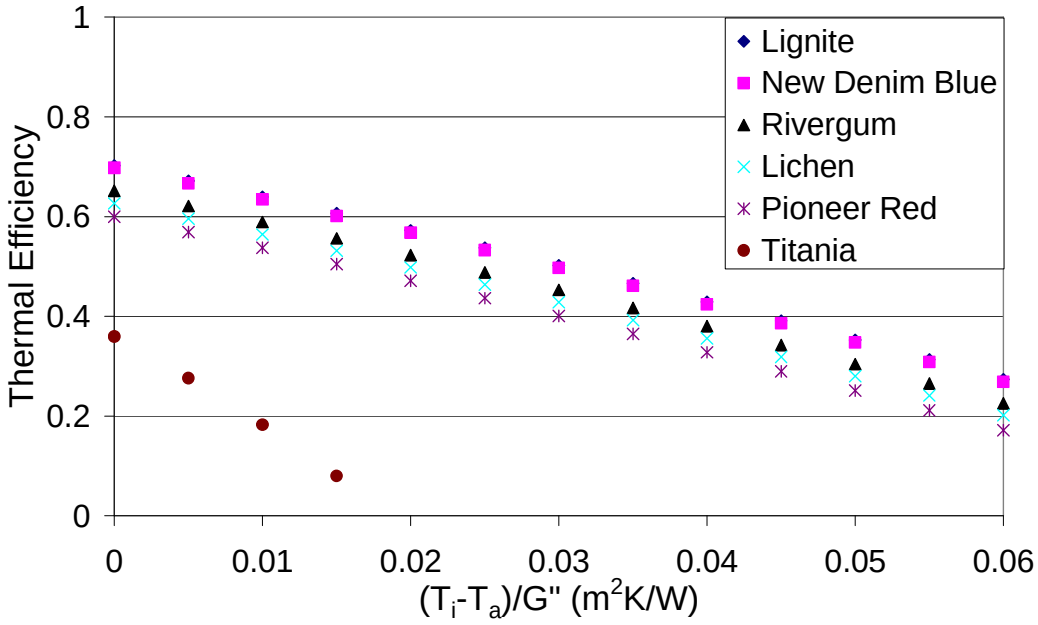

Figure 39: Electrical efficiency of coloured BIPVT collectors with 40% packing factor

It was previously noted that the transmittance/absorptance product of 0.80 could be improved by altering the lamination method and the PV cells. Another simple method is to remove the glazing (cover) from the PVT panel. The presence of glazing means that not all the available radiation is transmitted to the PV cells as some is absorbed or reflected by the glazing. As such removing the glazing should improve the maximum electrical efficiency.

However, it should also be noted that in an unglazed situation the thermal efficiency of the collector is strongly related to the external wind speed. In essence, a glazed collector has a "pocket" of air trapped between the absorber plate and the glazing that reduces the heat loss due to forced convection by the wind. As this layer of air is not present in an unglazed collector the convection heat loss significantly affects the performance of the collector.

The influence of glazing is clearly illustrated in Figure 40 where it can be seen that the maximum thermal efficiency is lower than that of the glazed collector, and reduces significantly at increasing wind speeds. This reduction in efficiency is principally due to the heat loss to the environment by radiation and convection. Conversely however, the increased heat loss means that the electrical efficiency is greater than that observed previously, and increases with increasing wind speed as shown in Figure 41.

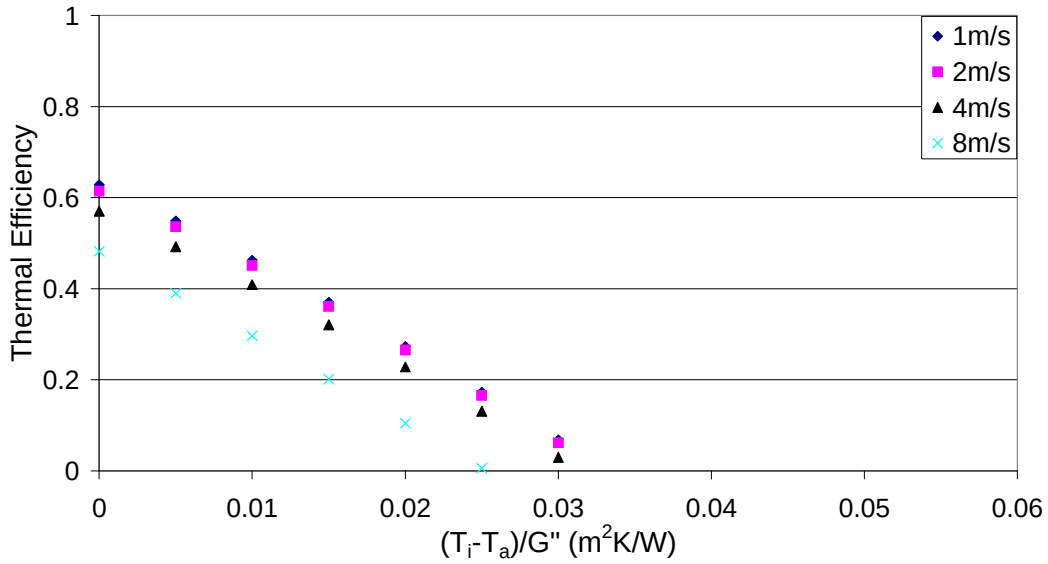

Figure 40: Unglazed BIPVT thermal efficiency

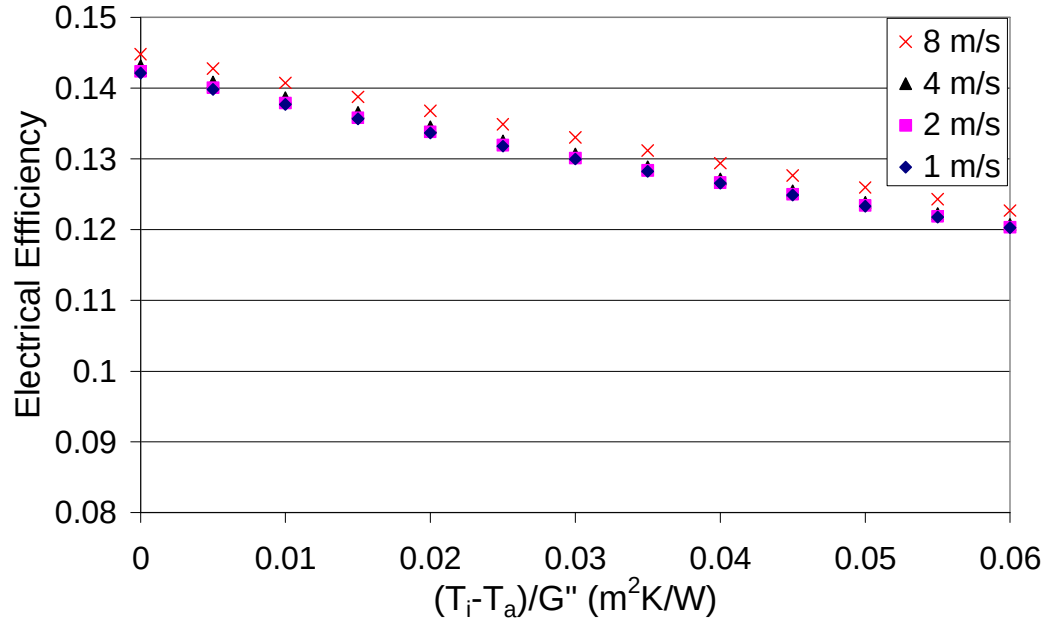

Figure 41: Unglazed BIPVT electrical efficiency

It should be noted that the reduced thermal efficiency due to an increased heat loss coefficient is not necessarily an entirely negative point. If the system were to be coupled with a heat pump system, the lower inlet temperatures, typically below

ambient (Anderson and Morrison, 2007), would mean that the heat loss coefficient of the unglazed BIPVT would be advantageous. This is due to the thermal and electrical efficiencies of the BIPVT collector increasing when the inlet temperature (T_i) is lower than the ambient temperature (T_a).

The analysis that has been presented has treated the BIPVT collector as a typical solar collector, however, it should be noted that it is also a roofing or façade element. In New Zealand it is common for buildings to use insulation at the ceiling level rather than at the rear of the roof and so it was decided to examine the effect of varying the insulation thickness at the rear of the panel. In Figure 42 it can be seen that by treating the BIPVT as a "stand-alone" solar collector, reducing the thickness of insulation reduces the thermal efficiency. However, it can also be seen that the 100mm of insulation specified in Table 1 is equivalent to having 100mm of static air trapped behind the collector.

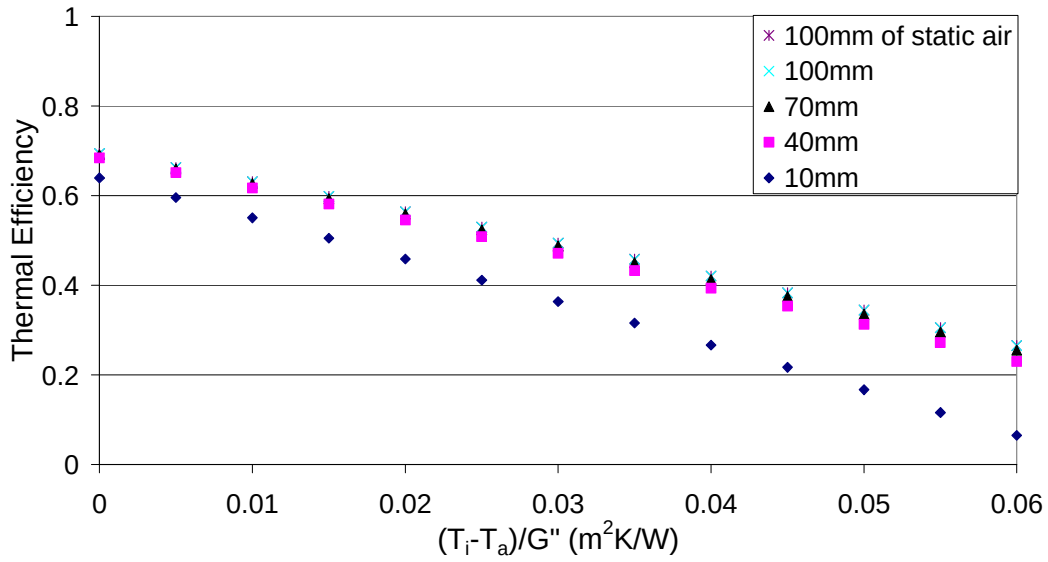

Figure 42: BIPVT thermal efficiency for varying levels of insulation

Given that air could provide the same level of insulation as an insulating material there is scope for reducing the cost of materials in the construction of BIPVT by doing this. At the most basic level it may be possible to rely on the low natural convection heat transfer coefficients in attic spaces or wall cavities to provide a degree of insulation. The possibility of using the attic space behind a roof integrated collector is examined in Chapters 4 and 5.

3.5 Modelling Summary

From the results and validation presented, it was shown that there are a number of parameters that can be varied in the design of a BIPVT collector. The fact that collector material made little difference to the thermal efficiency of the BIPVT suggests that lower cost materials, such as coated mild steel, could be utilised for these systems. The disadvantage of using steel is that the electrical efficiency would be decreased marginally.

To a certain extent this disadvantage can be overcome by maximising the ratio of the cooling tube width to the tube spacing so the fin efficiency approaches unity. This parameter was shown to improve both the thermal and electrical efficiency. Similarly, it was highlighted that good thermal contact between the PV cells and the absorber needs to be made; this could be achieved using thermally conductive adhesives. This would improve both the electrical and thermal efficiencies of the system.

Additionally, any modifications that can be made to improve the absorption of long-wave radiation should be considered. It was shown that increasing the transmittance/absorptance product of the photovoltaic cells and/or the absorber results in a significant increase in thermal efficiency, without greatly reducing the electrical efficiency. It was also noted that the use of unglazed BIPVT systems in conjunction with heat pumps could present interesting possibilities.

Finally, there appears to be significant potential to utilise the low natural convection heat transfer coefficients in the attic at the rear of the BIPVT to act as an insulating layer rather than using traditionally insulation materials. The use of this air layer may allow the material costs in such a system to be significantly reduced and so is explored in the following chapters.

Chapter 4: Numerical Modelling of Convection in an Attic Shaped Enclosure

4.1 Introduction

In Chapters 2 and 3, a concept was presented for integrating photovoltaic/thermal solar water heaters into sheet metal roofing for a building. At the conclusion of Chapter 3 it was suggested that the triangular air space in an attic could serve as the "insulation" for the rear surface of this solar collector thereby reducing the need for insulating materials. The problem of heat transfer due to natural convection in unventilated triangular enclosures is quite common and has application to buildings, solar collectors and greenhouses (Boussaid et al., 2003). However, compared to rectangular, square and cylindrical enclosures, the problem of natural convection heat transfer in triangular or attic-style enclosures has received relatively little attention.

Although not as common as studies on other geometries, work on triangular enclosures has not been entirely ignored. Flack et al (1979) performed one of the earliest studies on a triangular enclosure using an experimental apparatus in which the base of an isosceles triangle was insulated, and treated as adiabatic, while the two inclined walls were isothermally heated and cooled. Flack et al. found that for apex angles between 60 and 120 degrees, and Grashof numbers in the range 2.9 $x10^6$ to 9.0 x 10^6, the results were similar to those of inclined rectangular enclosures and isothermal plates. Flack et al. however noted that the apex region exhibited a complex thermal-fluid interaction not observed in rectangular

enclosures. A further study by Flack and Witt (1979) on the same enclosure showed that the velocity within the enclosure was qualitatively similar to that occurring on an inclined flat plate, and that the flow was in the "boundary layer regime". In a similar study by Karyakin et al. (1985) it was shown, computationally, that the greatest heat transfer occurred in the apex of an isosceles triangular enclosure.

Akinsete and Coleman (1982) performed a study on a base cooled right triangular enclosure in which the inclined wall was heated and the vertical wall was assumed to be adiabatic. They also observed an increase in heat transfer near the apex of the heated and cooled walls. In their study Akinsete and Coleman observed a single convection cell in their simulations, as did Poulikakos and Bejan (1983a). However Poulikakos and Bejan (1983b) found that at a Bénard-type instability existed at higher Rayleigh numbers resulting in the presence of a lateral multi-cellular structure, in their right triangular enclosure. Furthermore, they found that this structure was related to the vertical aspect ratio of the cavity and that at increasing ratios it was not apparent. Similar observations of this multi-cellular structure were observed by Asan and Namli (2000 and 2001) and by Aramayo et al. (2002 a and b) with these authors also noting the relationship to aspect ratio.

Holtzman et al. (2000) however, demonstrated computationally and experimentally that the multi-cellular structure was asymmetric in an isosceles triangular enclosure. They suggested that the use of symmetry boundary conditions would not accurately predict the flow above a critical Grashof number

dependent on the cavity's geometry. This finding was supported by Ridouane et al. (2006) and studied in greater detail by Ridouane and Campo (2007).

Based on the observations made in the previous studies, it was apparent that the apex between the heated and cooled sides of a triangular enclosure or attic was a point of relatively significant heat transfer. Moukalled and Acharya (2001) attempted to prevent this by including a series of offset baffles from the floor and inclined sides in a trapezoidal enclosure. They showed that the use of these baffles resulted in a decrease in heat transfer. Similarly, Ridouane and Campo (2007) showed that by attaching baffles to the inclined walls of an isosceles triangular attic they could also reduce heat transfer. Given these findings, it suggested that the effectiveness of air as an insulator in the BIPVT solar collector, as recommended in Chapter 3, could be improved by the use of baffles in the attic.

4.2 Problem Formulation, Boundary Conditions and Meshing

To determine the influence of natural convection heat transfer in a triangular attic shaped enclosure a model was formulated in Cosmos FloWorks, a commercial CFD solver based on the finite volume method (Cosmos, 2006). In order to reduce computational complexity it was assumed that the trusses normally present in an attic could be ignored, and that a simple triangular enclosure would provide an adequate prediction of the flow behaviour occurring within an attic. Additionally it was assumed that the flow could be treated as steady state, to allow easy comparison with Flack et al.' (1979) steady state experimental results.

As an initial point for investigating the natural convection heat transfer a scale model of an attic was modelled, using the dimensions of Flack et al.' (1979) experimental enclosure. As such a 3-dimensional right triangular enclosure with a vertical aspect ratio of 0.5 and a longitudinal aspect ratio of 3.3 was examined, as shown in Figure 43.

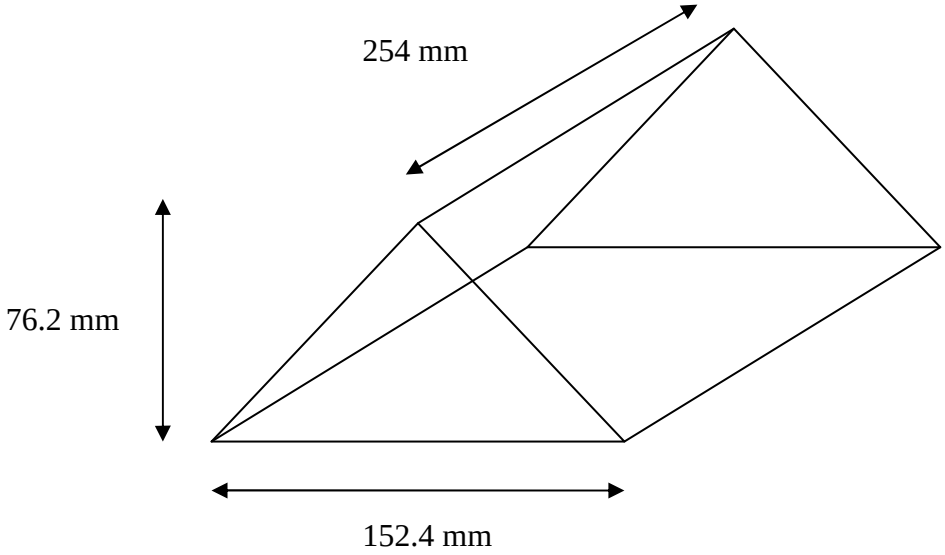

Figure 43: Computational domain

For this study, it was assumed that one of the inclined walls was held at a constant temperature (T_h) while the base and other inclined wall were held at a lower constant temperature (T_c). It was also assumed that the end walls were adiabatic and that heat transfer due to radiation between the surfaces was negligible. This is a simplified representation of what would occur in a dwelling where one of the inclined faces of the roof is oriented for maximum solar gain and where low emmissivity coatings are used to reduce internal radiation heat transfer.

The cold walls (T_c) were assumed to be at 0°C for all cases, while the hot wall temperature was varied to achieve ΔT values in the range of 20 to 80K. These conditions correspond to Grashof Numbers in the range of 10^6 to 10^7 and were similar to those values used in the experimental tests performed by Flack et al. (1979). In addition, a mesh sensitivity analysis was performed to determine the ideal number of mesh elements to provide the shortest solution time of sufficient accuracy. For this analysis, meshes consisting of 60,000, 120,000 and 360,000 cells were examined.

In order to model the influence of baffles in an attic space it was decided to use a different approach to that used by Moukalled and Acharya (2001) and Ridouane and Campo (2007). Where Moukalled and Acharya used multiple vertically oriented baffles attached to the inclined wall and base of their enclosure, and Ridouane and Campo used a single baffle mounted perpendicularly inward from the mid point of the inclined wall, this study examined the use of a single baffle protruding vertically down from the apex of the enclosure, the three configurations are shown in Figure 44.

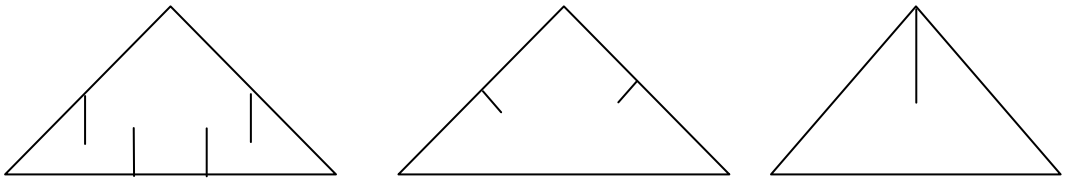

Figure 44: Baffles used by a) Moukalled and Acharya , b) Ridouane and Campo and c) this study

Through the use of a passive baffle system, the intention was to create a "hot side" in the roof enclosure where heated air passing along the inclined heated side could not easily reach the "cold side" of the roof, to be cooled. It was assumed that the baffle could be treated as a thin adiabatic fin that extended downwards between 25 and 75% of the enclosure height. This was done to examine how the proportions of such a baffling system influenced both the heat transfer and the flow within the enclosure.

4.3 Numerical Modelling

Cosmos Floworks is intended to be a general finite volume based CFD tool to aid designers in the development of fluid systems. It uses the Reynolds averaged Navier-Stokes equations in the prediction of turbulent flows (Cosmos, 2006).

In its treatment of turbulence, Floworks employs transport equations for the turbulent kinetic energy and turbulence dissipation rate using the k-ε model. In the turbulence model the standard values for the constants in the transport equations are used, those being C_μ = 0.09, $C_{\varepsilon 1}$ = 1.44, $C_{\varepsilon 2}$ = 1.92, σ_ε = 1.3 and σ_k = 1 (Versteeg and Malalasekera, 1995). These constants are fixed in Floworks and are unable to be changed. Although the standard values of the constants were also utilised by Ridouane et. al (2006) in their study of natural convection in a triangular enclosure, they modified the terms C_μ , $C_{\varepsilon 1}$, and $C_{\varepsilon 2}$ to act as a low Reynolds number turbulence model. They achieved this by multiplying the constants with the wall damping functions. However, Cosmos (2006) showed an

accurate prediction of natural convection in a square enclosure, when compared with de Vahl Davis' (1983) benchmark numerical solution.

It should also be noted that Floworks utilises the same transport equations in solving laminar flows and also allows transitions from laminar to turbulent flow to be modelled. However, for purely laminar flows the turbulent eddy viscosity and turbulent kinetic energy are given a zero value.

In its treatment of turbulence, Floworks uses a laminar/turbulent boundary layer model to describe the near wall flow. This model is based on the Modified Wall Function approach where a Van Driest's profile is utilised in favour of a logarithmic profile. This treatment allows both laminar and turbulent flow in the wall region to be characterised while also allowing transitions between laminar and turbulent flow to be described. Cosmos (2006) suggest that this provides accurate velocity and temperature boundary conditions in the conservation equations.

Because the study was examining natural convection it was critical to account for the buoyancy effects due to the temperature differences that drive the heat transfer. One approach to model changes in density is the Boussinesq approximation whereby density changes are treated as varying linearly over small temperature differences however for gas flows as studied here, Floworks uses the equation of state for ideal gases to determine the density.

Arguably, one of the most important points in any CFD study is the meshing and discretisation scheme. As a finite volume solver, Floworks uses a Cartesian coordinate system to spatially distribute a rectangular computational mesh. The solver utilises a cell-centred approach to obtaining a conservative approximation of the governing equations. By integrating these over the cell control volume it then approximates the cell-centred value of the basic variables.

The second-order upwind approximations for the fluxes are treated using the QUICK scheme and a Total Variation Diminishing (TVD) method (Cosmos, 2006). This is done to reduce over- and under-shooting and produce an oscillation free solution (Versteeg and Malalasekera, 1995). Finally, a SIMPLE-like approach and an operator-splitting (PISO) technique are used in the treatment of time-implicit approximations made in the continuity and convection/diffusion equations. It has been claimed that this resolves problems with pressure-velocity decoupling (Cosmos, 2006).

4.4 Computational Results and Discussion

Before examining the problem of natural convection in the enclosure in great detail it was necessary to perform a mesh sensitivity analysis. In Figure 45, it can be seen that by varying the number of cells in the mesh between 60,000 and 360,000, that there was not a large variation in the solution. It was decided that the use of a mesh with 120,000 cells provided sufficiently accurate results for this study.

While performing the simulations, the opportunity was taken to examine how the predicted heat transfer coefficient for the model compared with those of a real attic. Anderson and Ward (1981) measured the heat transfer coefficient in the tiled "cold roof" attic (with a mean temperature of 10°C) of a terrace house for six weeks and found it to be approximately 3.5W/m^{2}K. As can be seen in Figure 45, the heat transfer coefficient predicted by the CFD solver was within the error range of Anderson and Ward's study. This suggests that the behaviour in the small scale enclosure modelled was similar to that occurring in a large attic space.

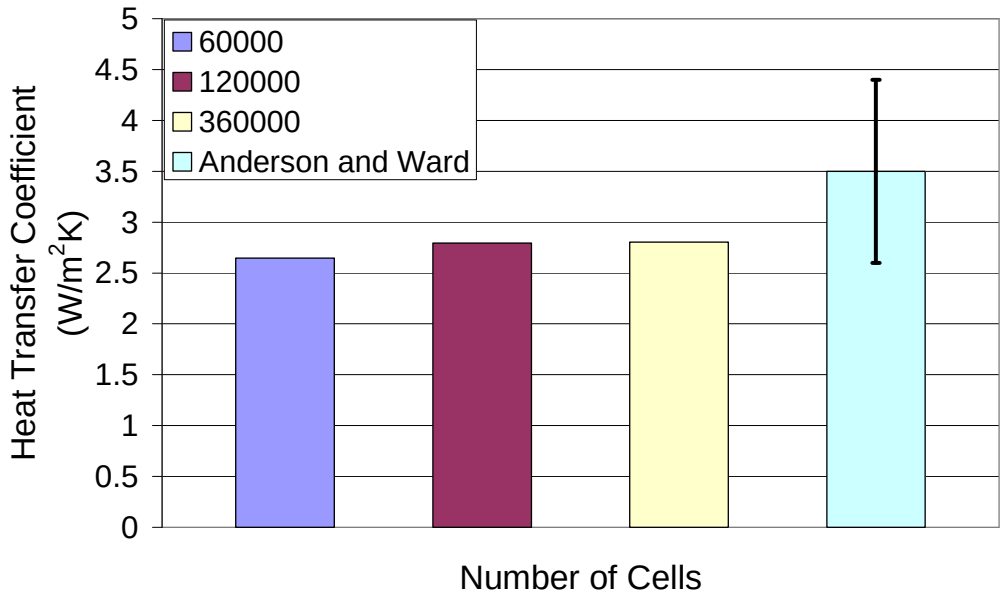

Figure 45: Mesh sensitivity and ability to represent heat transfer in a real attic space

Having reached a mesh independent solution that was of similar magnitude to that from a real attic, the flow in the enclosure was examined. In Figure 46 it can be seen from the temperature contours that a thermal plume appears to form along the heated (left) wall of the enclosure. As the plume moves higher in the cavity it

begins to thicken, however at the apex there is a discontinuity where the heated and cooled wall meet. This discontinuity results in a sharp temperature gradient as was observed in the experimental work of Flack et al. (1979).

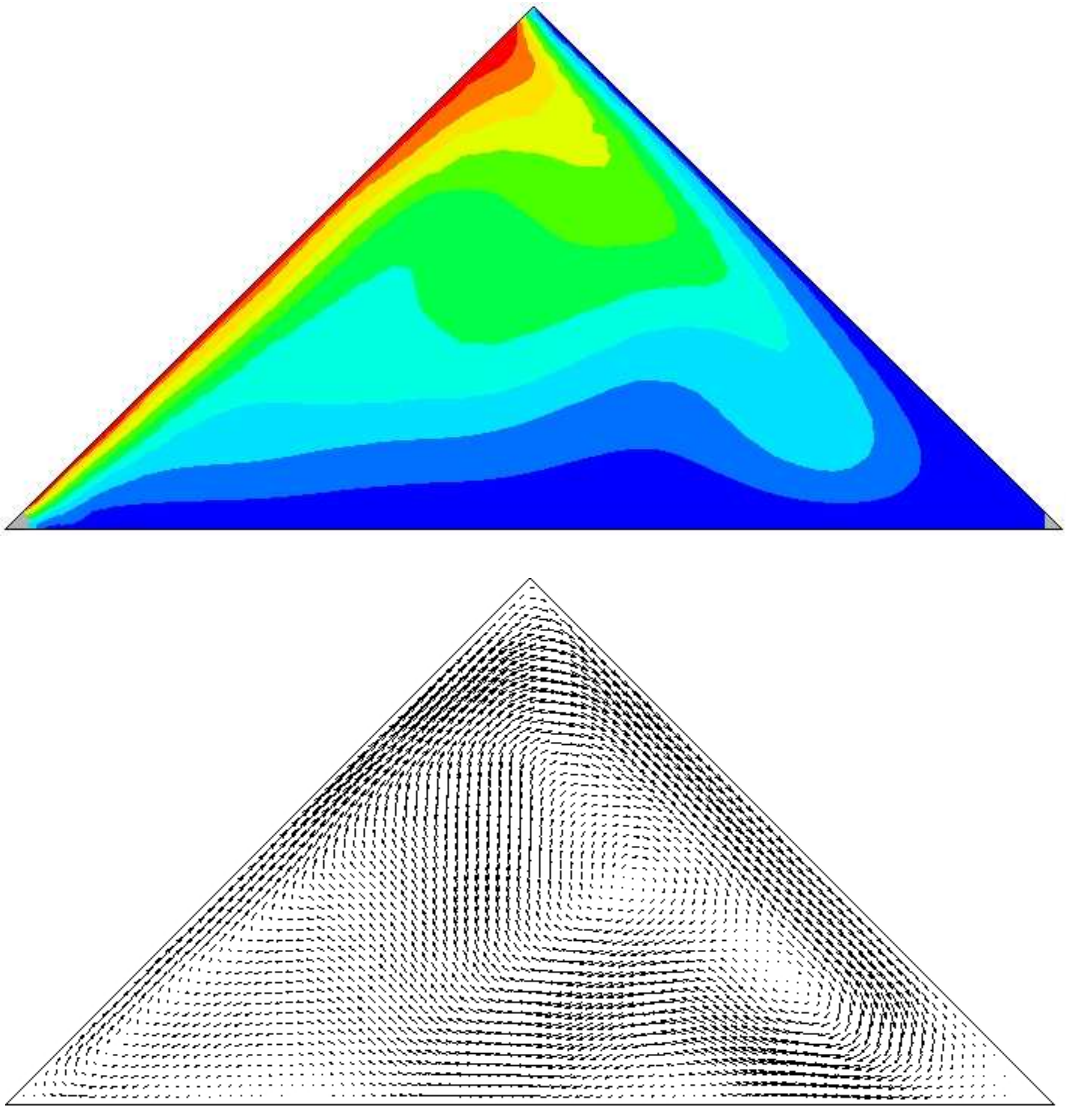

Figure 46: Temperature contours and velocity vectors at lateral centreline of enclosure for a temperature difference of 20K

By increasing the temperature difference from 20K to 40K it can be seen, in Figure 47 that the thermal plume becomes much larger and there is significant separation from the heated wall. With this temperature increase there is also a large scale separation that results in a greater amount of mixing in the flow, which thereby reduces the degree of stratification in the cavity.

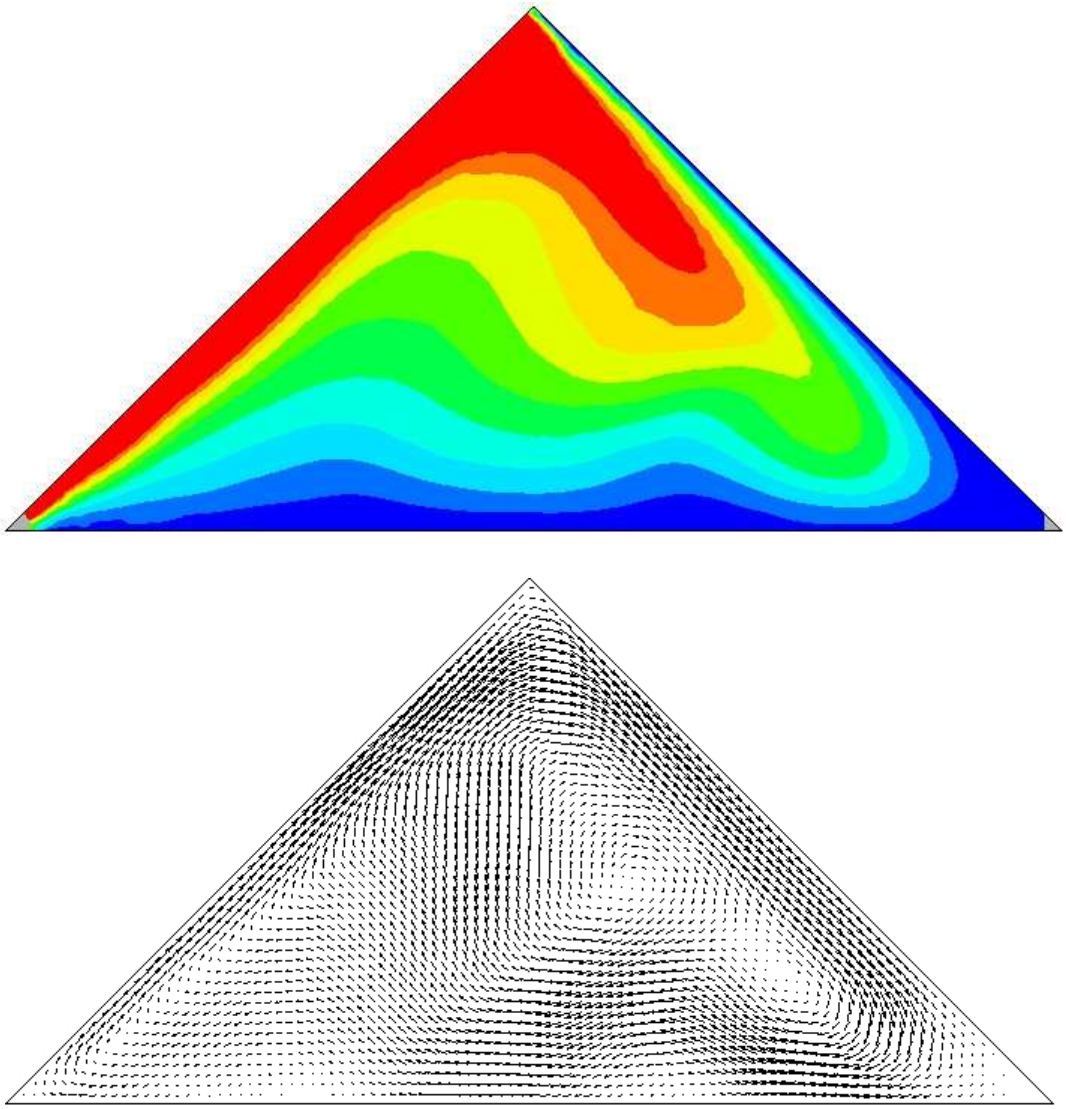

Figure 47: Temperature contours and velocity vectors at lateral centreline of enclosure for a temperature difference of 40K

With an 80K temperature differential the plume becomes the dominant feature of the cavity, as shown in Figure 48. The obvious outcome of such a large and widespread thermal plume is that a greater amount of the heated air passes adjacent to the cold wall. The large amounts of the heated air coming into contact with the cold side of the enclosure cause an increase in the heat loss.

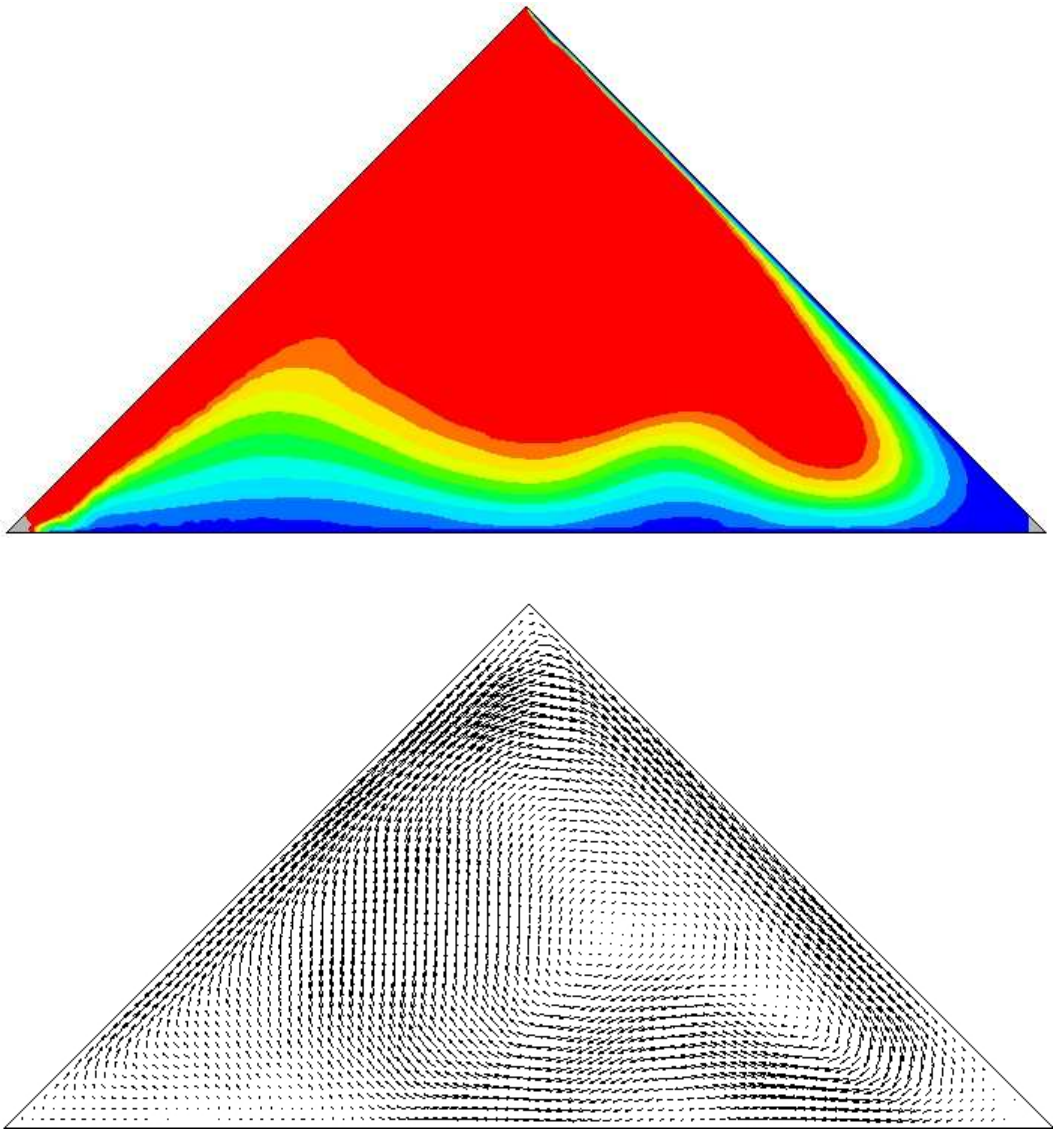

Figure 48: Temperature contours and velocity vectors at lateral centreline of enclosure for a temperature difference of 80K

The increase in the heat loss is characterised by an increase in the value of the Nusselt number in the enclosure. Ridouane and Campo (2005) suggested that for air in a triangular enclosure this could be represented by Equation 30, where *A* is the vertical aspect ratio.

$$Nu = 0.286\,A^{-0.286}Gr^{1/4} \tag{30}$$

This correlation provided a good approximation of the cavity Nusselt number calculated by the simulations. As can be seen in Figure 49, it may be possible to achieve a similar degree of accuracy using a simple power-law fit, given by Equation 31. However, this power-law fit does not consider the influence of the aspect ratio.

$$Nu = 0.0124Gr^{0.4393} \tag{31}$$

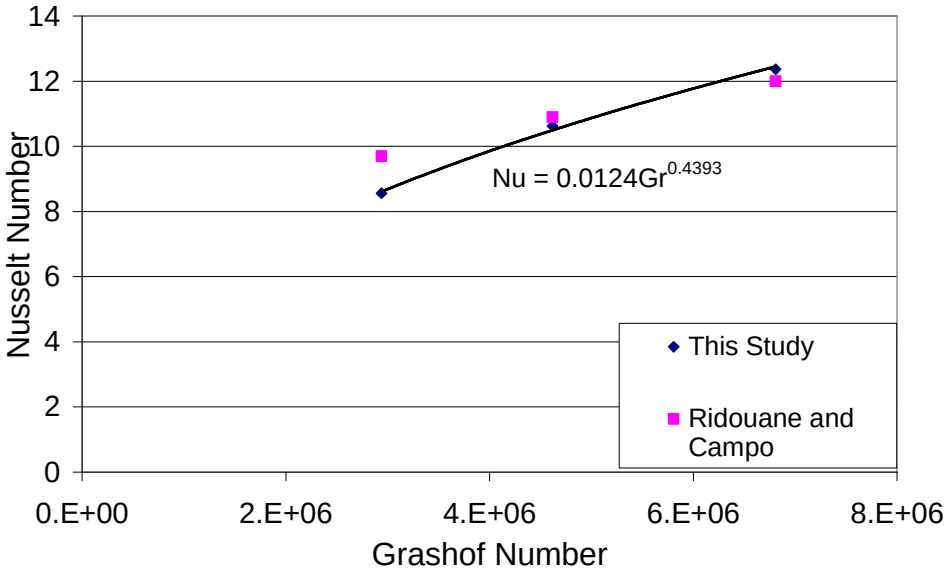

Figure 49: Nusselt number v Grashof number in a triangular enclosure

From observation of the temperature profiles in the triangular enclosure, and the increase in heat transfer at increased Grashof numbers, it was apparent that the use of baffles to direct or divert air could reduce the Nusselt number. In this study three baffle lengths were modelled, 25%, 50% and 75% of the vertical height.

The principal perceived benefit of placing baffles in the enclosure was to limit the progression of the thermal plume towards the cold wall. By achieving this there would be a reduction in the induced natural convection flow and subsequently the rate of heat transfer. In Figure 50 it can be seen that, with a temperature difference of 20K, the shortest of the baffles appears to achieve this to a certain extent. From this it can be seen that the highest temperature portion of plume is trapped against the baffle and lower temperature air is drawn toward the cold wall.

Similarly in Figure 51 and Figure 52 it is shown that the addition of the baffle traps a pocket of hot air against the baffle. When the baffle extends down 50% of the height, there is a much larger portion of air trapped in this region. However Figure 52 most clearly illustrates the benefit of having the baffle in place. In this figure it can be clearly seen that a stratified, high temperature layer develops and is trapped against the hot wall with only a relatively low temperature plume moving towards the cold wall.

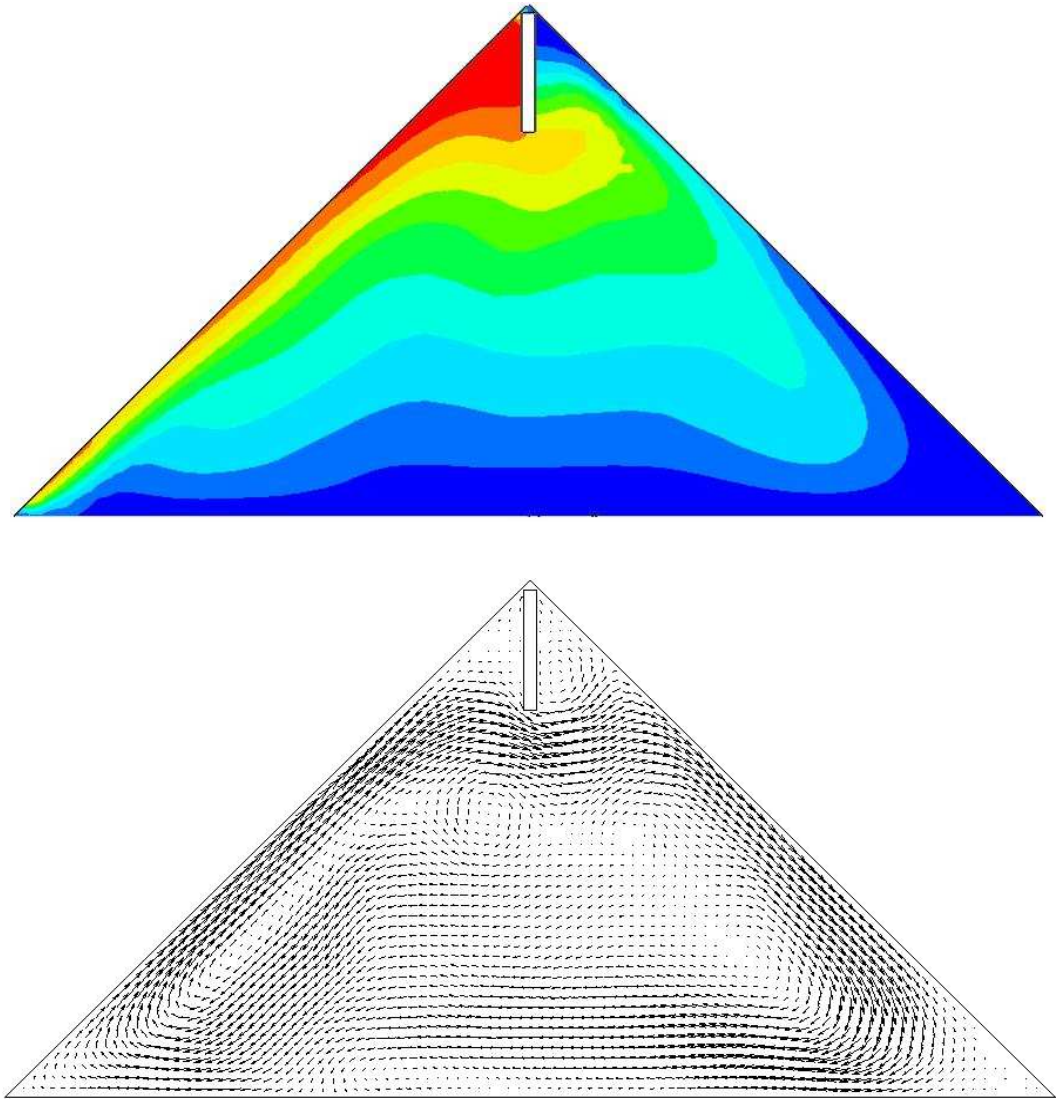

Figure 50: Temperature contours and velocity vectors for a baffle of 25% of enclosure height

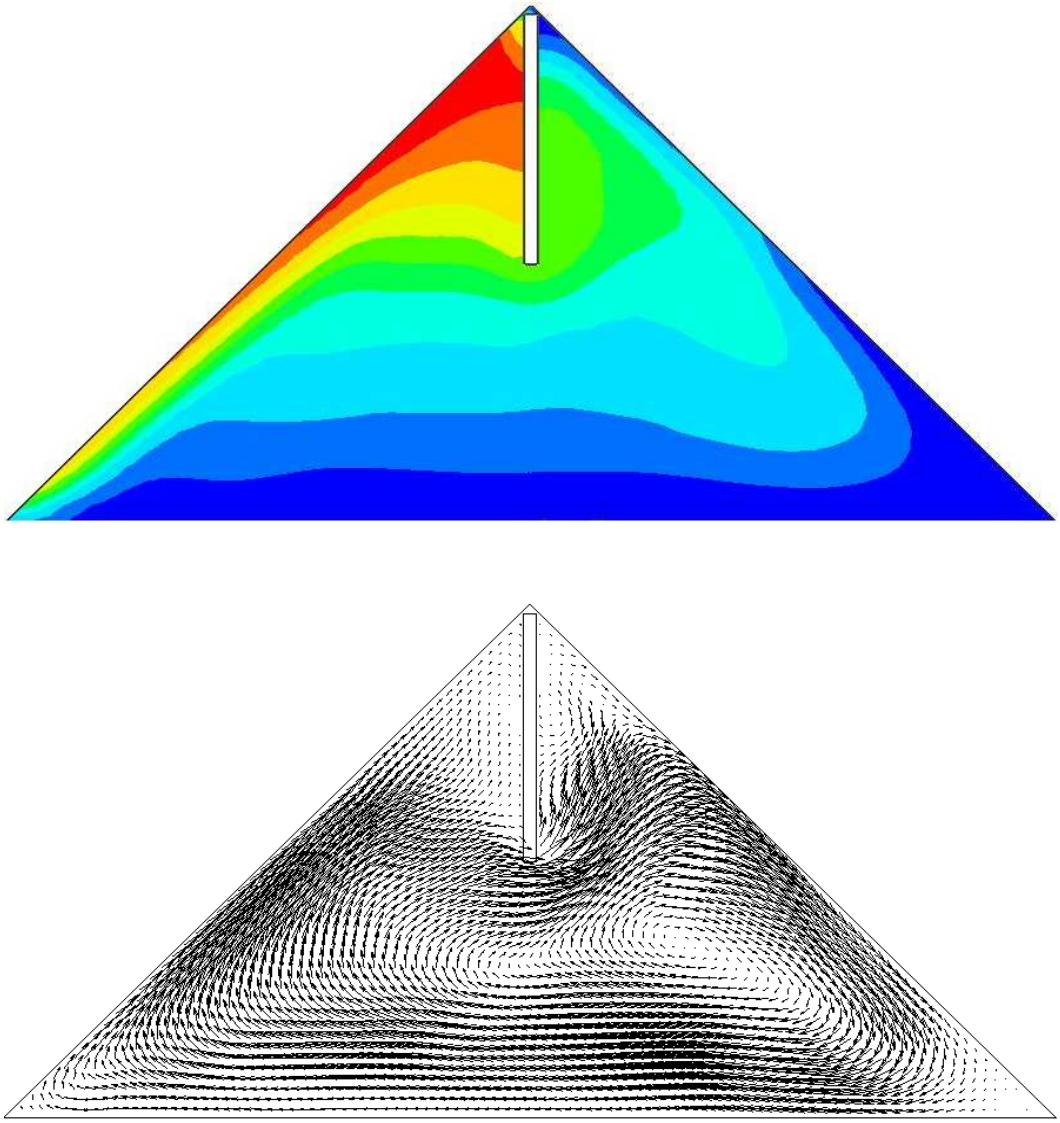

Figure 51: Temperature contours and velocity vectors for a baffle of 50% of enclosure height

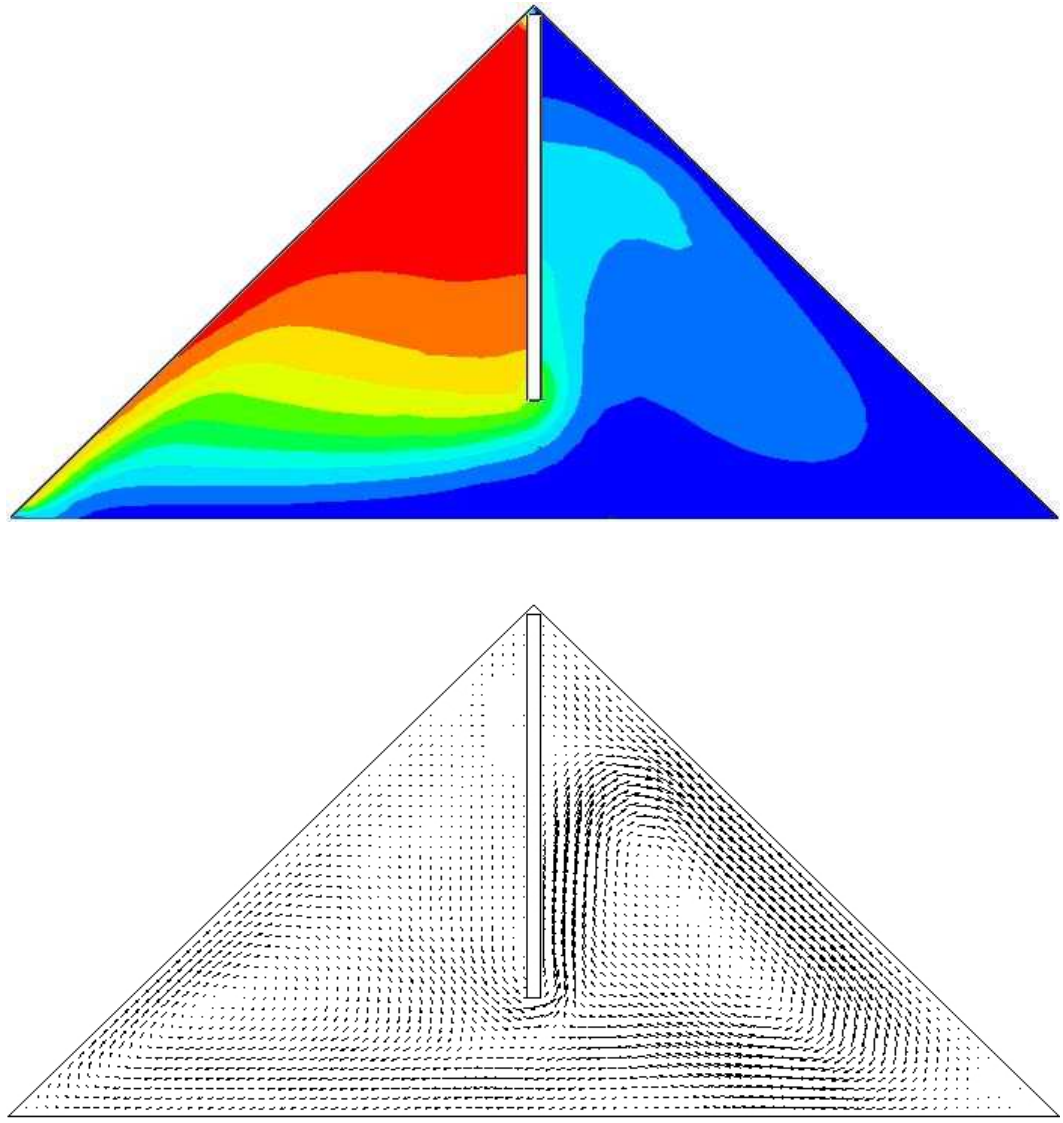

Figure 52: Temperature contours and velocity vectors for a baffle of 75% of enclosure height

By trapping the high temperature plume, and restricting its movement, there is a marked decrease in the movement of heat from the hot to the cold wall. This is due to the buoyant nature of the high temperature air, which tends to resist downward motion. The benefit of the baffle is illustrated quantitatively in Figure 53. Here it can be seen that a greater than 50% reduction in the heat transfer

coefficient could potentially be achieved by using a simple vertically mounted baffle arrangement. As such, the use of baffling could present a simple and effective alternative to insulation on building integrated solar collectors.

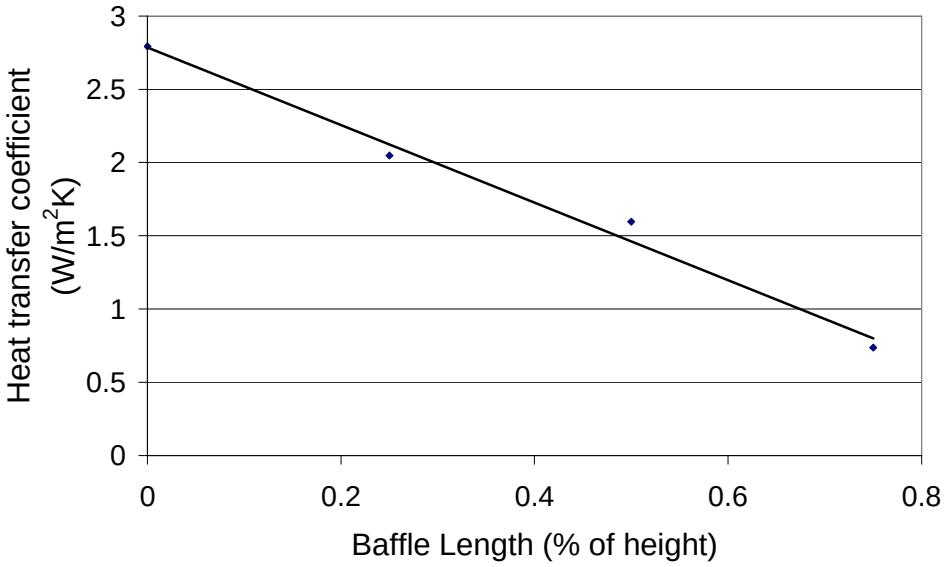

Figure 53: Heat transfer coefficient v baffle length

While analysing the flow in the enclosure, it was observed that the temperature distribution along the centreline longitudinal axis was highly non-uniform, as shown in Figure 54. In this figure it can be seen that a series of convection cells are present along this longitudinal axis. Although one could suggest that the presence of these cells is not entirely unexpected (Flack, 1980 observed them for base heated flow in a triangular enclosure) they have not been discussed in the literature. This is principally due to the fact that almost all the studies have treated enclosures as two-dimensional spaces.

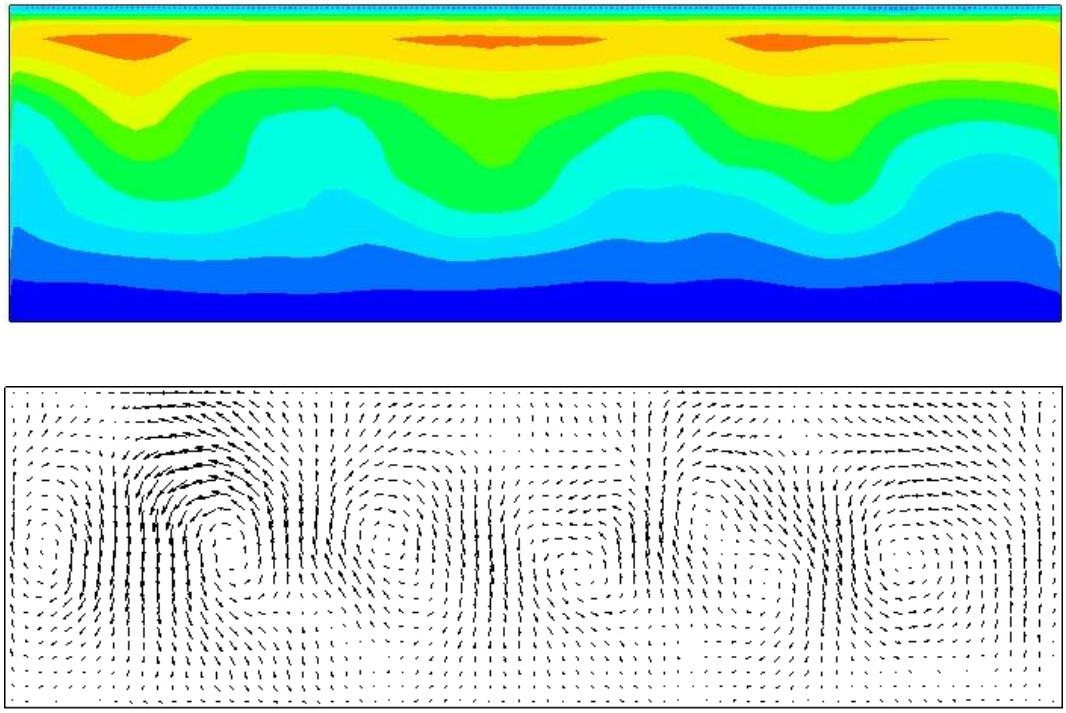

Figure 54: Convection cells along the longitudinal axis of the enclosure

Given the lack of discussion on the presence of these cells it was decided to examine whether the behaviour of these cells was influenced by the presence of baffles. This was achieved by placing a single laterally positioned baffle at the mid-length of the enclosure extending downwards for 50% of the height, as shown in Figure 55. The presence of this baffle was found to increase the heat loss from the enclosure, giving a higher heat transfer coefficient as illustrated in Figure 56.

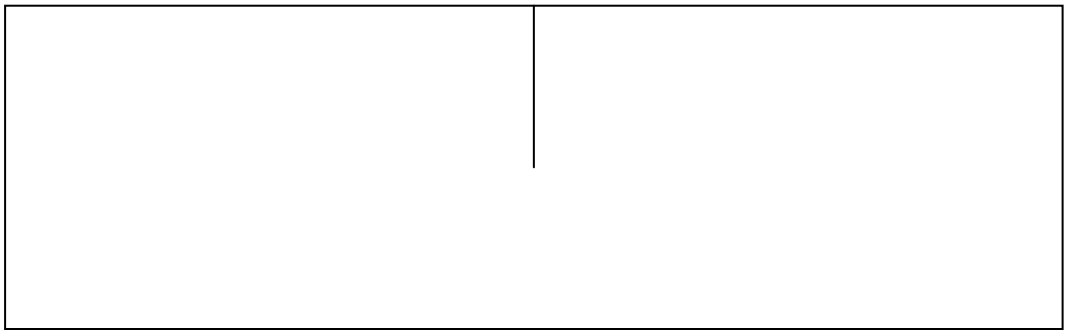

Figure 55: Laterally mounted baffle in triangular enclosure

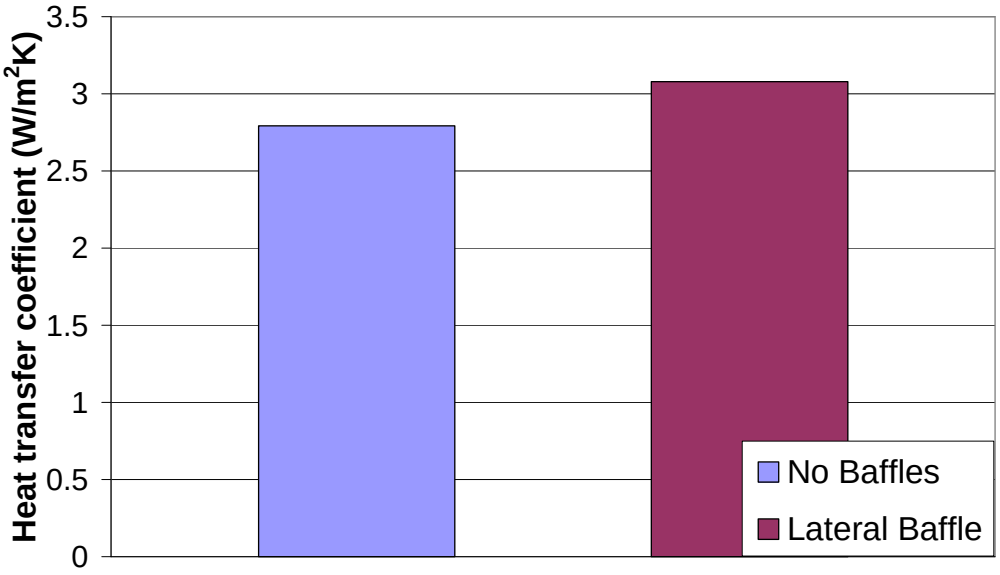

Figure 56: Effect of lateral baffle on heat transfer

Though the reasons for this increased heat transfer are not immediately apparent, it was observed that the centre cell in Figure 54 was split by the baffle, as shown in Figure 57. The splitting of this cell gave rise to a larger number of smaller cells, and, it is probable that the larger number of cells resulted in the increase in heat transfer as a result of increased "end effects", where any longitudinal flow meets an impermeable wall. This would suggest that by adding the baffle the enclosure is forced to act as two separate enclosures with very weak flow and thermal coupling. It is suggested that the influence of the cavity's longitudinal aspect ratio

is an area that requires further investigation; however it is beyond the scope of this work.

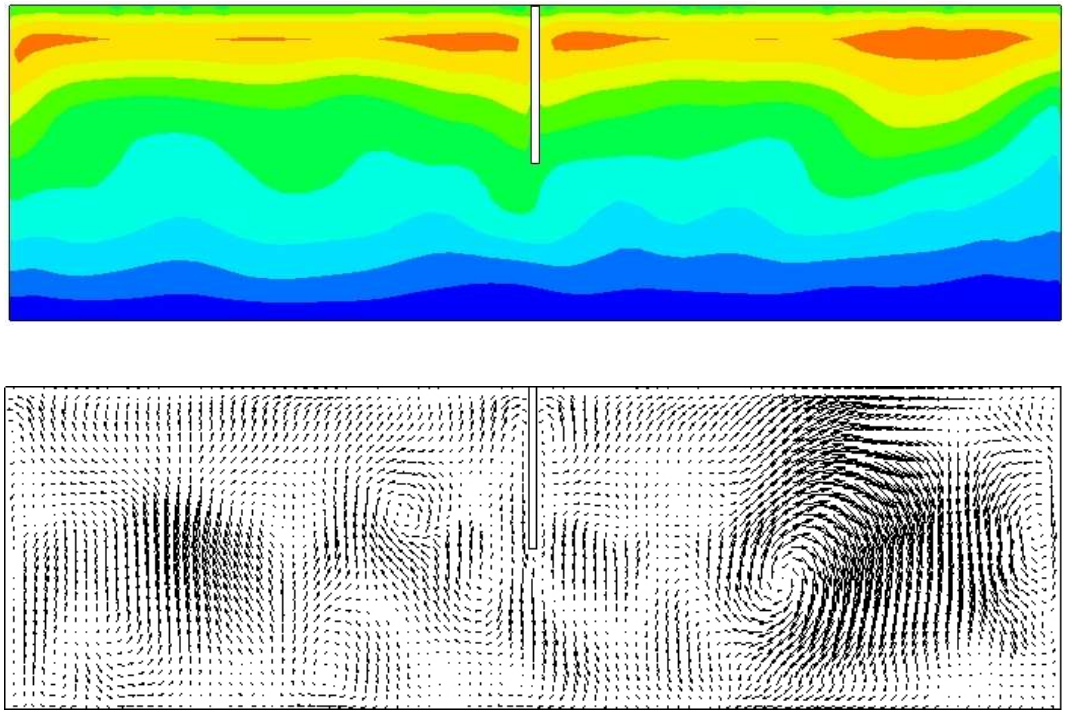

Figure 57: Convection cells in laterally baffled enclosure

4.5 Conclusions from Numerical Modelling

The use of air as an insulating medium for building integrated solar collectors presents an interesting possibility. To date, many of the studies examining these types of collectors have treated them in the same manner as standalone collectors, with little or no coupling between them and the building. However, this study has shown that the heat transfer coefficient in an attic style enclosure is relatively low. By taking advantage of this there is the opportunity to remove the need to insulate the rear surface of building integrated solar collectors in “cold roof” buildings.

Where previous studies have examined the use of multiple baffles in triangular and attic style enclosures to reduce natural convection, this study demonstrated that the use of a single longitudinal baffle mounted downwards from the apex of the enclosure could be an effective solution in suppressing convective heat losses. It was shown that the natural convection heat transfer coefficient could theoretically be reduced simply by increasing the proportions of the baffle relative to the enclosure, possibly resulting in a thermal resistance similar to that provided by 50mm of mineral wool insulation. In essence this created a hot and cold side in the enclosure, and in doing so effectively reduced the heat loss.

It was also observed that convection cells were present along the length of the cavity. By adding a lateral baffle, it was found that the heat transfer coefficient was actually increased. This, it was suggested, may be the result of increased end effects and the disturbance of the cells. The presence of these cells has not been discussed in the literature and so represents an area of study requiring further work. It is possible that these cells are related to the cavity's longitudinal aspect ratio and therefore, it is suggested that this is an area that should be examined in the future. Finally, there is the possibility that by using both the single longitudinal baffle and a series of laterally mounted baffles that the heat transfer could be further reduced. However this is an area that requires further investigation.

Chapter 5: Experimental Analysis of Convection in an Attic Shaped Enclosure

5.1 Introduction

In Chapter 4 it was noted that there have been a large number of computational studies that have examined natural convection in triangular enclosures. However, there is a distinct lack of generalised correlations to predict the heat transfer in these spaces (Cengel 1998, Holman 1997, Incropera and DeWitt 2002). Al-Shariah and Ecevit (1992) were perhaps the first to present a truly generalised equation for heat transfer in a triangular enclosure. In their study they examined a right triangular enclosure with one heated and one cooled side and found that the heat transfer could be expressed as a function of the Rayleigh number, the enclosure aspect ratio and the inclination of the cavity to the horizontal.

However for isosceles triangular enclosures, perhaps the most notable experimental work is that of Flack et al. (1979) and Flack (1980). In these studies one side of an air filled isosceles triangular enclosure was heated, while the other was cooled and the base was treated as being adiabatic. They performed a number of experiments for varying aspect ratios and also Grashof Numbers in the range 2.9×10^6 to 9×10^6. Using their data they subsequently developed a series of correlations for predicting heat transfer in such enclosures.

Recently however, Ridouane and Campo (2005) re-examined the data from Flack's work and presented the results as a single generalised correlation expressed in terms of the enclosure Grashof number and aspect ratio. The greatest shortcoming of this correlation however, is that it was based on data from a relatively narrow range of Grashof numbers. For large attic spaces in a tropical or warm climate such as those of Australia or New Zealand, the Grashof numbers could exceed those covered by the correlation of Ridouane and Campo (2005) by several orders of magnitude, with values of up to and possibly exceeding 10^{10}. For example, consider a "typical" pitched roof with a height (i.e. the characteristic length) at the ridgeline of 1.7m experiencing a temperature difference between the hot and cold sides of 10K and a mean temperature inside the attic space of 298K. Under these conditions the Grashof number is approximately 7×10^9, which is far in excess of the existing correlations range.

In light of the lack of experimental data relating to higher Rayleigh and Grashof number flows, it was decided to experimentally examine the issue of natural convection of air in an isosceles triangular enclosure and develop a correlation that is valid over a wider range of Grashof number conditions.

5.2 Experimental Method

To determine the heat transfer by natural convection it was necessary to build an appropriate experimental apparatus. For this study, the aim was to develop a generalised correlation suitable for use under higher Grashof number conditions that could be experienced in an attic. As such the scale of the enclosure was

increased from 152.4mm x 76.2mm x 254mm in the Flack's previous studies (and the CFD study in Chapter 4) to an enclosure 707.1mm x 353.6mm x 1500mm, Figure 58, as a means of changing the characteristic length and therefore the Grashof number.

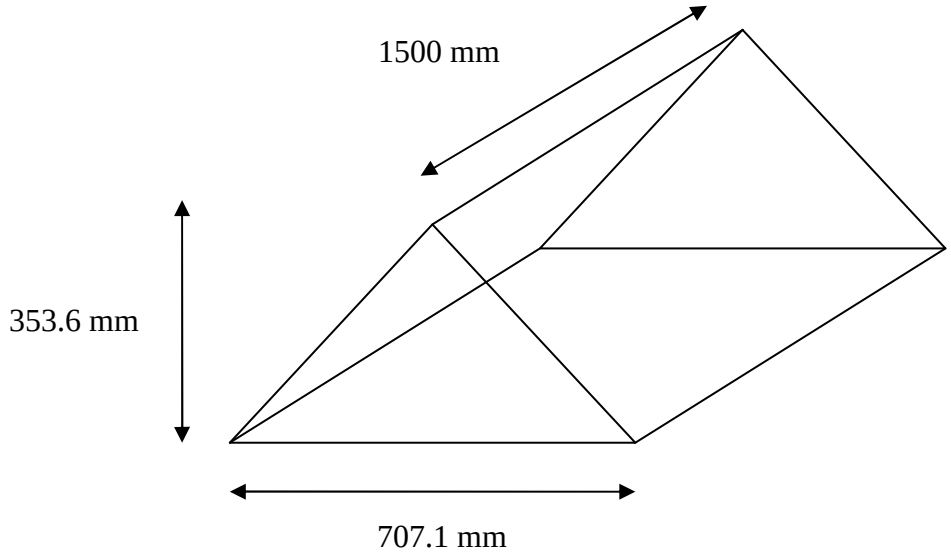

Figure 58: Dimensions of experimental enclosure

In order to create a temperature gradient within the enclosure, a flexible aluminium foil resistance heater (750W nominal) was attached to a 2mm aluminium plate and used as one of the inclined sides of the enclosure. The aluminium plate, having a high thermal conductivity, was used to minimise temperature variation on the heated surface inside the enclosure. To minimise heat loss from the rear surface of the heater, it was insulated with approximately 100mm of mineral wool fibre insulation with a nominal R-value of 2.2 and a sheet of 20mm plywood.

Similarly, the base of the enclosure was made from 100mm of the mineral wool fibre insulation between two layers of 20mm plywood. The ends were fabricated from a single layer of 20mm plywood. The second inclined surface was constructed from 2mm aluminium plate to ensure that there would be minimal thermal resistance across this surface. Additionally, the inclined aluminium plate was cooled by forced convection by a fan providing a free stream velocity of approximately 4m/s. This step was taken to ensure that the surface would be the main source of heat loss in the enclosure. Finally, all edges of the enclosure were sealed with high temperature duct tape to ensure that no air leakage from the enclosure could occur. The layout of the physical enclosure is illustrated in Figure 59.

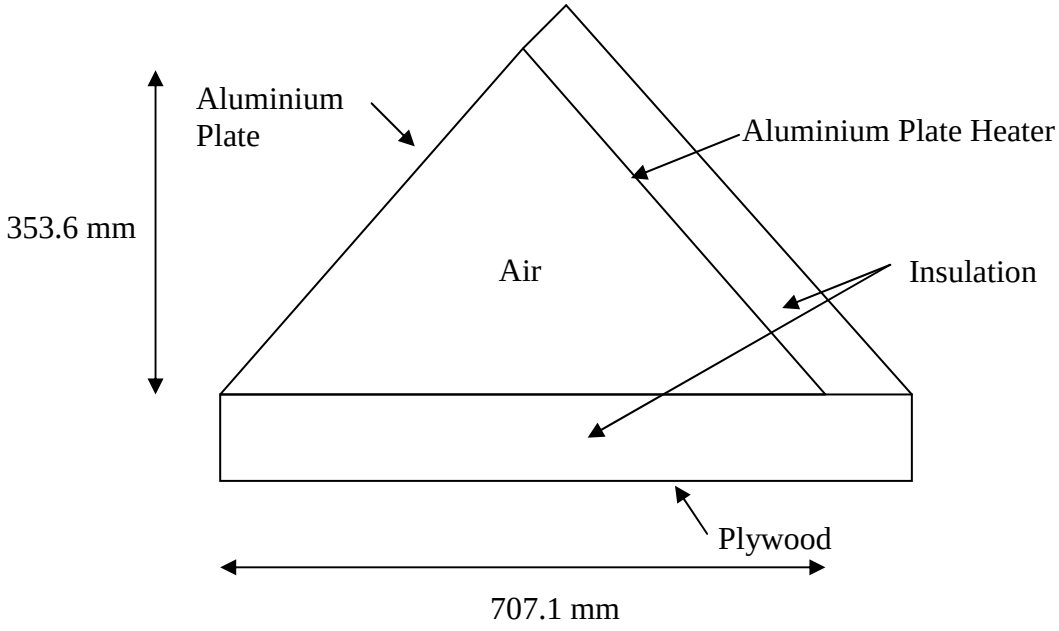

Figure 59: Layout of experimental enclosure

In order to vary the Grashof number conditions, it was necessary to vary the temperature difference across the enclosure. To achieve this, the power supplied

to the electrical resistance heater was varied using a variable power transformer (Variac) and measured using a single phase EMU Elektronik power meter.

To determine the temperature gradient occurring with the enclosure the mean temperature of the heater was measured using a series of six copper-constantan (T-type) thermocouples that were uniformly distributed over and attached to the heater surface (an examination of the temperature data found that the temperature variation was less than 5% across the surface of aluminium plate), while a seventh thermocouple was used to measure the ambient temperature. Before undertaking the measurements these thermocouples were calibrated against a platinum resistance thermometer and were found to be accurate to with ±0.3K across the temperature measurement range. The thermocouples were connected to a Picolog TC-08 eight channel thermocouple DAQ system and recorded by a computer via the USB interface. The configuration of the power and temperature measurement system and instrumentation is illustrated schematically in Figure 60.

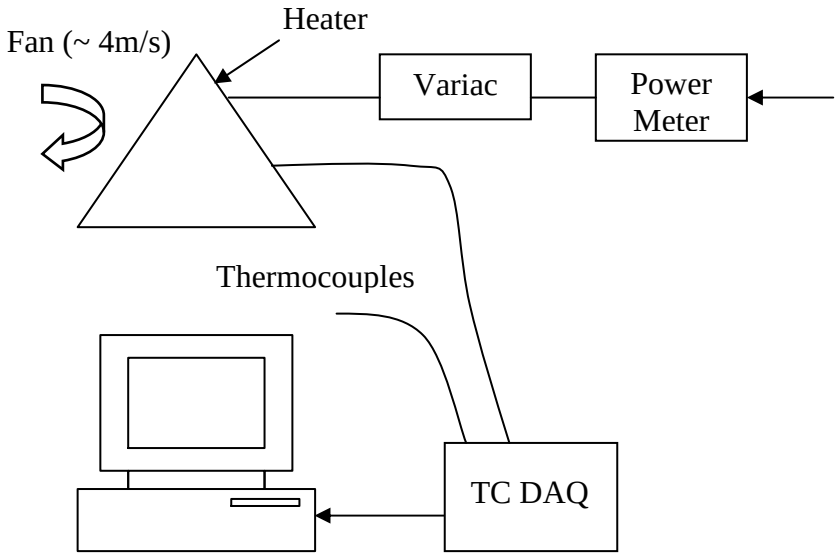

Figure 60: Schematic of measurement system

To accurately determine the heat transfer coefficient within the enclosure it was necessary to allow the system to reach steady state conditions. To do this, the heater power was set and the ambient and heater temperature were monitored. When the variation of the temperature difference between the heater and the ambient was not more than 0.6K over a 30 minute period, it was assumed that the system had reached a steady state, as shown in Figure 61. Subsequently, the readings taken during this period were used to determine the natural convection heat transfer coefficient, the uncertainty of which is described in Appendix A.

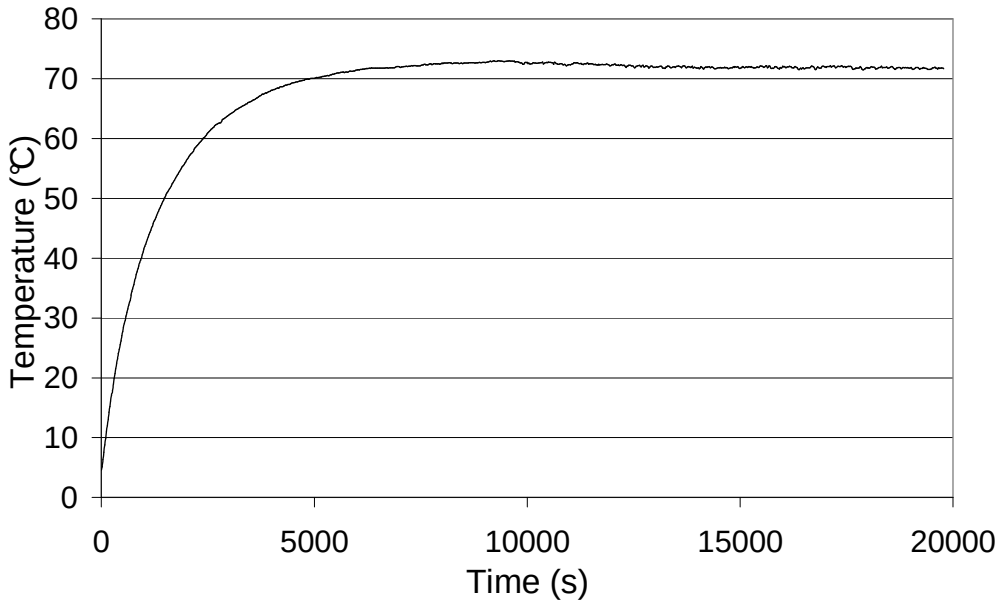

Figure 61: Temperature v time showing steady state

5.3 Analysis

From the experimental measurements it is relatively straight-forward to determine the overall heat loss coefficient for the experimental rig. Under steady state conditions the rig heat loss coefficient (U) is represented by a function of the input electrical power (Q_e), the difference between the heaters mean temperature (T_p)

and the ambient temperature (T_a), and the heater area (A_h), as shown in Equation 32.

$$U = \frac{Q_e}{A_h\left(T_p - T_a\right)} \tag{32}$$

However, although this provides a crude estimate of the heat transfer coefficient inside the enclosure it was necessary to undertake a full heat balance to identify the heat that was being transferred by convection. For this study the heat balance could be given by Equation 33: where Q_e was the electrical input power, $Q_{end,cond}$ was the heat loss though the ends of the enclosure by conduction based on the mean enclosure temp (T_e, taken as the average of T_p and T_a), $Q_{back,cond}$ was the heat loss from the heater by conduction through the insulation on its rear surface, $Q_{base,cond}$ was the heat loss through the base by conduction based on the mean enclosure temp and Q_{rad} was the radiation heat loss.

$$Q_e - Q_{end,cond} - Q_{back,cond} - Q_{base,cond} - Q_{rad} = Q_{convection} \tag{33}$$

The remaining term, $Q_{convection}$ was the heat transferred from the heated to cooled inclined wall by convection. This term incorporates the thermal resistance due to natural convection, the inclined aluminium plate wall and the external forced convection as shown in Figure 62, the thermal resistance network. However, the thermal resistance through the aluminium wall and the resistance due to external forced convection are small relative to the natural convection and as such these

terms were neglected (testing showed that these terms contributed less than 3% of the total heat transfer).

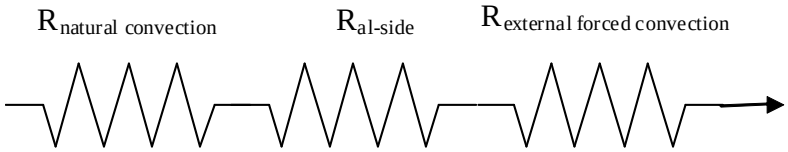

Figure 62: Thermal resistance network for natural convection heat transfer coefficient

The calculation of heat loss by conduction (Q_{cond}) through the walls (i.e. $Q_{end,cond}$, $Q_{back,cond}$ and $Q_{base,cond}$) was given by Fouriers law (Equation 34) over the area (A) of the wall of interest, where k is the thermal conductivity of the wall and L is the thickness of the wall or alternatively R (m^2K/W) is the thermal resistance of the wall.

$$Q_{cond} = \frac{kA(T_e - T_a)}{L} = \frac{A(T_e - T_a)}{R} \tag{34}$$

Calculation of the radiation heat transfer in an enclosure of this nature is somewhat more complicated. However it was recognised that for this case, heat transfer by radiation between the heated and cooled sides would be relatively small, given that both inclined sides were made from aluminium plate ($\varepsilon_p \approx 0.06$). Furthermore, the base of the enclosure was essentially adiabatic and therefore could be discounted from any radiation calculations. Finally the view factor from the heated surface to the end walls for a cavity of this size are relatively small (less than 0.3) (Siegel and Howell, 2002), as was their area ($0.125m^2$), thereby reducing the potential radiation heat transfer.

To verify that radiation could be neglected, it was assumed that radiation heat transfer would only occur between the wooden ends (where there was the least insulation), and the aluminium heater. Therefore it was assumed that the radiation heat transfer could be treated as being analogous to having two parallel plates, essentially a "worst case" scenario. With these assumptions the equation for the radiation heat transfer could be simplified to Equation 35 for a two surface enclosure where the two surfaces are: the heater of area (A_h) made of aluminium with emissivity ε_p, and the other made of wood with emissivity ε_w and an area (A_w) equal to the sum of the areas of the ends and base of the enclosure and where the view factor (F) between the plates is equal to unity (Cengel 1998).

$$Q_{rad} = \frac{\sigma\left(T_p^4 - T_e^4\right)}{\frac{1-\varepsilon_p}{A_h\varepsilon_p} + \frac{1-\varepsilon_w}{A_w\varepsilon_w} + \frac{1}{A_p F}} \tag{35}$$

From the analysis of Q_{rad} it was found that, based on the assumptions listed above, that radiation heat transfer accounted for less than 5% of the heat being transferred, and so was assumed to be negligible. Similar calculations showed that using this conservative approximation of the radiation between the hot and cold side accounted for less than 1% of the heat transfer. It should also be noted that the radiation and external convection term, discussed earlier, act in opposite directions and are of similar magnitude essentially cancelling each other.

Hence, based on the energy balance, and the outlined assumptions, it was then reasonable to determine the heat transfer by convection between the heated and cooled surfaces from Equation 36.

$$h_c = \frac{Q_{convection}}{A_h(T_p - T_a)} \tag{36}$$

5.4 Results

Having established an appropriate experimental methodology and means of analysing the natural convection heat transfer in the enclosure a number of experiments were undertaken to determine the heat transfer coefficient.

As mentioned previously, the power to the heater was varied in order to change the temperature gradient. In this study the power was varied such that the mean heater temperatures were between 30°C and 120°C under steady state conditions. By recording this period of steady state data it was then possible to determine the heat transfer coefficient. For this study, the range of plate temperatures equated to Grashof numbers in the range of 10^7 to 10^9, where the characteristic length was taken to be the vertical height of the enclosure and the physical properties were taken at the mean enclosure temperature.

In Figure 63, it can be seen that with an increasing temperature gradient in the enclosure there is an increase in the natural convection heat transfer coefficient. This is characteristic of natural convection flows, as with higher temperature

gradients there are significant buoyancy forces resulting in a higher degree of turbulence and therefore heat transfer.

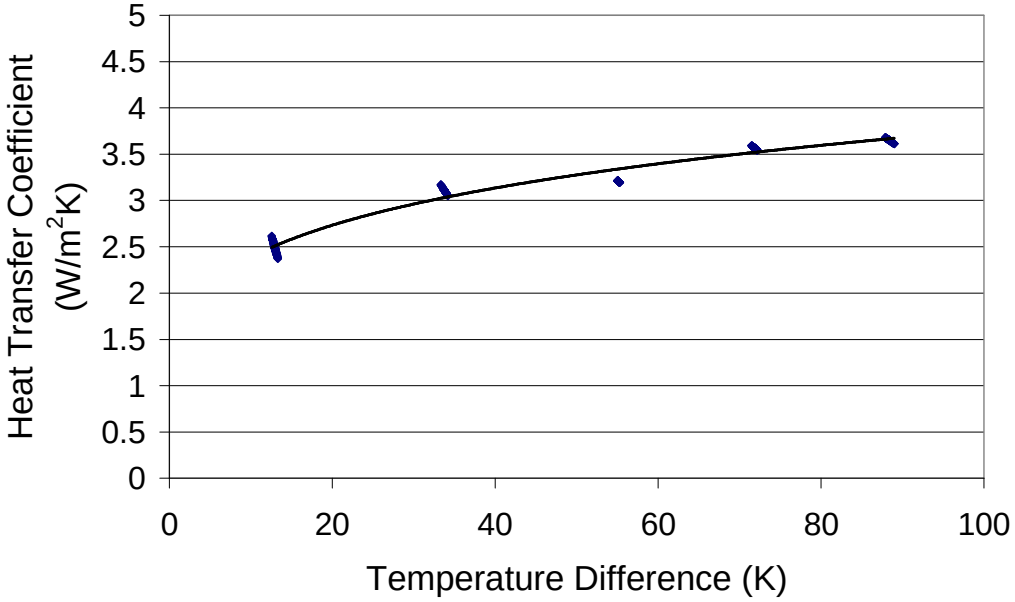

Figure 63: Heat transfer coefficient v enclosure temperature difference

Although Figure 63 demonstrates that the heat transfer coefficient increases for increasing temperature gradient, it is not a dimensionless correlation and so cannot be readily translated to enclosures of a different size. This is readily overcome by translating the data into a non-dimensional form. In Figure 64 it can be seen that there exists a relationship between the Nusselt number and Rayleigh number that can be represented in the general form of Equation 37 and more specifically as shown in Equation 38.

$$Nu = cRa^{n} \tag{37}$$

$$Nu = 1.2Ra^{0.2} \tag{38}$$

This is typical of the relationship that exists for turbulent natural convection where an exponent value of n = 0.2 would commonly be used for surfaces of constant heat flux (Bejan, 2004), as was the case here.

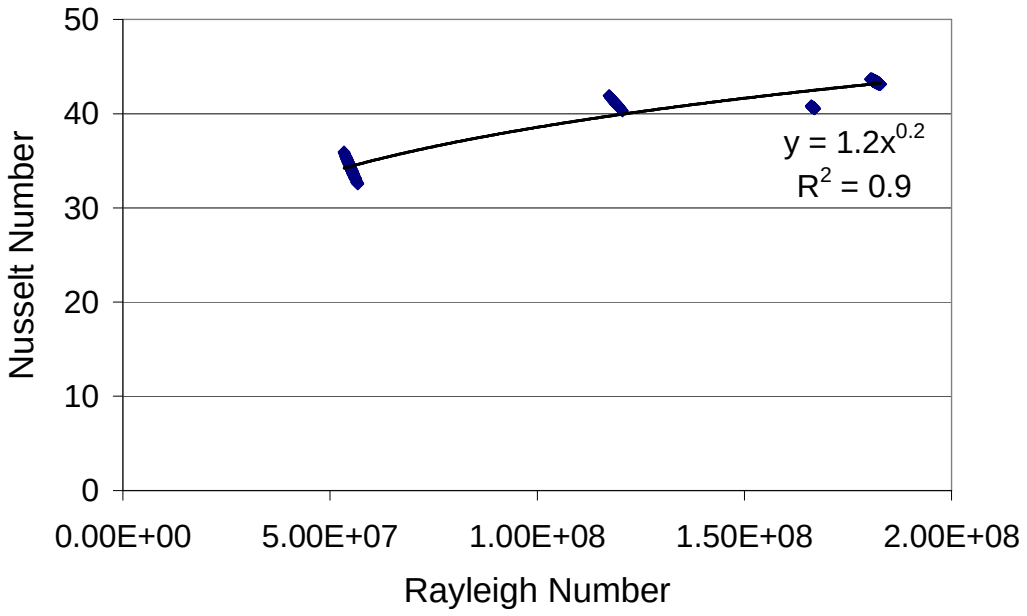

Figure 64: Nusselt number v Rayleigh number

A shortcoming of this correlation however, is that it is based on a relatively narrow range of Rayleigh numbers and does not account for aspect ratio. As such, it was decided to examine how well the existing correlation (Equation 39) of Ridouane and Campo (2005) that accounts for aspect ratio could predict the heat transfer in the experimental enclosure. A similar shortcoming of Ridouane and Campo's work was that it also was based on a narrow range of Grashof numbers.

$$Nu = 0.286 A^{-0.286} Gr^{1/4} \tag{39}$$

In Figure 65 it can be seen that although Equation 39 was developed for Grashof numbers in the range 2.9 x 10^6 to 9 x 10^6 it provides predictions within 5% of the values achieved in the experiments conducted in this study, where the Grashof numbers were in the range of 10^7 to 10^9. This suggests that the correlation is well suited to use over a much wider range of conditions and is a suitable generalised representation of heat transfer in a triangular enclosure.

Furthermore, the use of Ridouane and Campo' (2005) generalised correlation was shown in the last chapter to be suitable for predicting the Nusselt number for Grashof numbers lower than were measured in this study. In Figure 65 it can be seen that there is a good relationship between the predicted values from this correlation and the experimental data from this work.

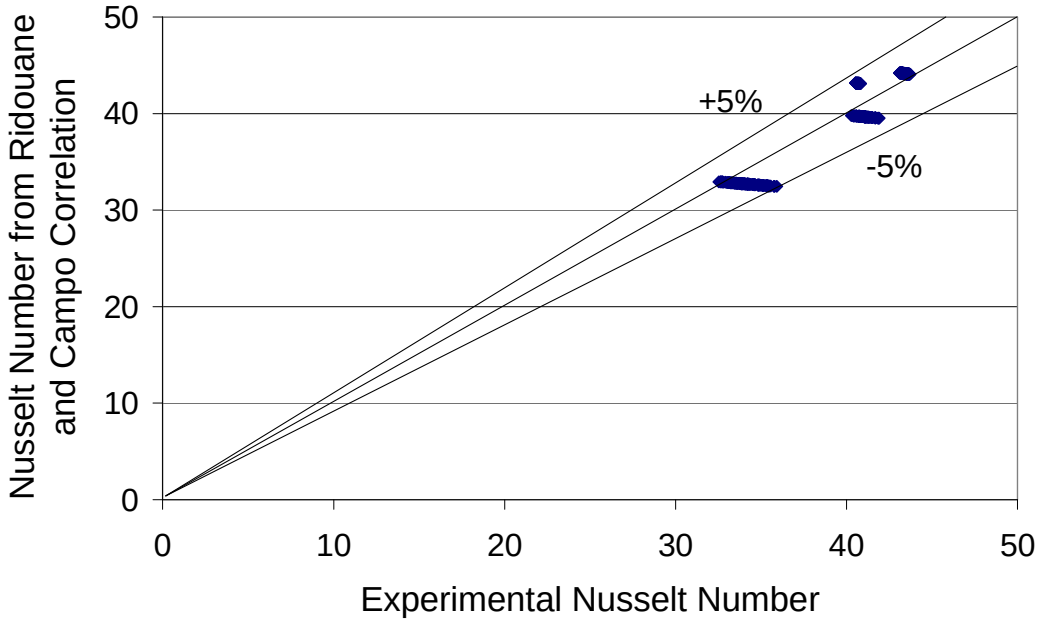

Figure 65: Relationship between Nusselt number from Ridouane and Campo's correlation and measured Nusselt number

5.5 Effect of a Baffle on Natural Convection Heat Transfer

In Chapter 4 it was concluded that the addition of a baffle could help reduce heat loss by natural convection inside an attic shaped space. To test this in practice the enclosure used in the experimental study was modified, by the addition of a 20mm thick polystyrene baffle, extending down from the apex of the enclosure, as shown in Figure 66.

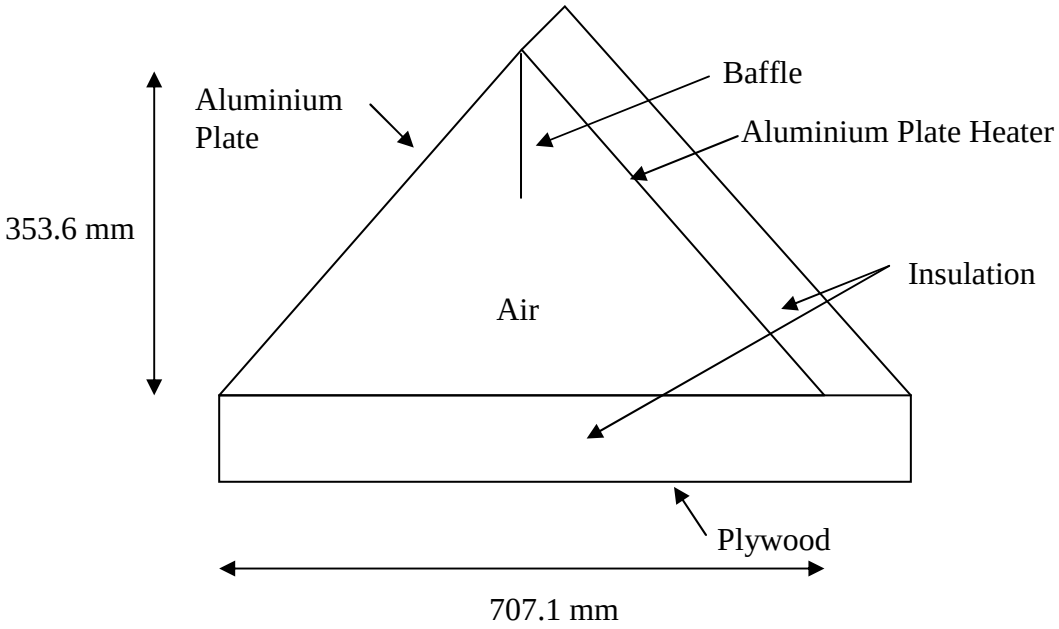

Figure 66: Layout of experimental enclosure with baffle added

From the CFD analysis in the previous chapter, it was expected that an adiabatic fin of this length would reduce the heat transfer coefficient in proportion to the length of the baffle. However, repeating the experiment, it was found that the addition of the baffle did not result in such a noticeable change in the heat transfer coefficient. Figure 67 shows that the heat transfer coefficient from the experiment is significantly different from what would be expected from the CFD analysis. Moreover, in Figure 68 it can be seen that the temperature difference does not affect the proportional change in the heat transfer coefficient.

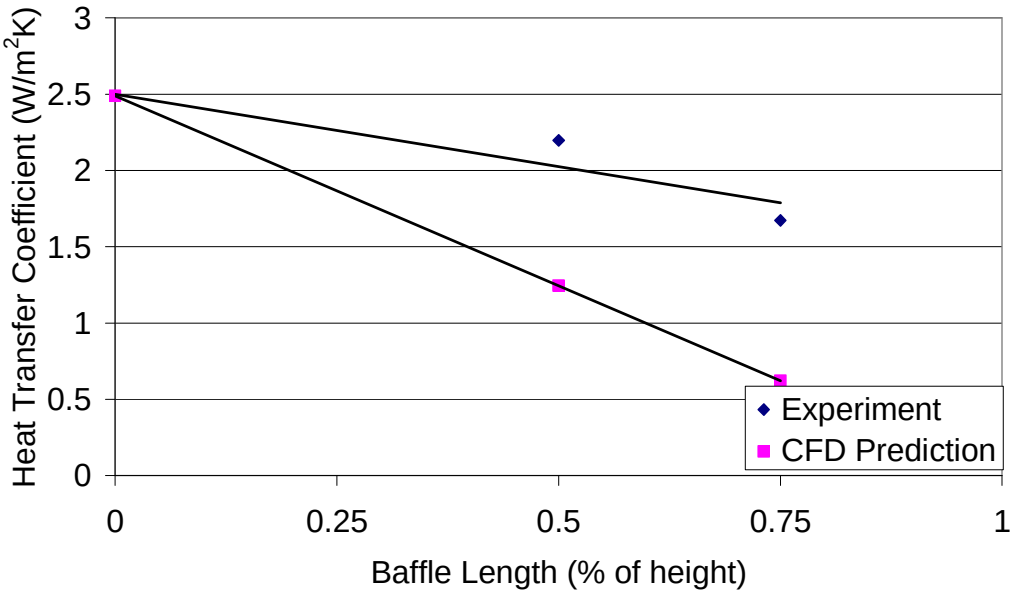

Figure 67: Heat transfer coefficient for baffled and non-baffled enclosures from experiments and CFD

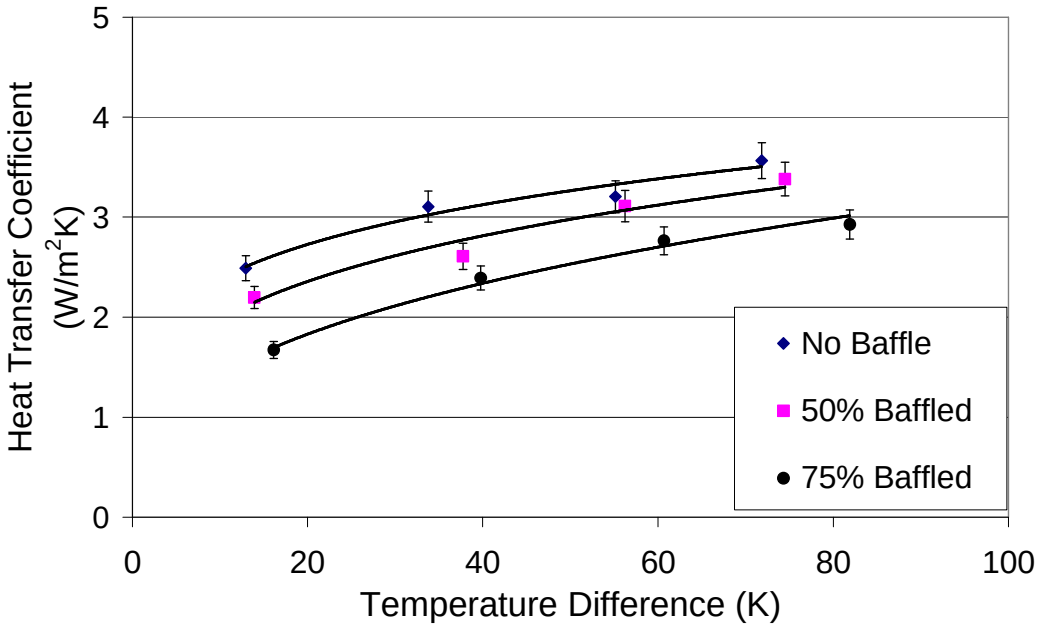

Figure 68: Change in experimental heat transfer coefficient for varying enclosure temperature gradient

Since the addition of a baffle did not reduce the heat transfer coefficient as significantly as predicted by the CFD study, it was decided to use flow visualisation to compare the flows in the experiments to those predicted by CFD.

To perform the flow visualisation, a small slot was cut in the bottom of the enclosure to allow the insertion of a laser light sheet. For this study it was decided to use a 5mW helium-neon laser with a wavelength of 543nm (green) focussed through a cylindrical lens to generate a light sheet with smoke used to seed the flow with particles.

The use of a green laser was chosen as this corresponds to the wavelength that modern CCD digital cameras are most sensitive to, thus ensuring the best quality image (Raffel, 1998). The layout of the flow visualisation experiment is shown in Figure 69.

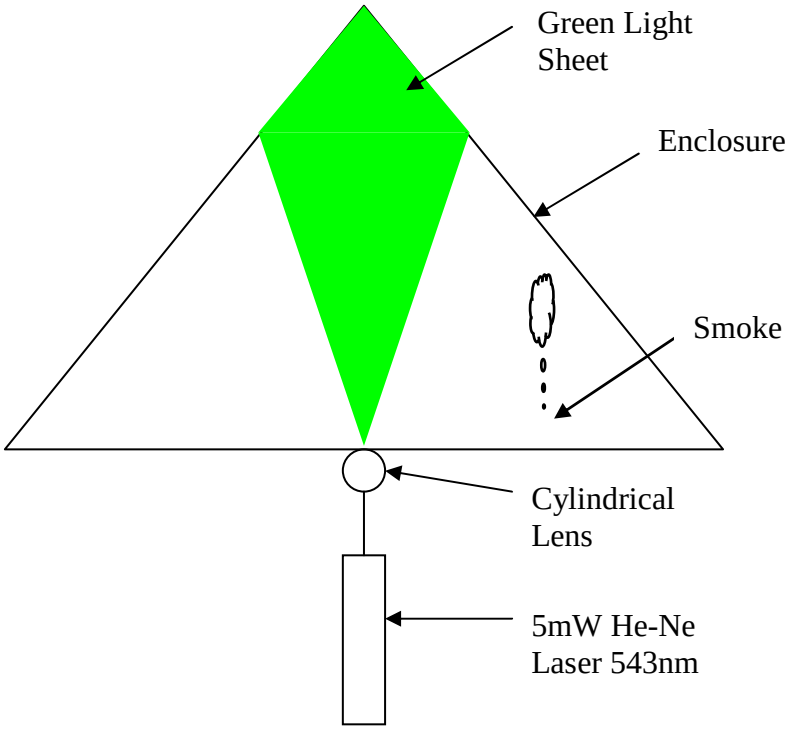

Figure 69: Flow visualisation experimental setup

As a baseline case, the flow in the non-baffled experimental enclosure was compared with that predicted from the CFD results. In Figure 70 and Figure 71 it can be seen that, qualitatively, the time-averaged flow in the experiment was similar to that predicted by the CFD, although unsteady flow patterns were also visually observed.

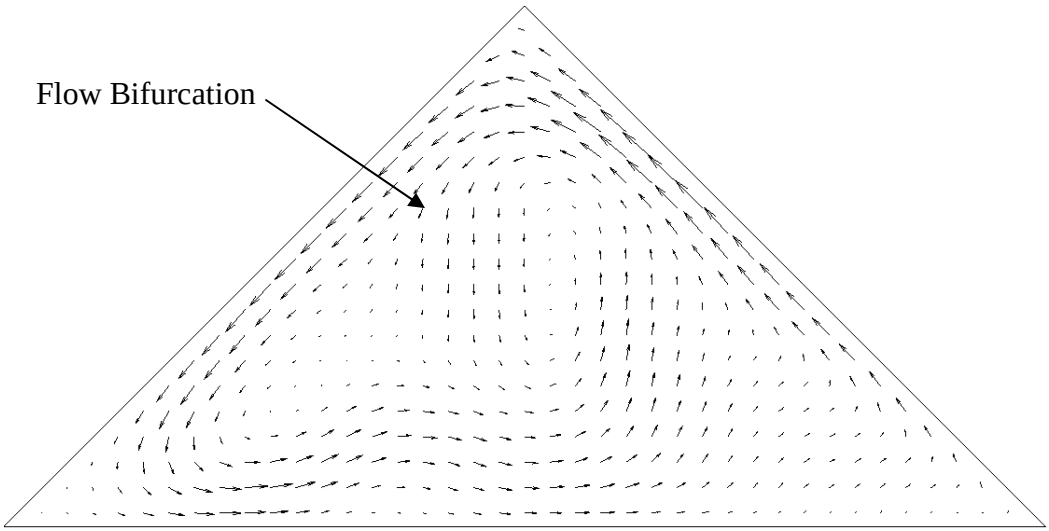

Figure 70: Typical flow field from CFD for non-baffled enclosure

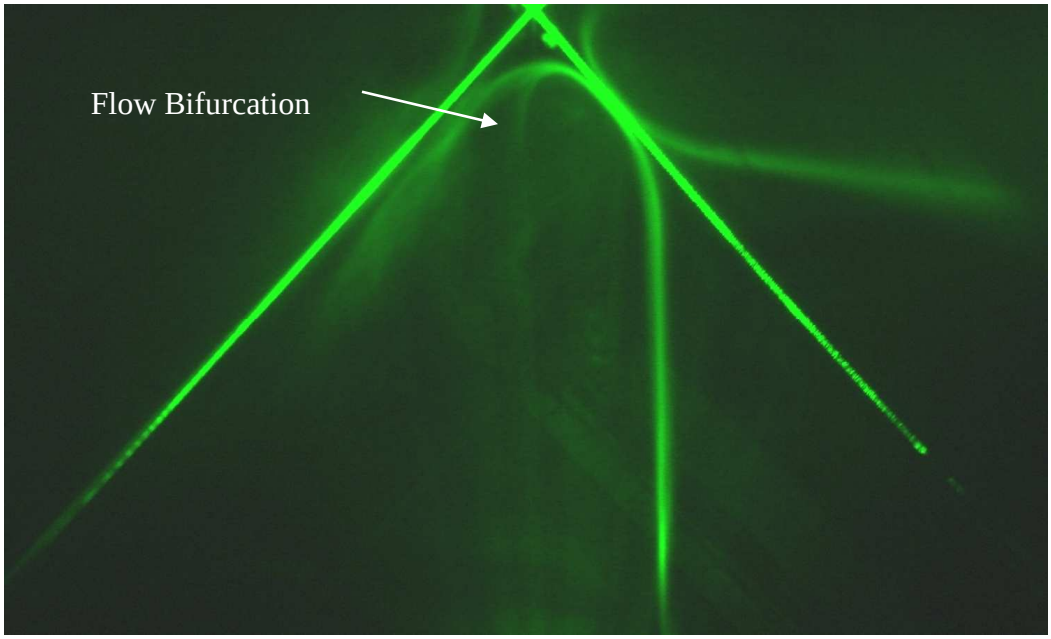

Figure 71: Experimental streamlines from flow visualisation

However, when a baffle was added to the enclosure, it was found that the flow predicted by CFD was somewhat different from that observed in the flow visualisation. In Figure 72 it appears that the flow near the apex of the enclosure

was relatively weak, however in Figure 73 and Figure 74 it can be seen that there was a recirculation zone on the heated (right) side of the baffle.

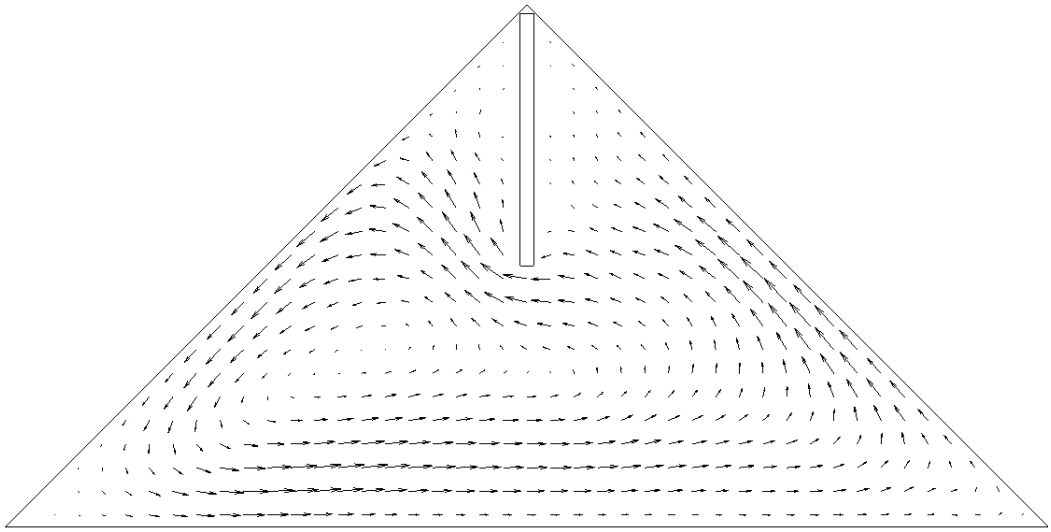

Figure 72: Typical flow in an enclosure with an adiabatic baffle, as predicted by CFD

The presence of this recirculation could suggest that significant heat was being transferred by conduction through the baffle; however given the low thermal conductivity of the baffle (R~ 0.9 m^2K/W) this is highly unlikely. More likely, is the scenario that the flow has a much higher velocity or momentum than predicted by the CFD in which the baffle was treated as an adiabatic surface. This momentum may be driving flow into the space between the heated side and the baffle. As the flow cannot get through or around the baffle it is forced downwards and around the bottom of the baffle. In doing this it appears that some of the flow is being returned into the plume rising along the heated wall and thereby forms a recirculation zone. In addition in Figure 74 it can be seen that there is significant mixing on the cooled side of the enclosure, as this is far less coherent than the

CFD results suggest, it may be contributing to higher levels of heat transfer in this area.

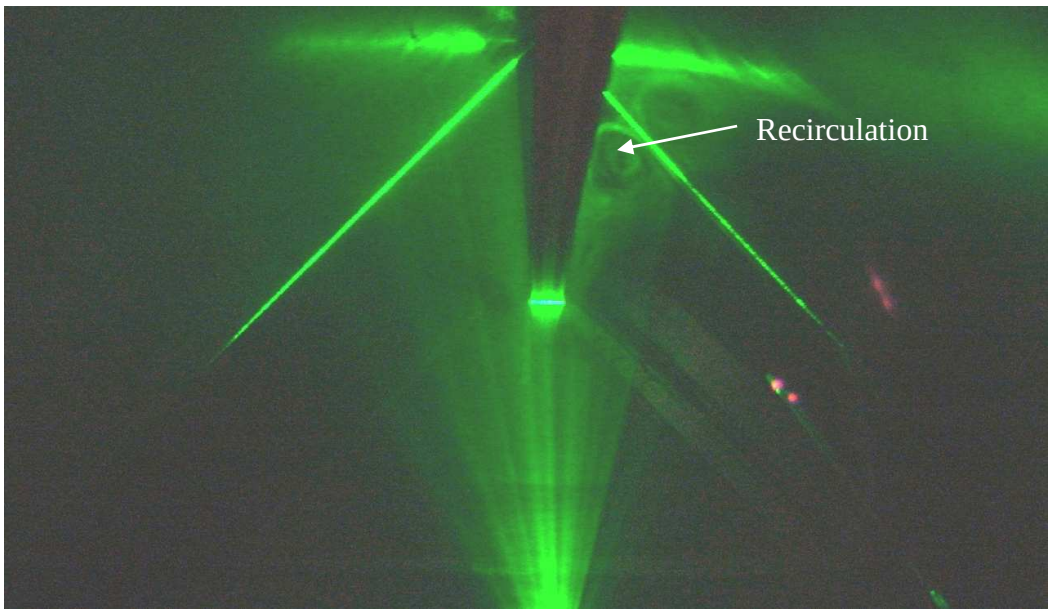

Figure 73: Visualised flow in experimental enclosure with a baffle

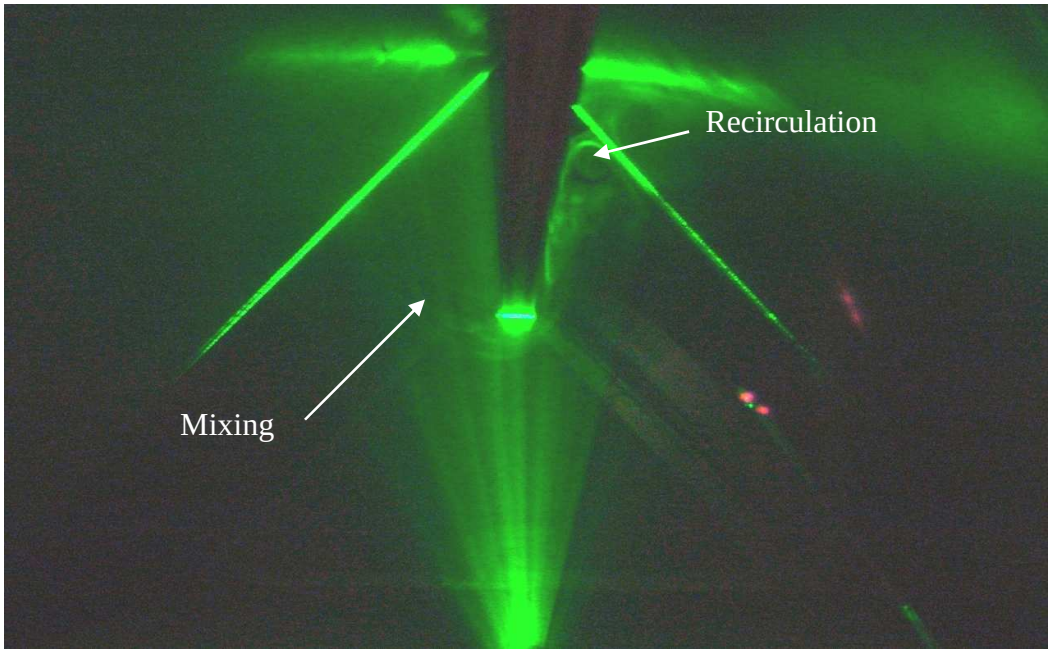

Figure 74: Flow in experimental enclosure showing mixing and recirculation

Another observation that was made when the baffle was added was the flow acceleration that occurred through the contraction between the baffle and the base of the enclosure. Although present in the CFD analysis, the influence of this was not as apparent as when observed in the flow visualisation. However, visualisation of the flow in the enclosure with a baffle extending down 75% of the height of the enclosure most clearly illustrated this flow acceleration.

Whereas in Figure 75, CFD suggests that the flow entering into the heated side of the enclosure is very weak, in Figure 76 it can be seen that there was a large recirculation and significant flow down and under the baffle due to the low pressure created by the contraction and flow acceleration.

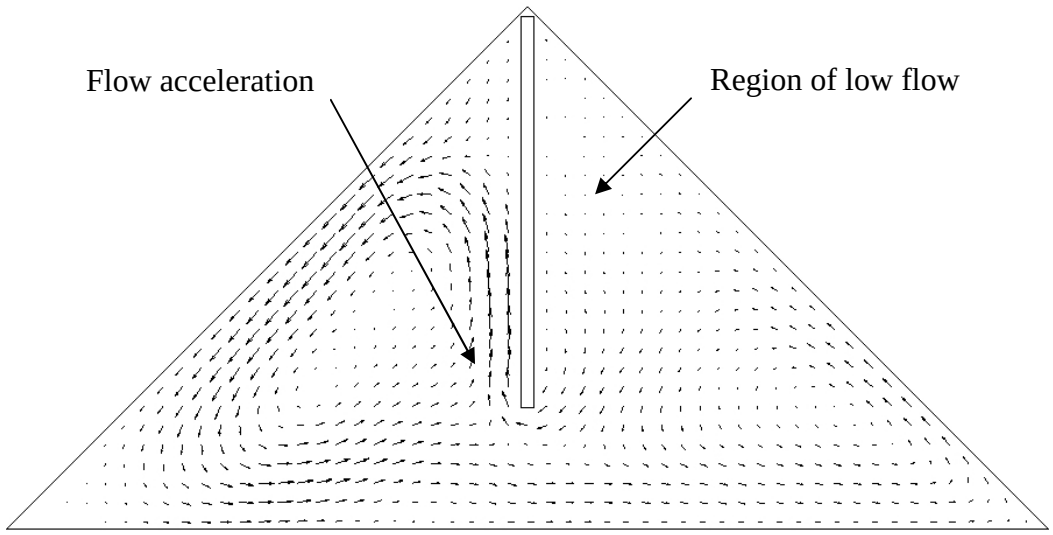

Figure 75: Typical flow in an enclosure with an adiabatic baffle extending 75% of the height

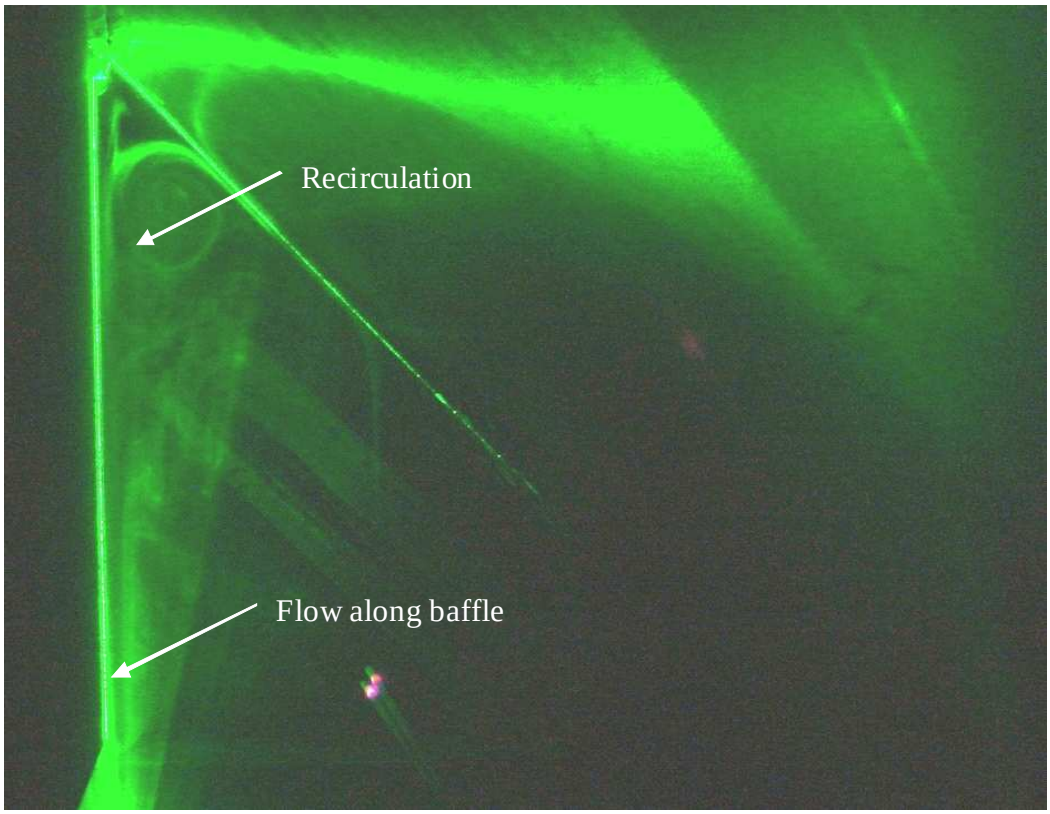

Figure 76: Flow visualisation of flow in enclosure with a baffle extending 75% of the height

From the experimental measurements of the heat transfer coefficient and the flow visualisation it was apparent that the baffles had a noticeable effect on the flow. However, as there was only qualitative similarity between the CFD and experimental results it was decided to examine if the baffle could be relocated to improve the convection suppression. Therefore the enclosure was again modified with the baffle being mounted on the floor of the enclosure and extended upwards towards the apex as shown in Figure 77.

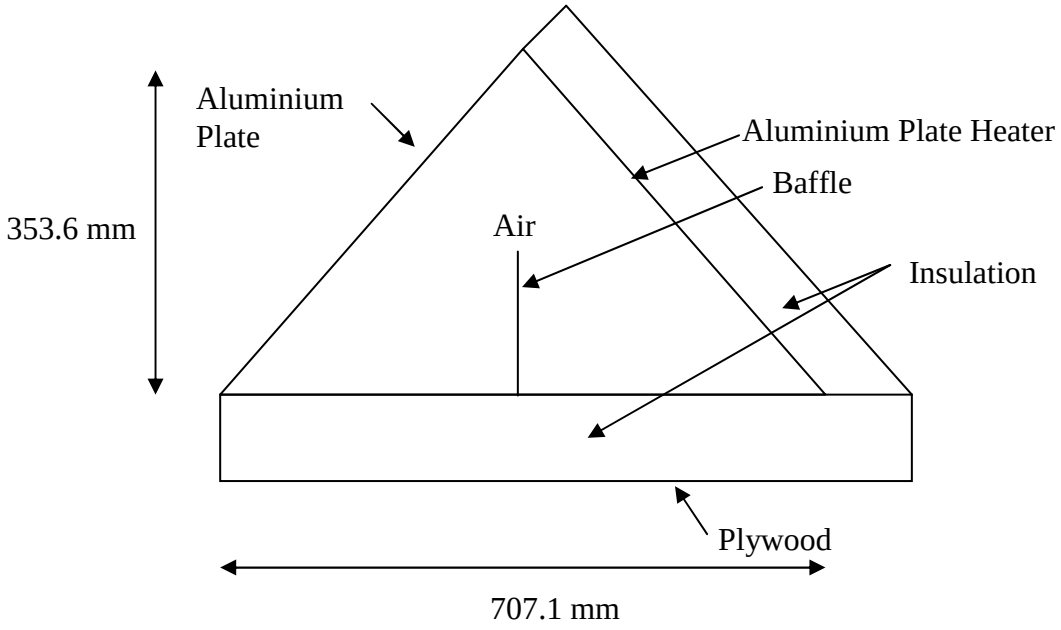

Figure 77: Floor mounted baffle in enclosure

As before, the heat transfer coefficient was determined over a range of Grashof Numbers, and again it was found that the baffle provided a noticeable degree of convection suppression. In Figure 78 it can be seen that as before the greater the length of the baffle, the greater the reduction in the heat transfer coefficient.

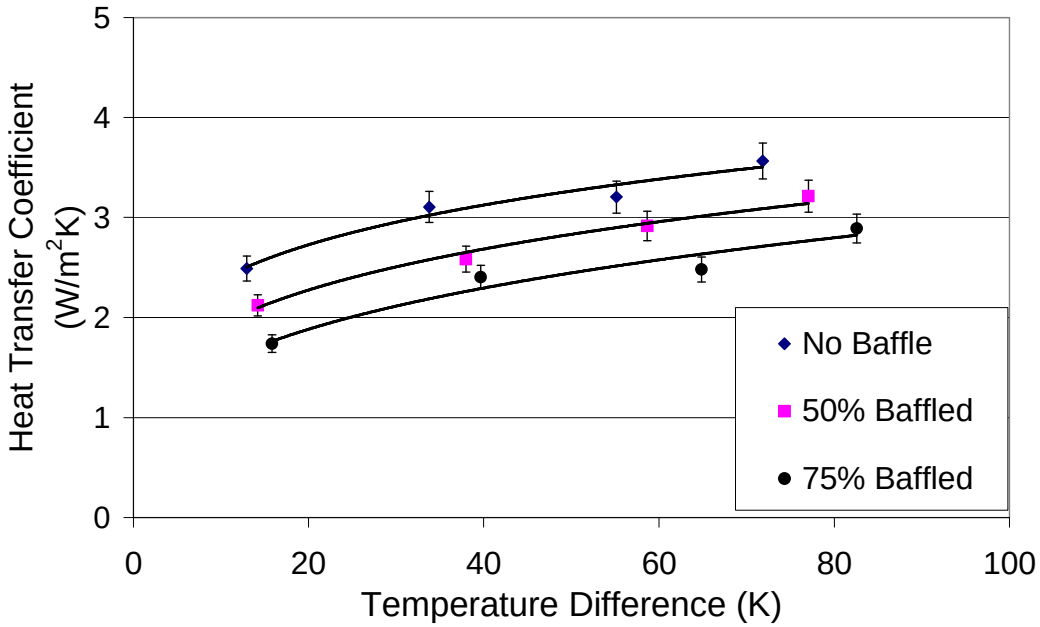

Figure 78: Heat transfer coefficients in a bottom baffled enclosure

A comparison of Figure 68 and Figure 78 shows that there is negligible difference between placing the baffle on the bottom of the enclosure or by suspending it from the apex down.

Previously it was shown that the experimental data for an unbaffled enclosure could be represented by a correlation developed by Ridouane and Campo (2005), however when a baffle is placed in the enclosure this correlation no longer holds. In Figure 79 it can be seen that this correlation would result in an over prediction of the Nusselt number if applied to a baffled enclosure.

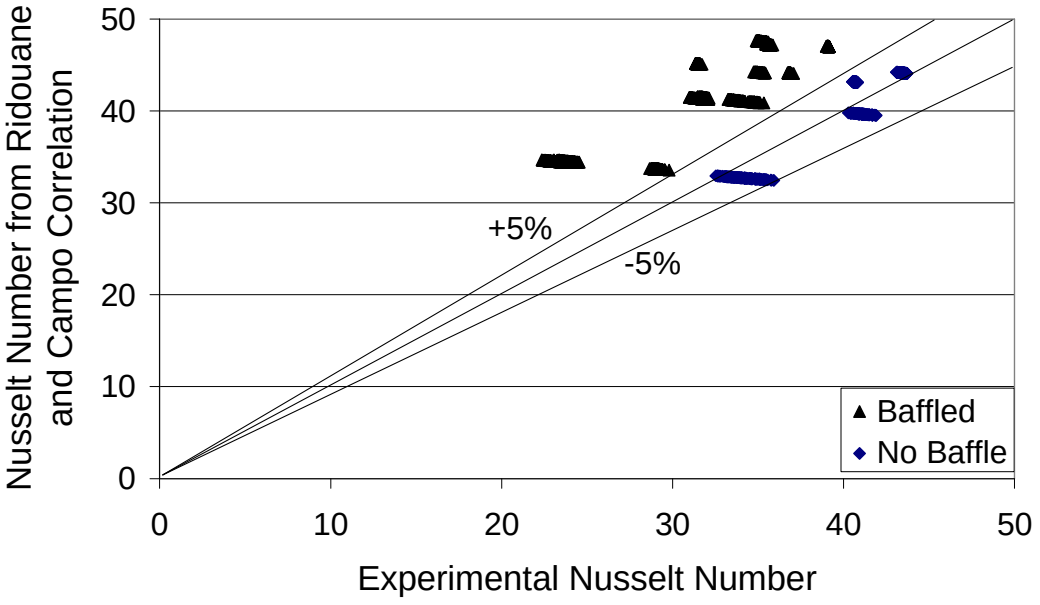

Figure 79: Nusselt number in a baffled enclosure, showing over-prediction by Ridouane and Campo's correlation

In order to account for the presence of the baffle, it was decided to modify the existing correlation. To do this a non-dimensional length parameter (the blockage ratio) represented by the ratio of the baffle length (L) to the enclosure height (H) was added to the correlation as given by Equation 40. It was found that this correlation provided a good degree of correlation with the experimental data, both with and without a baffle, shown in Figure 80.

$$Nu = 0.286 A^{-0.286} Gr^{0.25} \left(1 - \frac{L}{H}\right)^{0.2} \tag{40}$$

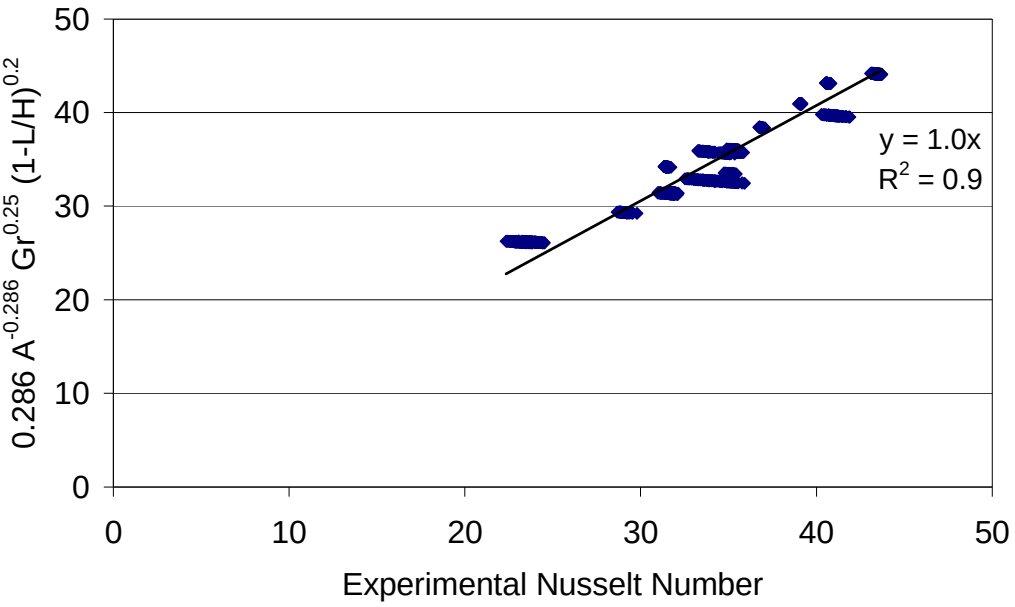

Figure 80: Experimental Nusselt number versus modified Ridouane and Campo correlation

However Equation 40 and the method used to derive it cannot be applied when the blockage ratio is equal to unity. Using the methodology described previously the Nusselt number will equal zero thus implying an adiabatic chamber, and in reality this cannot occur. Rather by increasing the length of the baffle so the blockage ratio is equal to one, the enclosure becomes two right triangular enclosures separated by a partition. Therefore alternative correlations would need to be used to determine the heat loss and the thermal resistance of the partition would also need to be considered. In fact the situation may occur where the losses through the ends of the enclosure begin to outweigh the losses between the inclined sides of the enclosure. This may mean that some of the existing correlations may not predict the behaviour accurately and so could require further investigation.

5.6 Conclusions from Natural Convection Experiments

From the numerical modelling of the BIPVT collector in Chapter 4 it had been suggested that natural convection in the attic of a cold roof building could serve as an insulating medium for BIPVT collectors. A correlation had been developed by Ridouane and Campo (2005) to describe natural convection in attic style enclosures; however this was based on Grashof Numbers in the range 2.9×10^6 to 9×10^6. For a tropical or warm climate such as that of Australia or New Zealand, the Grashof numbers in an attic space could conceivably exceed those previously studied by several orders of magnitude. In light of the shortcomings of the data relating to natural convection in attic shaped enclosures, the experimental work undertaken in this chapter extended the validity of this correlation to Grashof Numbers in the range of 10^7 to 10^9.

Furthermore, the potential for using a single baffle to suppress heat loss presented and computationally examined in the CFD study of the preceding chapter was verified experimentally. Although it was found that the CFD results tended to over-predict the reduction in heat transfer, the general trend of increasing baffle length resulting in lower heat transfer coefficients was found to hold true. Additionally, it was shown using flow visualisation that, qualitatively, CFD was able to provide an acceptable estimate of the streamlines in an unbaffled triangular enclosure. However the CFD simulation was not able to predict the flow observed in the baffled enclosure which could explain the difference between the computational and measured heat transfer coefficients.

The experimental work also showed that the baffle could be placed either downwards from the apex of the enclosure, or upwards from the floor. From the measurements it was shown that the heat transfer coefficient of the two scenarios had almost identical dependence on the baffle length. On this basis a new generalised correlation was presented that could be used to predict the natural convection heat transfer coefficient in both baffled and unbaffled triangular enclosures in the range of Grashof Numbers from 2.9×10^6 to 10^9.

Given the much wider range of Grashof Numbers that the correlation has been validated for, there is obviously significant potential for it to be used in the analysis of roof integrated BIPVT collectors. In Chapter 6, the use of this correlation shall be examined to verify the hypothesis that natural convection in an attic space can serve as the insulation for a BIPVT collector.

Chapter 6: Designing a Building Integrated Photovoltaic Thermal System

6.1 Introduction

In the preceding chapters, the experimental testing of a prototype BIPVT collector, the development and validation of an optimisation model for the collector and a computational and experimental study on heat transfer in attic shaped enclosures were examined. In this chapter the results of the experimental BIPVT testing and optimisation are combined with the correlations developed for the heat transfer coefficients in attic shaped enclosures discussed in Chapters 4 and 5, and typical meteorological year data for Hamilton NZ (Appendix D) to model and assess the long term performance of a BIPVT collector system.

6.2 Effect of Natural Convection on the Performance of a BIPVT Solar Collector

As was noted in Chapter 1, many studies on PVT style collectors have treated them as they would with any other stand-alone solar water heater. During the experimental testing and numerical modelling of the BIPVT it was assumed that the BIPVT could be treated as a stand-alone unit, however, in reality this would not be the case as in a cold roof there is thermal coupling between the roof and the air beneath it.

From the experimental and computational work it has been shown that the heat transfer in an idealised attic shaped enclosure can be represented by the correlation of Ridouane and Campo (2005) shown in Equation 41.

$$Nu = 0.286\,A^{-0.286}Gr^{1/4} \tag{41}$$

In the numerical modelling of the BIPVT design it was assumed that the BIPVT collector was insulated on its rear surface by an insulating material similar to the mineral wool used in the experimental testing. By treating the heat loss from the rear surface of the BIPVT in this manner, the efficiency of the collector would vary with the thickness of insulation, as is shown again in Figure 81.

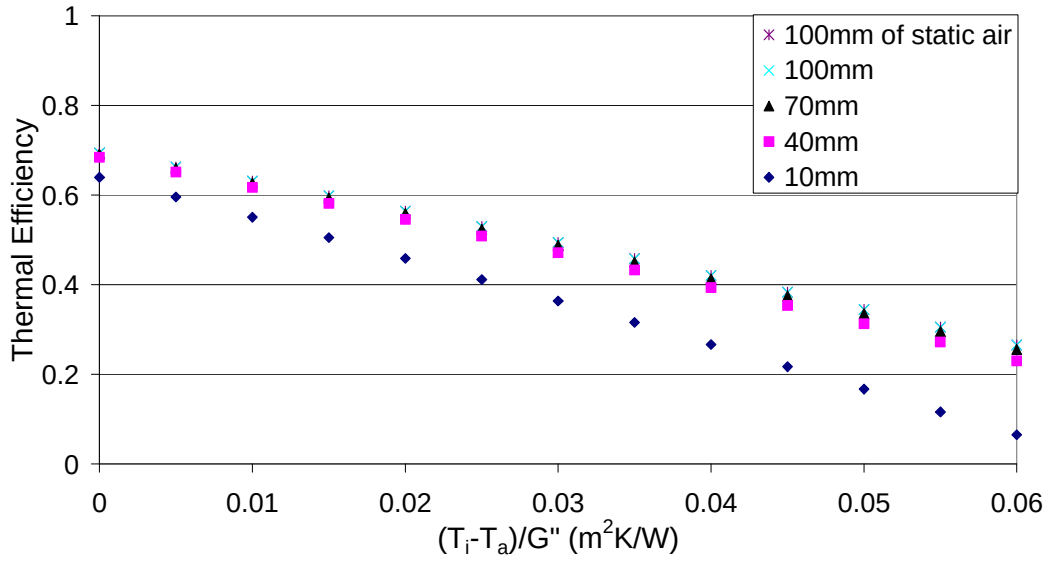

Figure 81: Thermal efficiency of BIPVT with varying insulation thickness

However, in a cold roof this layer of insulation would normally be placed above the ceiling of the building rather than on the rear of the roofing panels. As has been shown, the heat transfer coefficient in an attic shaped enclosure is relatively

low (Anderson and Ward reported a value of 3.5W/mK for a real attic), therefore it may be possible to rely on this large air gap as an insulating barrier, as opposed to insulating the rear of the BIPVT collector and the ceiling. By doing this it is conceivable that the cost of a BIPVT could be reduced by approximately \$20/m^2 (Rawlinson's, 2005). Furthermore, in the experimental and numerical analysis of the natural convection in an attic style enclosure, it was shown that the use of passive baffling could readily be implemented as a means of reducing the heat transfer coefficient further.

Therefore, assuming that an attic space is weather-tight and has minimal ventilation, the optimisation model presented in Chapter 3 can be modified to examine the effect of using an attic space as insulation on the BIPVT performance. Rather than calculate the rear surface heat transfer coefficient by taking the inverse of the insulation's R-value (ie. K_b/L_b), as was done in the numerical optimisation of the BIPVT design (Chapter 3), it can be taken as being the heat transfer coefficient from Ridouane and Campo's correlation, where the Grashof number is based on the temperature difference between the mean collector temperature (T_{pm}) and the ambient temperature (T_a) (Anderson et al., 2009) (Appendix E).

Figure 82 shows that under these conditions the optimisation model predicts that reducing the inclination of the BIPVT also reduces the thermal efficiency. This is particularly pronounced at low roof inclinations with high temperature gradients. This suggests that if natural convection in an attic space is used as an alternative

to insulating the rear surface of a BIPVT collector, the pitch (angle) of the roof has a significant influence on the BIPVT thermal efficiency. However, this effect becomes less pronounced as the pitch is increased.

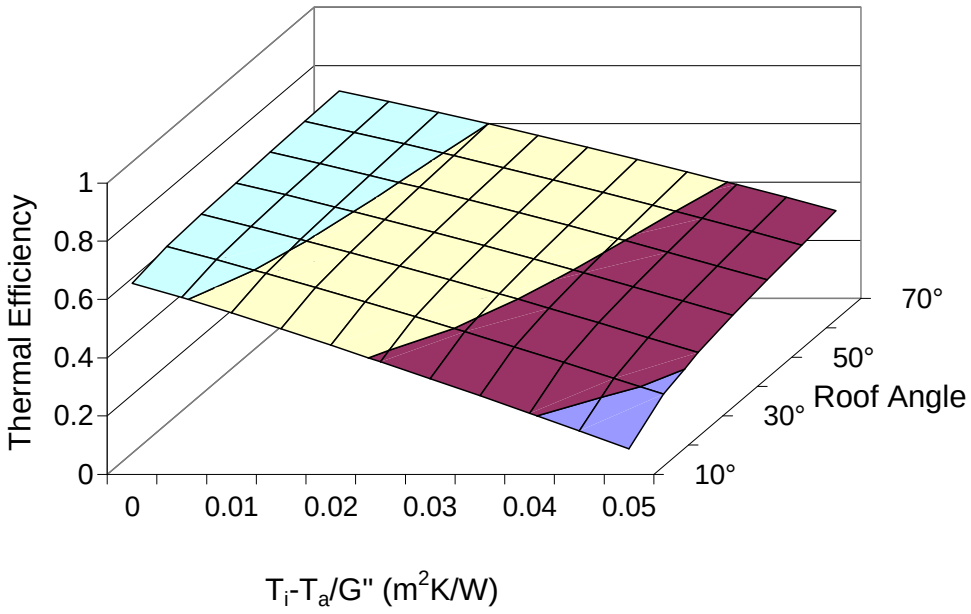

Figure 82: Thermal efficiency of BIPVT for varying roof pitch

There is however a counterpoint to the improved thermal efficiency gained by increasing the pitch of the roof. In Figure 83, it can be seen that by increasing the roof pitch there is a decrease in the electrical efficiency of the BIPVT. The decrease in thermal efficiency at low pitch angles is the result of the higher heat loss meaning that the BIPVT is operating at lower temperatures and therefore has a higher electrical efficiency. However, as the pitch is increased the heat loss is reduced, thus giving improved thermal efficiency but also higher PV cell temperatures and therefore lower electrical efficiencies.

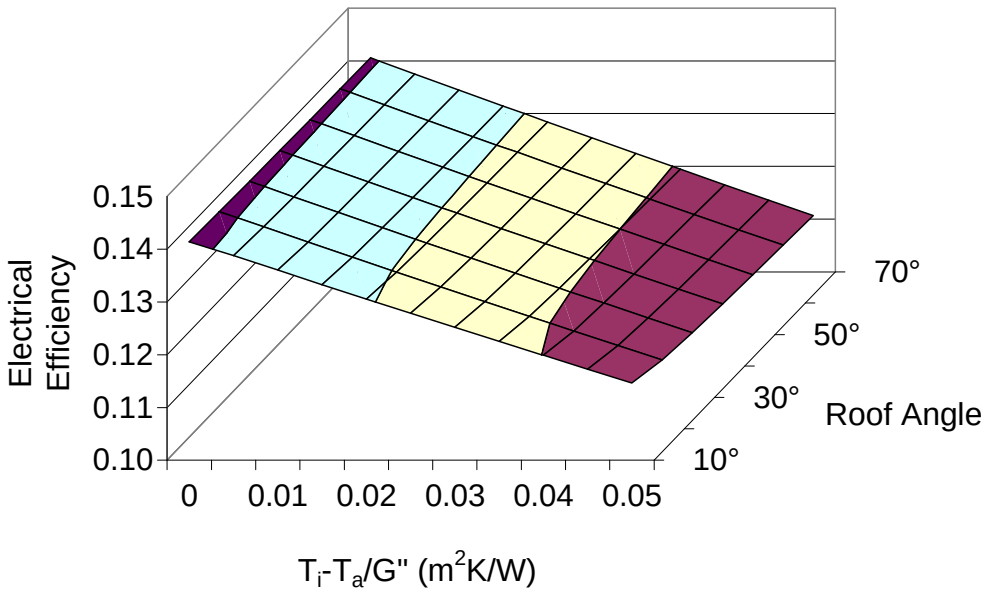

Figure 83: Electrical efficiency of BIPVT for varying roof pitch

The use of the attic space as an insulating medium can be taken further by the addition of a passive baffle and implementing the new Nusselt number correlation derived in Chapter 5 from the experimental results, as shown in Equation 42.

$$Nu = 0.286 A^{-0.286} Gr^{0.25} \left(1 - \frac{L}{H}\right)^{0.2} \tag{42}$$

Figure 84 shows that the addition of a baffle to an attic with a roof pitch of 45° would, as expected, provide a further increase in the thermal efficiency, or more specifically, a lower heat loss from the panel. Therefore, from the modelling, the inclusion of a baffle in an attic space should provide a degree of further insulation by acting to suppress the natural convection.

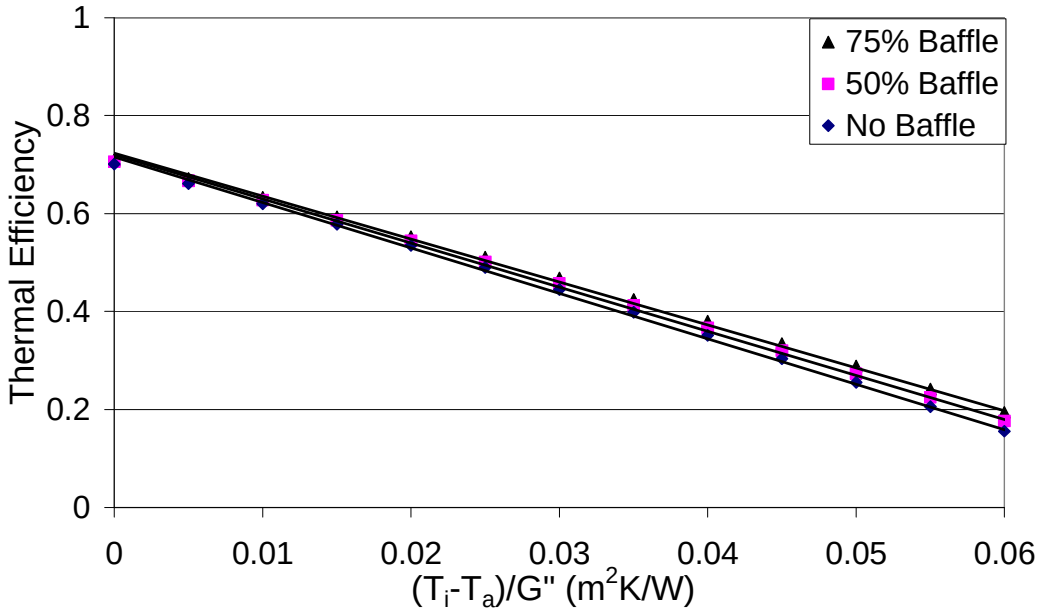

Figure 84: Effect of a baffle on BIPVT thermal efficiency

6.3 Development of a Long Term Simulation for BIPVT Performance Analysis

In order to assess the long-term performance of the BIPVT, a simulation was performed using TRNSYS (SEL, 2007) and the typical meteorological year (TMY) data for Hamilton developed by Anderson et al. (2007) (Appendix D).

TRNSYS is a widely used software tool for conducting transient simulations of solar thermal energy systems using quasi-steady models. The mathematical representations of the components of the solar energy system are presented as algebraic or ordinary differential equation models, which the software interconnects depending on energy and mass flows. Its flexible nature allows the

user to configure any number of systems and to determine their performance at a large number of sites worldwide.

To demonstrate the performance of the BIPVT collector it was modelled using the TRNSYS photovoltaic/thermal collector model (Type 50). This model uses a similar method of analysis to that of the theoretical flat plate collector model (Type 1), and is based on the modified Hottel-Whillier equations (Chapter 3). For the simulations it was assumed that the BIPVT was coupled to a stratified tank (Type 4) as shown in Figure 85.

The weather data from the TMY was read using the user defined weather function (Type 109). This function allowed the radiation on an inclined surface to be determined using the isotropic sky model. Although it has been suggested that the correlation of Reindl provides the best accuracy for determining the beam and diffuse components on an inclined surface (SEL, 2007), it was found that in these simulations, at low solar angles (sunrise and sunset) the Reindl model would over-predict the radiation levels. However, the work of Benseman and Cook (1969) suggests that the application of an isotropic sky model provides an accurate prediction of radiation on inclined surfaces in New Zealand.

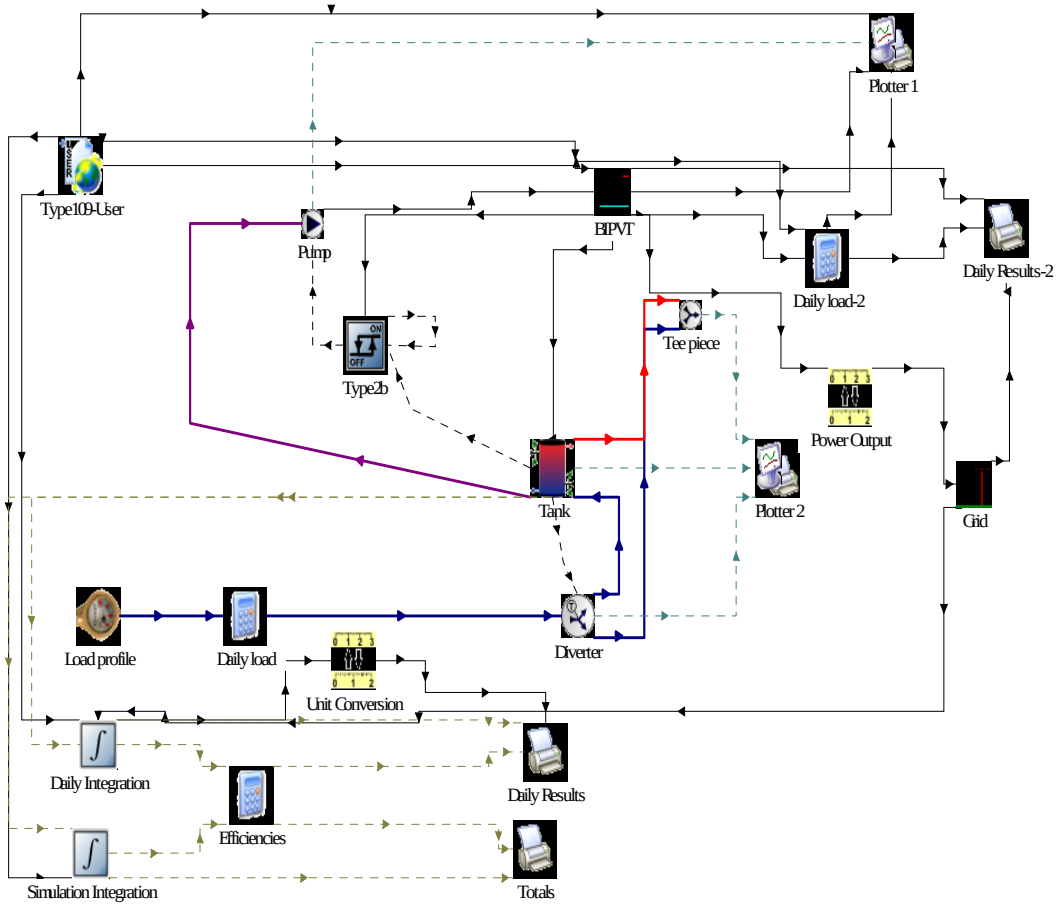

Figure 85: TRNSYS model of BIPVT system

For the simulation it was decided to examine a small scale BIPVT system suitable for use in a single residence. As such, a collector of 4m^2 mounted at 45° was assumed to be used in conjunction with a 300 L storage tank in Hamilton, NZ. Furthermore, the water use profile of the system was given by Figure 86 and is typical of the use in an Australian or New Zealand residence (AS 4234:1994).

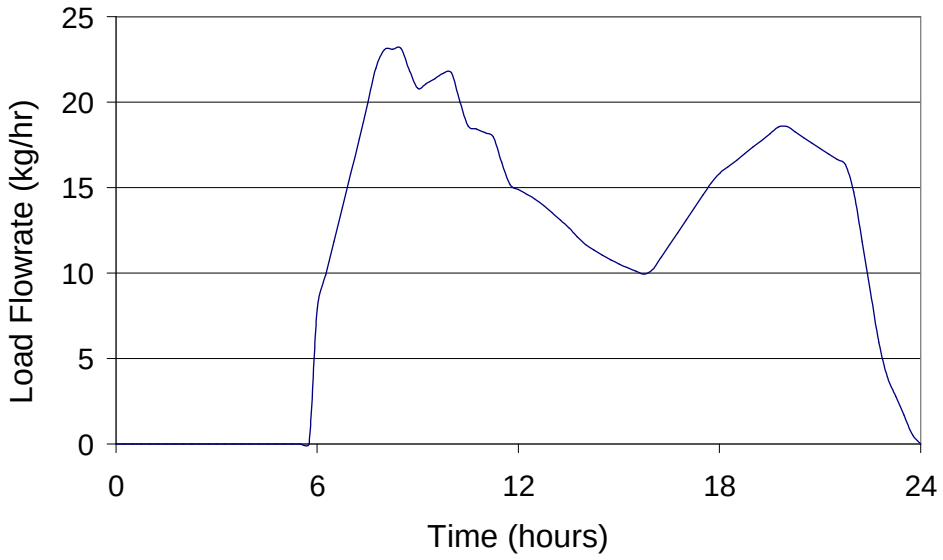

Figure 86: Hot water load profile

6.4 Long Term Performance of a BIPVT System

In Chapter 2 it was shown that the thermal efficiency of the glazed prototype BIPVT could be represented by Equation 43. Therefore, as a benchmark case, the performance of this collector was compared with that of a theoretically optimised BIPVT collector (using the method discussed in Chapter 3) with a thermal efficiency given by Equation 44. It should be noted that for this chapter an "optimised" BIPVT collector was taken as being one with the properties listed in Table 6 and a packing factor of 40% mounted above a 75% baffled attic.

$$\eta = 0.6 - 5.55\frac{T_i - T_a}{G''} \tag{43}$$

$$\eta = 0.73 - 8.78\frac{T_i - T_a}{G''} \tag{44}$$

Based on the collector efficiencies shown in Equations 43 and 44 it can be seen in Figure 87 that, during a week of operation during summer (January), there is only a small difference in the daily solar heating fraction of the panels. However, if we examine the daily electrical output in Figure 88, we can see that the optimised design provides a noticeable increase in performance. This suggests that it is necessary to optimise the BIPVT, from the experimental prototype, in order to improve the electrical efficiency and output.

Furthermore, the higher thermal (and electrical) output from the "optimised" collector clearly shows that the combined effect of natural convection and a passive baffle provide a sufficient degree of insulation so as to negate the need for additional layers of insulation in a cold roof attic space.

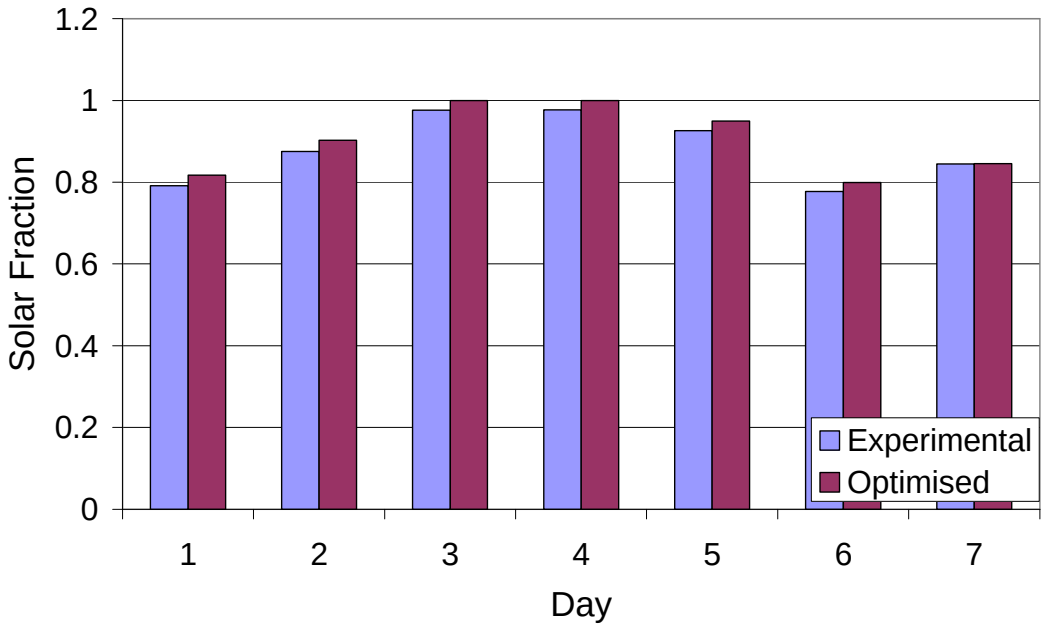

Figure 87: Solar heating fraction of BIPVT panels for a summer week in Hamilton

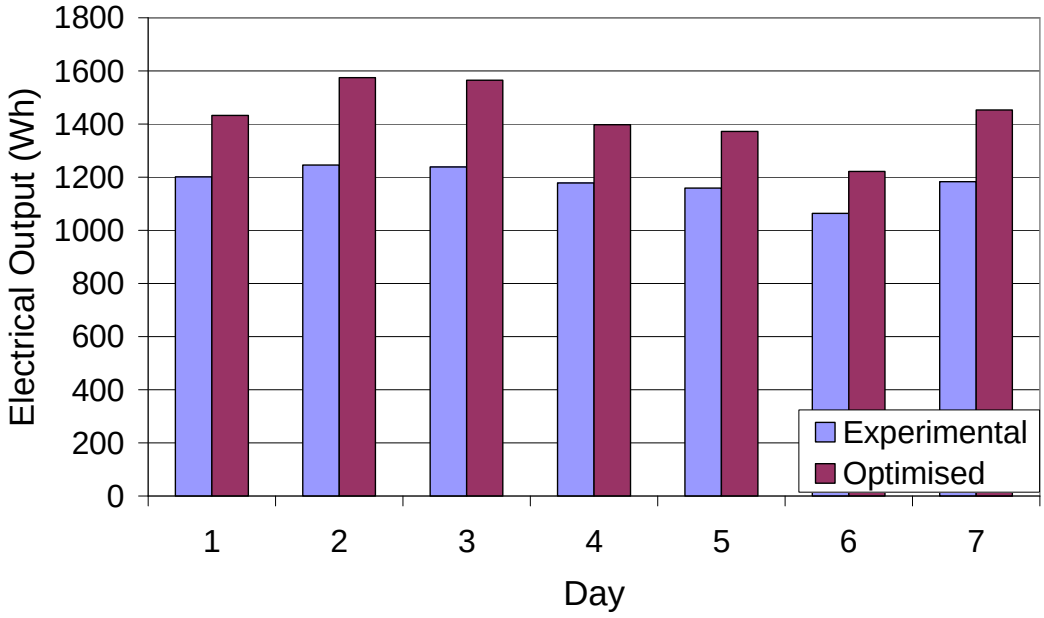

Figure 88: Daily electrical output from BIPVT panels for a summer week in Hamilton

During a winter week (June) the solar fraction is almost zero as shown in Figure 89. The reason for this is the particularly low levels of solar radiation and also the low ambient temperatures that result in increased heat loss. Under low temperature conditions, PV panels typically perform well, even without active cooling; however in Figure 90 it can be seen that the electrical output of an optimised collector is still higher than the experimental collector.

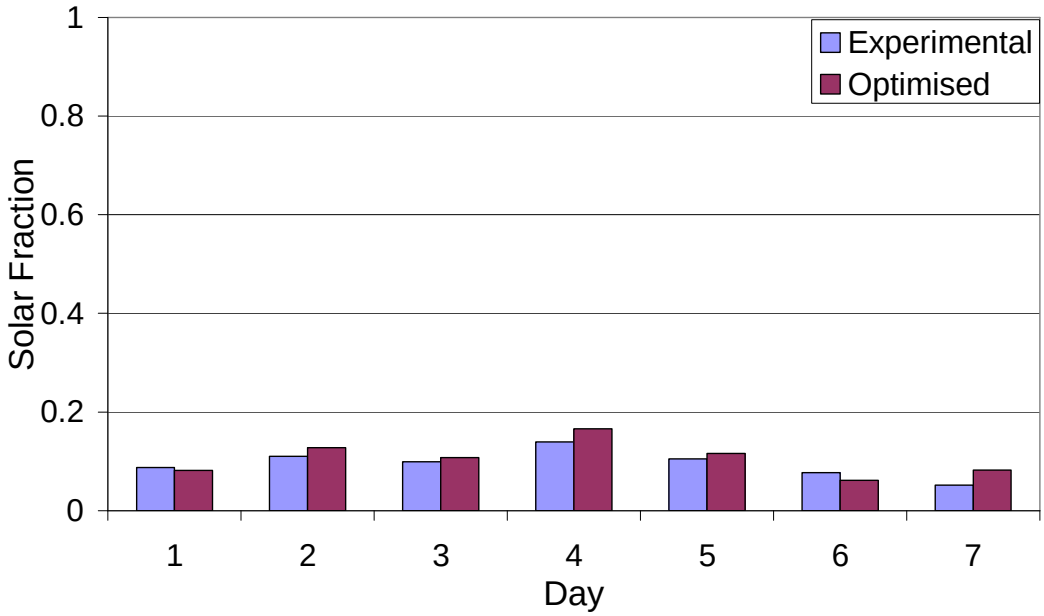

Figure 89: Solar heating fraction of BIPVT panels during a winter week in Hamilton

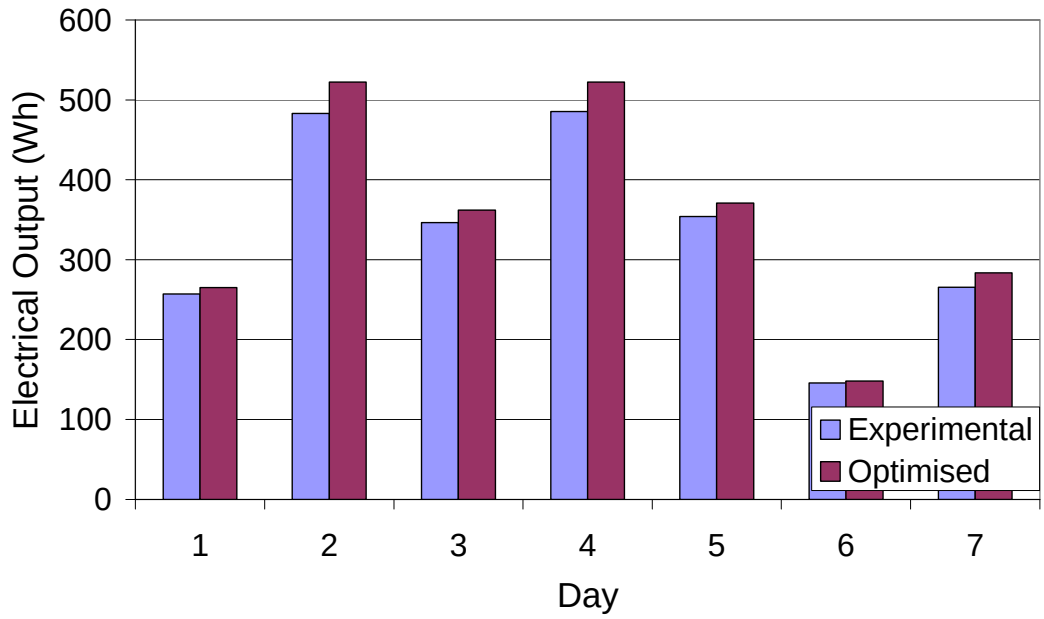

Figure 90: Daily electrical output from BIPVT panels during a winter week in Hamilton

6.5 Comparative Performance of Glazed and Unglazed BIPVT Systems

In addition to the glazed collectors that have been analysed there is also potential for unglazed collectors to be used, particularly for low temperature applications such as swimming pool heating. In Chapter 2 it was found that the efficiency of an unglazed collector could be represented by Equation 45. Therefore a simulation was conducted to determine the performance of an unglazed collector in the same heating application.

$$\eta = 0.36 - 9.22\frac{T_i - T_a}{G''} \tag{45}$$

Figure 91 shows that the solar fraction is significantly less than for a glazed collector, which is principally due to the higher heat loss and lower optical efficiency of the collector. However, the electrical output from the unglazed experimental collector, shown in Figure 92, shows a marked improvement over the glazed collector. This improvement is due to the fact that the glazing absorbs some of the incoming radiation that could otherwise be absorbed by the PV cells. Furthermore, its presence acts to reduce thermal losses and thus results in a higher panel temperature, which also affects the electrical efficiency of a BIPVT.

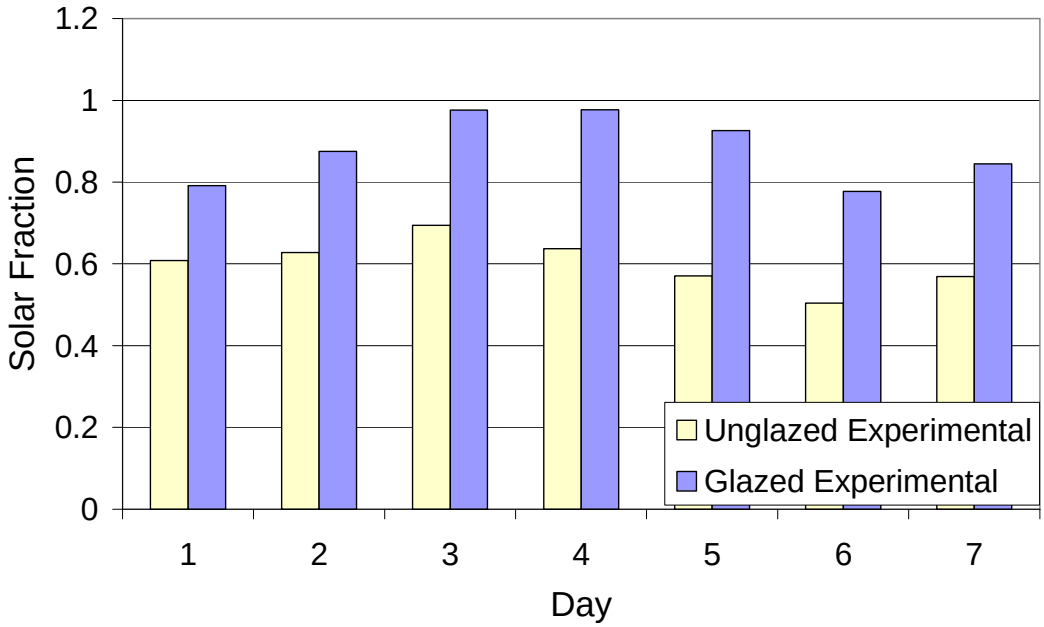

Figure 91: Solar heating fraction of prototype BIPVT panels during a summer week in Hamilton

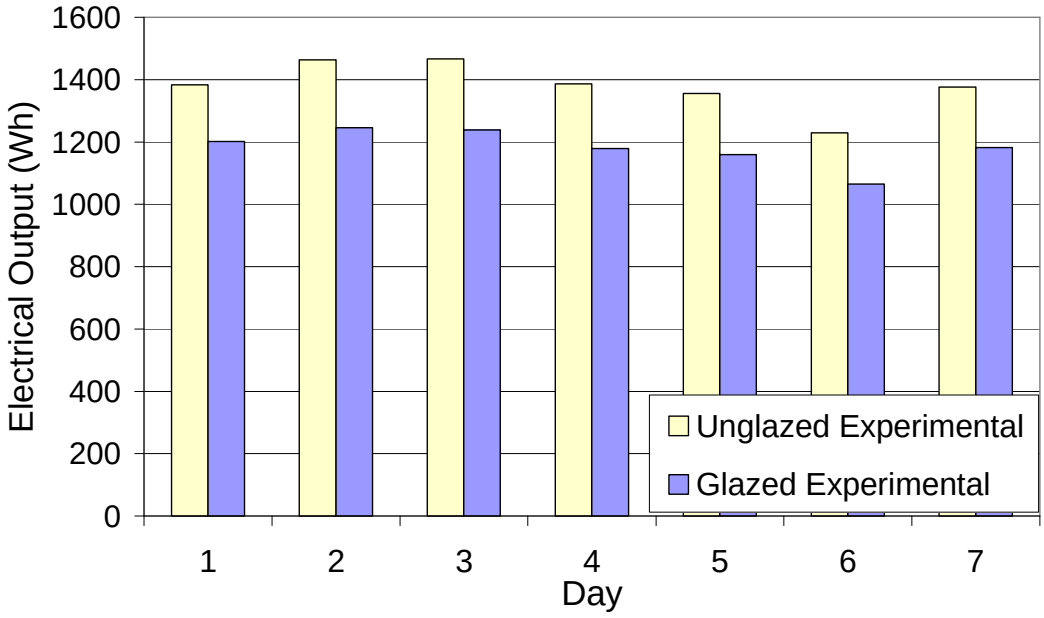

Figure 92: Daily electrical output from prototype BIPVT panels during a summer week in Hamilton

Previously, it was noted that the reason for the difference in the electrical efficiency for the glazed and unglazed collector is due to an increase in the temperature of the PV cells when a glazing layer was added to the BIPVT. To illustrate this point, the optimisation model presented in Chapter 3 can be used to determine the thermal efficiencies of "optimised" glazed (Equation 46) and unglazed (Equation 47) BIPVT collectors.

$$\eta = 0.73 - 8.78\frac{T_i - T_a}{G''} \tag{46}$$

$$\eta = 0.57 - 17.97\frac{T_i - T_a}{G''} \tag{47}$$

In Figure 93 it can be seen that there is a significant difference between the temperatures of the PV cells in the "optimised" BIPVT when the glazing layer is present and when it is removed. This supports the explanation given for the decrease in electrical output from a glazed BIPVT panel.

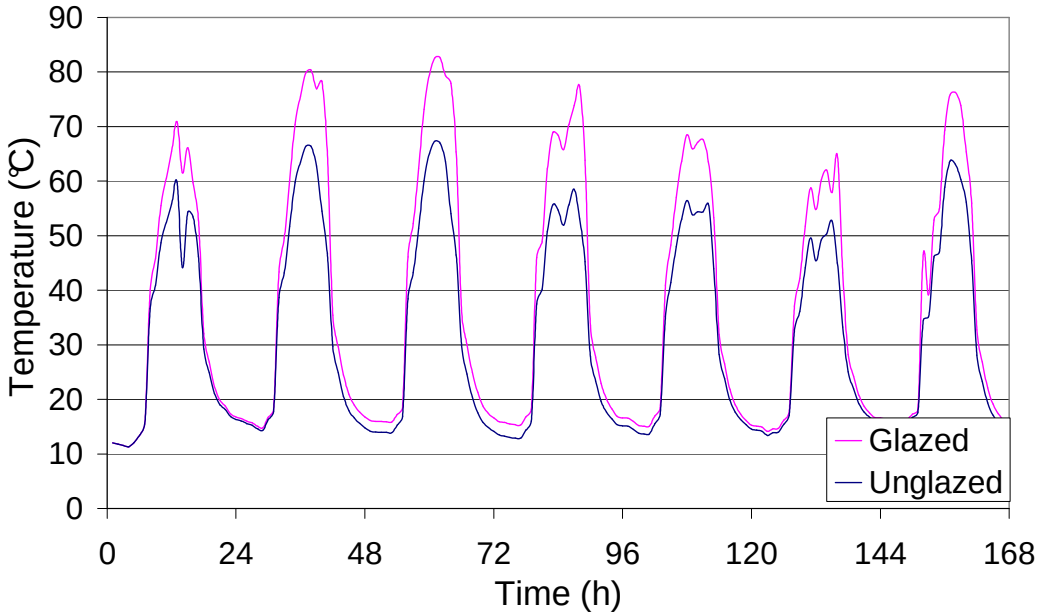

Figure 93: Cell temperatures for optimised glazed and unglazed BIPVT collectors during a summer week in Hamilton

6.6 Potential Pitfalls in the Design of BIPVT Systems

When looking at the design of the BIPVT the effect of "off design" operating conditions on the collector need to be considered. In the majority of the studies relating to PVT style collectors little, if any, consideration has been paid to the effect of non-ideal conditions on their performance. Given the sensitivity of these collectors to temperature, it is important to demonstrate not only the "ideal" performance but also to consider the effect of "poor" system design or failure on its performance.

6.6.1 The Effect of Stagnation on BIPVT Performance

One extreme example that needs to be taken into consideration for the design of a BIPVT is the effect of stagnation on the collector. In Figure 93 it was shown that the cell temperature was higher for a glazed collector than an unglazed collector. Now it is possible that in the event of a pump failure on a BIPVT system the collector could be subjected to severe stagnation conditions, particularly if no load is being drawn from the tank.

In Figure 94 it can be seen that under such conditions, the PV cell temperature would exceed 140°C. As this is in excess of the melting temperature of many common EVA encapsulants, it highlights the need to use encapsulants that are stable at high temperature, such as silicones, in the design of BIPVT collectors.

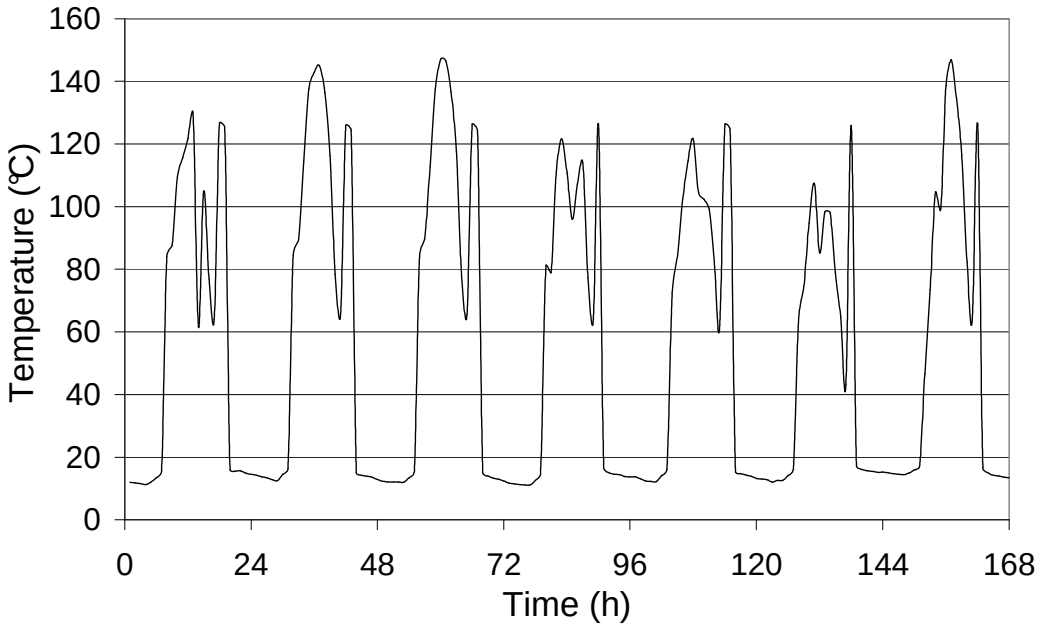

Figure 94: Cell temperatures in an optimised stagnating BIPVT collector during a summer week in Hamilton

6.6.2 The Effect of Oversizing on BIPVT Performance

Another potential problem that may occur during the operation of a BIPVT collector is the oversizing of the ratio of the collector area to storage volume. In the previous examples it has been assumed that a 4m^2 collector has been used with a 300L storage tank. However, if the same hot water load and collector area are maintained, but the storage volume is reduced by 50% to 150L the solar fraction is reduced (Figure 95) and the electrical output is also lowered (Figure 96). This is due to the tank being continually forced to operate at high temperatures which means that it dumps large amounts of hot water to avoid overpressure. Also the higher temperatures result in a significant decrease in the electrical efficiency.

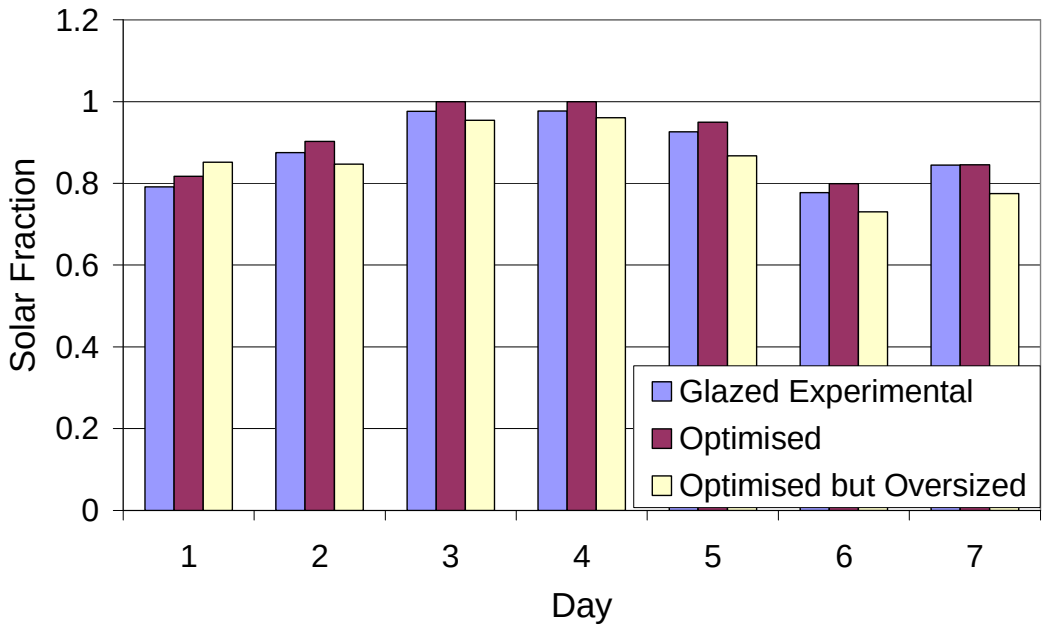

Figure 95: Solar fraction for an oversized BIPVT system during a summer week in Hamilton

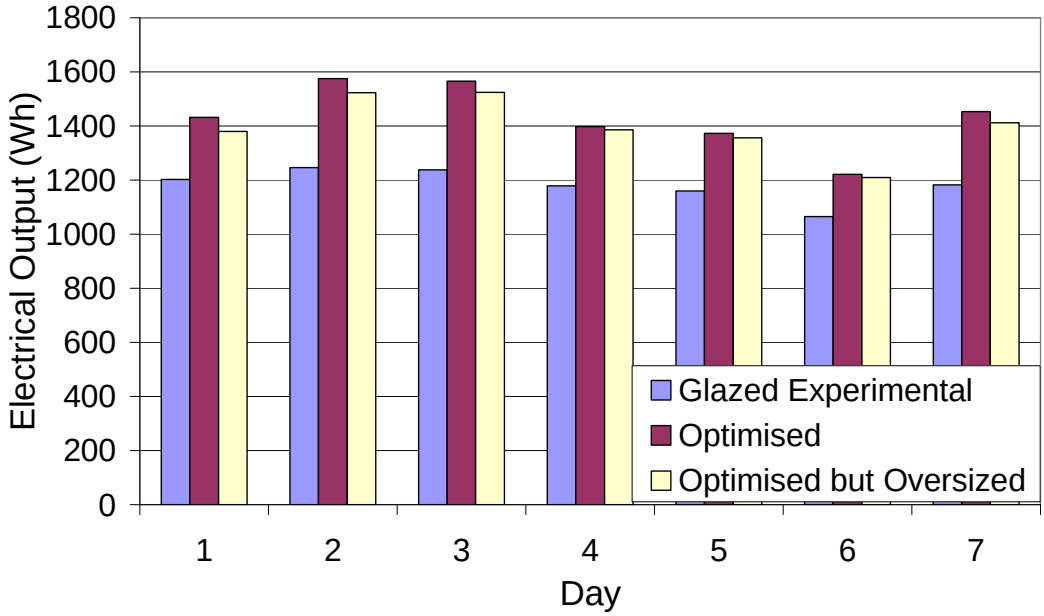

Figure 96: Daily electrical output from an oversized BIPVT system during a summer week in Hamilton

6.6.3 The Effect of Undersizing on BIPVT Performance

Taking the preceding example in the opposite direction, an undersized BIPVT system can also reduce performance. In the case of the $4m^2$ collector attempting to heat a storage volume of 900L the solar fraction is lower (Figure 97) due to the increased volume of water in the tank and the influence of stratification and thermal diffusivity on the delivered water temperature. However there is an advantage to having an oversized tank, namely that it tends to result in lower temperatures in the BIPVT, thereby improving electrical output (Figure 98).

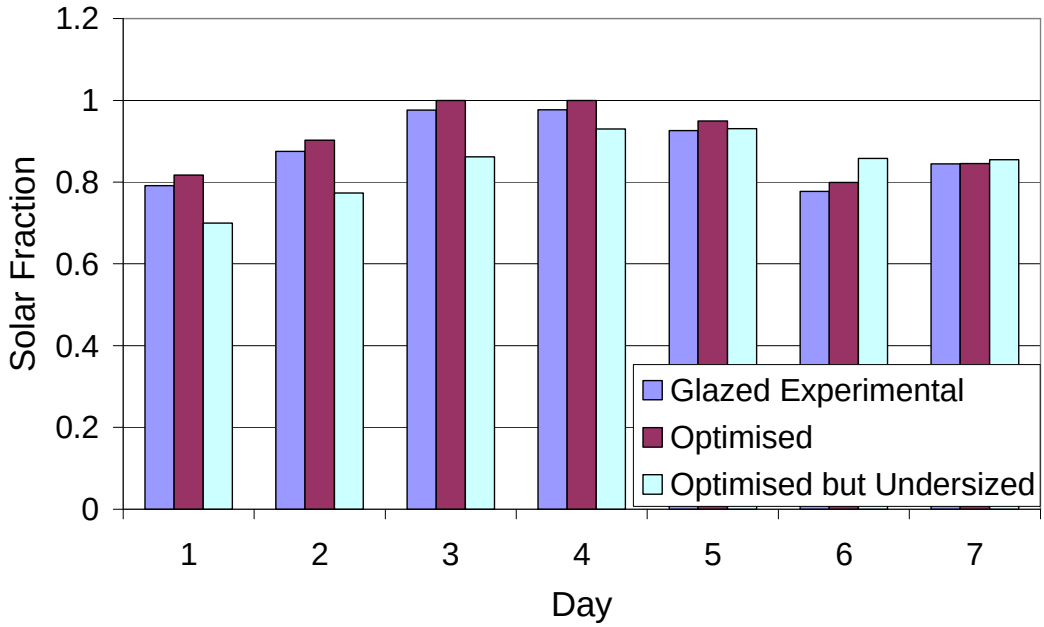

Figure 97: Solar fraction for an undersized BIPVT system during a summer week in Hamilton

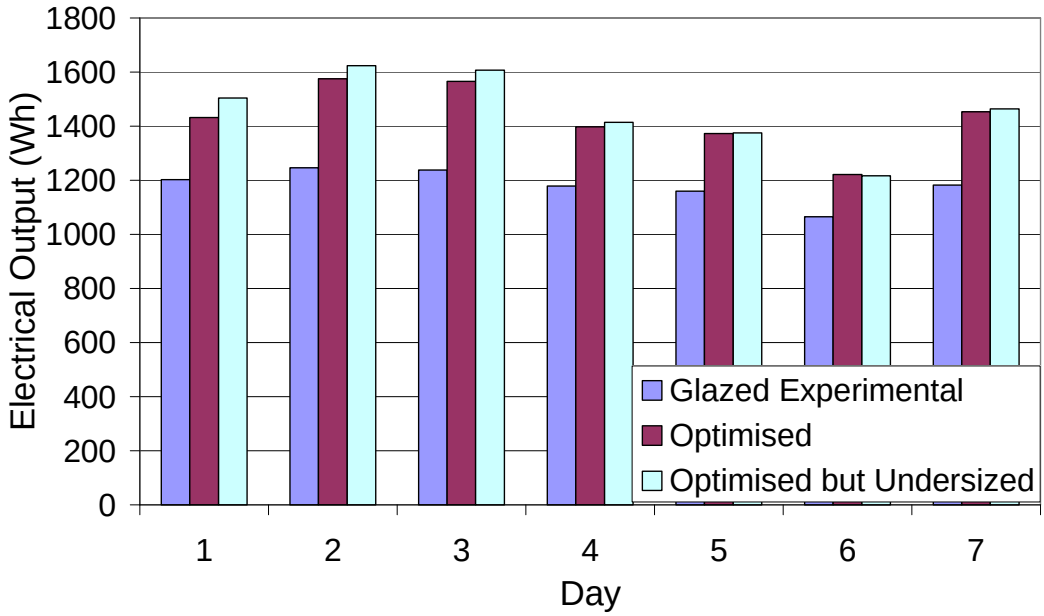

Figure 98: Daily electrical output from an undersized BIPVT system during a summer week in Hamilton

6.7 Conclusions from Long Term Performance Modelling of a BIPVT System

From the long-term modelling of the BIPVT system it is apparent that there are a number of issues to be addressed in the design of not only the system but also the collector.

The modelling showed that through optimising the collector, per the recommendations of Chapter 3, significant improvements could be made to the systems electrical and thermal output. Moreover, it was found that the use of the attic space as an insulation barrier, to reduce capital costs, did not significantly decrease the system's performance, if the collector was optimised.

Examination of some atypical operating conditions showed that the stagnation temperature of the collector could exceed 140°C and therefore potentially damage PV laminates with EVA encapsulation, thus suggesting the need for silicone encapsulation in glazed BIPVT.

Moreover, it was seen that both under- and over-sizing of the thermal storage could result in reduced thermal efficiency. The use of under-sized storage however is perhaps the worst situation, as it significantly reduces the electrical output from the collector, whereas an oversized system improves it.

Finally, the application that is chosen will most likely be determined by the economic assessment. Where generous subsidies exist for the generation of electricity from solar or renewable sources, there will be a drive to use an unglazed collector, as this will provide the highest electrical yield. However, in this situation the value of electrical energy in comparison to the value of thermal energy needs to be considered and ideally it should be considered for each particular location and the prevailing subsidisation arrangements.

Chapter 7: Conclusions and Recommendations for Future Work

7.1 Conclusions

In the current energy climate, in terms of both its consumption and supply, there is a growing need to consider the resources that are available and their sustainability for the future. This has led to an increased demand for the use of renewable energy sources and for more efficient use of energy.

The use of photovoltaic/thermal solar collectors presents a practicable alternative to traditional water heating methods. Furthermore, the use of building integrated cogeneration of heat and electrical power from solar energy is an area with significant potential growth. Although New Zealand's nearest neighbour, Australia, is a world leader in terms of the production of solar water heating systems and research in the field of photovoltaics, neither of these technologies have gained a significant foothold in the New Zealand market. However, there has been significant growth in the market worldwide for solar energy devices, and the use of a BIPVT has significant potential to harness this further.

In this study it was shown that there are some key points to be observed in developing a BIPVT collector and a number of areas where significant improvements can be made to the collectors' thermal performance. In particular the fin efficiency needs to be maximised if low conductivity coloured steel is to be used as the absorber. There is also a need to ensure a high level of thermal conductivity between the absorber and the PV cells (minimal bond resistance)

possibly through the use of high conductivity adhesives. Any improvements to increase the absorption of the PV cell should also be made to ensure that the smallest possible portion of the incident radiation is lost by reflection.

It was also demonstrated that when installing a BIPVT system, the insulation typically installed on the rear surface of a packaged solar water heating collector may be unnecessary for a cold-roof BIPVT collector. From the CFD and experimental work in this study it was found that the level of insulation provided by natural convection in an attic shaped enclosure was comparable to that encountered in a heavily insulated solar collector. When removing the rear insulation in a building-integrated situation, it needs to be considered that the heat loss from the BIPVT becomes particularly sensitive to the pitch of the roof. However, the heat loss from the rear surface of the collector can be suppressed by the addition of a passive baffle in the attic space; thus providing a low–cost alternative to installing any additional insulation.

Finally the transient analysis conducted in this study showed that when optimising the performance of a BIPVT system it is imperative to match the configuration and size of BIPVT with the intended application. In this study a number of potential applications were proposed, from swimming pool heating, to large combined heat and power systems for apartment complexes and individual houses. The transient simulation of a “typical” BIPVT system showed that the cooling provided by the system resulted in an improvement to the long-term

electrical output. Further, it was shown that the system was able to provide high solar-fractions of the typical water heating load for a residence in Hamilton.

The transient analysis conducted in this study also demonstrated that care needs to be taken in the selection of materials, particularly the PV encapsulant to ensure that it does not fail under stagnation conditions. Additionally, it showed that care needs to be taken in matching the collector size to the storage volume. If the storage volume is too small there is the possibility of overheating during summer and a subsequent reduction in electrical output, however if oversized, a portion of the heat input is lost through the cylinder venting at high temperatures to avoid over-pressure conditions.

Similarly, if the system is undersized the electrical performance will be good, but the solar heating fraction may be lower than required due to increased tank and mixing losses. Furthermore, the use of an unglazed collector may present a better alternative if high temperature heating is not required, such as an auxiliary or pre-heater or for swimming pool heating.

7.2 Recommendations for Future Work

Besides the remarks that have been made hitherto regarding the design of the BIPVT collector, there are a number of avenues that could be explored in the area in the future. In particular it would be interesting to examine control strategies and predictive controllers for energy management from a BIPVT. Such a system could

potentially be tailored to monitor weather conditions, and electricity prices on the spot market, to best determine when to buy, sell, store or dump energy.

It was noted that the BIPVT design had led to the development of low-cost building integrated thermal (BIT) systems (Appendix B) and also could be modified to form a water cooled V-trough concentrator. It is envisaged that these devices will also require significant development in the future, though many of the findings in this work translate directly to these.

Finally, apart from modifications to the design of the BIPVT collector, there is also a need to further our understanding of heat and mass transfer in the built environment. In particular, it was found in the CFD component of this study, that there appeared to be convection cells present along the length of the modelled enclosure. The presence of these cells has not been observed computationally in the studies of triangular enclosures, due to the assumption of 2-dimensional flow. The presence, behaviour and factors that affect these cells such as aspect ratio and the presence of baffles could present interesting challenges in the future.

References

Adelhelm, R. and Berger, D., 2003, "Requirements for a large area solar simulator regarding the measurement of MJ solar cells", *Proceedings of 3rd World Conference on Photovoltaic Energy Conversion*, May 2003, Osaka, pp. 821-824

Akinsete, V.A. and Coleman, T.A., 1982, "Heat transfer by steady laminar free convection in triangular enclosures", *International Journal of Heat and Mass Transfer*, Vol. 25, No. 7, pp. 991-998

Al-Shariah, A.M. and Ecevit, A., 1992, "Natural convective heat transfer in a triangular enclosure having various aspect ratios and inclination angles", *Doga Turkish Journal of Physics*, Vol. 16, No. 5, pp. 340-352

Anderson, T.N., 2004, *Advanced Heat Pump Water Heaters*, ME Thesis, University of New South Wales, Sydney

Anderson, T.N. and Morrison, G.L., 2007, "Effect of load pattern on solar-boosted heat pump water heater performance", *Solar Energy*, Vol. 81, pp. 1386–1395

Anderson, B.R. and Ward, T.I., 1981, "Measurements of the heat loss through an insulated roof", *Building Services Engineering Research and Technology*, Vol. 2, No. 2, pp. 65-72

Anderson, T.N., Duke, M. and Carson, J.K., 2007, "A Typical Meteorological Year for Energy Simulations in Hamilton, New Zealand", *Transactions of Engineers New Zealand, Engineering TreNZ*, 2007-003

Anderson, T.N., Duke, M. and Carson, J.K., 2009, "Performance of coloured solar collectors", *Proceedings of ICAE'09 1st International Conference on Applied Energy*, January 2009, Hong Kong

Anderson, T.N., Duke, M., Morrison G.L. and Carson, J.K., 2009, "Performance of a Building Integrated Photovoltaic/Thermal (BIPVT) Solar Collector", *Solar Energy*, Vol. 83, No. 4, pp. 445-455

Andrews, J.W., 1981, "*Evaluation of flat-plate photovoltaic/thermal hybrid systems for solar energy utilization*", US Department of Energy, Report No. BNL—51435

Aramayo A1., Esteban S. and Cardon L., 2002 (a), "Conveccion natural a elevado numero de Rayleigh en recintos triangulares rectangulares enfriados por arriba Parte I: flujo de calor", *Avances en Energías Renovables y Medio Ambiente*, Vol. 6, No. 2, pp. 8.43-8.48

Aramayo A1., Esteban S. and Cardon L., 2002 (b), "Conveccion natural a elevado numero de Rayleigh en recintos triangulares rectangulares enfriados por arriba

Parte II: patrones de flujo del fluido", *Avances en Energías Renovables y Medio Ambiente*, Vol. 6, No. 2, pp. 8.49-8.53

Asan, H. and Namli, L., 2000, "Laminar natural convection in a pitched roof of triangular cross-section: Summer day boundary conditions", *Energy and Buildings*, Vol. 33, No. 1, pp. 69-73

Asan, H. and Namli, L., 2001, "Numerical simulation of buoyant flow in a roof of triangular cross-section under winter day boundary conditions", *Energy and Buildings*, Vol. 33, No. 7, pp. 753-757

Assoa, Y.B., Menezo, C., Fraisse, G., Yezou, R. and Brau, J., 2007, "Study of a new concept of photovoltaic-thermal hybrid collector", *Solar Energy*, Vol. 81, No. 9, pp. 1132-1143

AS/NZS 2535.1, 1999, "*Test methods for solar collectors Part 1: Thermal performance of glazed liquid heating collectors including pressure drop*", Standards Australia, Homebush

AS 4234-1994, 1994, "*Solar water heaters- Domestic and heat pump- Calculation of energy consumption*", Standards Australia, Sydney

Bakker, M., Zondag, H.A. and van Helden, W.G.J., 2002, "Design of a dual flow photovoltaic/thermal combi-panel", in *PV in Europe*, Rome, 2002

Bartelsen, B., Rockendorf, G., Vennemann, N., Tepe, R., Lorenz, K., and Purkarthofer, G., 1999, "Elastomer-metal-absorber: development and application", *Solar Energy*, Vol. 67, Nos. 4–6, pp. 215–226

Bazilian, M.D., Leenders, F., van Der Ree, B.G.C. and Prassad, D., 2001, "Photovoltaic cogeneration in the built environment", *Solar Energy*, Vol. 71, No. 1, pp.57-69

Bazilian, M.D., Kamalanathan, H., and Prasad, D., 2002, "Thermographic analysis of a building integrated photovoltaic system", *Renewable Energy*, Vol. 26, No. 3, pp. 449-461

Bejan, A., 2004, "*Convection Heat Transfer*", Wiley, New York

Benseman, R.F. and Cook, F.W., 1969, "Solar radiation in New Zealand – The standard year and radiation on inclined surfaces", *New Zealand Journal of Sciences*, Vol. 12, pp. 696-708

Bergene, T. and Lovvik, O.M., 1995, "Model calculations on a flat-plate solar heat collector with integrated solar cells", *Solar Energy*, Vol. 55, No. 6, pp. 453-462

Blach, A.E., Hoa, V.S., Kwok, C.K. and Ahmed, A.K.W., 1990, "Rectangular pressure vessels of finite length", *Journal of Pressure Vessel Technology, Transactions of the ASME,* Vol. 112, pp. 50-56

Boussaid, M., Djerrada, A, and Bouhadef, M., 2003, "Thermosolutal transfer within trapezoidal enclosure", *Numerical Heat Transfer, Part A*, Vol. 43, pp. 431–448

Boyle, G., 2004, "*Renewable Energy: Power for a sustainable future*", Oxford University Press, Oxford

Brinkworth, B.J., 2006, "Optimum depth for PV cooling ducts", *Solar Energy*, Vol. 80, pp.1131-1134

Canadian Renewable Energy Network, 2006, [cited 13/09/2006], http://www.canren.gc.ca

Cengel, Y.A., 1998, "*Heat Transfer-A Practical Approach*", McGraw Hill, Boston

Chow, T.T., He, W. and Ji, J., 2006, "Hybrid photovoltaic-thermosyphon water heating system for residential application", *Solar Energy*, Vol. 80, pp. 298-306

Chow, T.T., He, W. and Ji, J., 2007, "An experimental study of facade-integrated

photovoltaic/water-heating system", *Applied Thermal Engineering*, Vol. 27, pp. 37–45

Colon, C.J., and Merrigan, T., 2001, "Roof integrated solar absorbers: The measured performance of "invisible" solar collectors", *Proceedings of the International Solar Energy Conference 2001*, Washington D.C., pp. 151-159

Cosmos, 2006, "*COSMOSFloWorks Fundamentals*", Solidworks Corporation, Concord

Coventry, J.S., 2004, *A solar concentrating photovoltaic/thermal collector*, PhD Thesis, Australian National University, Canberra

Coventry, J.S., 2005, "Performance of a concentrating photovoltaic/thermal solar collector", *Solar Energy*, Vol. 78, No. 2, pp. 211-222

Crawley, D.B., 1998, "Which weather data should you use for energy simulations of commercial buildings?", *ASHRAE Transactions*, Vol. 104, pp. 498-515

de Vahl Davis, G., 1983, "Natural convection of air in a square cavity: a benchmark numerical solution", *International Journal for Numerical Methods in Fluids*, Vol. 3, No. 3, pp. 249-264

de Vries, D.W., 1998, *Design of a photovoltaic/thermal combi-panel*, PhD Thesis, Eindhoven University, Eindhoven

Dietz, A.G.H., 1954, "Diathermous materials and properties of surfaces", in *Space Heating with Solar Energy*, MIT Press, Cambridge, Massachusetts

Duffie, J.A. and Beckman, W.A., 2006, "*Solar engineering of thermal processes*", Wiley, New York

Duke, M.D., 2006, "An energy conversion system", *New Zealand Patent 546718*

EECA, 2001, "*Solar Energy Use and Potential in New Zealand*", Energy Efficiency and Conservation Authority, Wellington

EECA, 2004, "*Code of Practice for Manufacture and Installation of Solar Water Heating Systems in New Zealand*", Energy Efficiency and Conservation Authority, Wellington

EECA, 2006, "*EECA Energy End Use Database*" [cited 28/08/2006], http://www.eeca.govt.nz/enduse/index.aspx

Eicker, U., 2003, *Solar technologies for buildings*, John Wiley and Sons, Chichester

Flack, R.D., Konopnicki, T.T. and Rooke, J.H., 1979, "The measurement of natural convective heat transfer in triangular enclosures", *Journal of Heat Transfer, Transactions of the ASME,* Vol. 101, No. 4, pp. 648-654

Flack, R. D. and Witt, C. L., 1979, "Velocity measurements in two natural convection air flows using a laser velocimeter", *Journal of Heat Transfer, Transactions of the ASME,* Vol. 101, No. 2, pp. 256-260

Flack, R. D., 1980, "The experimental measurement of natural convection heat transfer in triangular enclosures heated or cooled from below", *Journal of Heat Transfer, Transactions of the ASME,* Vol. 102, pp. 770-772

Florschuetz, L.W., 1979, "Extension of the Hottel-Whillier model to the analysis of combined photovoltaic/thermal flat plate collectors", *Solar Energy*, Vol. 22, No. 4, pp. 361-366

Fuentes, M.K., 1987, "*A simplified thermal model for flat-plate photovoltaic arrays*", Sandia National Laboratories Report, SAND85-0330-UC-63, Albuquerque

Garg, H.P. and Adhikari, R.S., 1999, "Performance analysis of a hybrid photovoltaic/thermal (PV/T) collector with integrated CPC troughs", *International Journal of Energy Research,* Vol. 23, No. 15, pp. 1295-1304

Garg, H.P. and Agarwal, R.K., 1995, "Some aspects of a PV/T collector/forced circulation flat plate solar water heater with solar cells", *Energy Conversion and Management*, Vol. 36, No. 2, pp. 87-99

Garg, H.P., Shukla, A.R., Indrajit, Madhuri, Agnihotri, R.C. and Chakravertty, S., 1985, "Development of a simple low-cost solar simulator for indoor collector testing", *Applied Energy*, Vol. 21, No. 1, pp. 43-54

Green, M., 1998, *Solar Cells: Operating Principles, Technology and System Applications*, The University of New South Wales, Kensington, Australia

Green, M.A. and Keevers, M.J., 1995, "Optical properties of intrinsic silicon at 300 K", *Progress in Photovoltaics: Research and Applications*, Vol. 3, No. 3, pp. 189-192

Guo, Y.Z. and Zeng, Z.J., 1997, "The six-plate analytical method for rectangular pressure vessels of finite length", *International Journal of Pressure Vessels and Piping*, Vol. 74, pp. 1-6

He, W., Chow, T.T., Lu, J., Pei, G., Chan, L., 2006, "Hybrid photovoltaic and thermal solar-collector designed for natural circulation of water", *Applied Energy*, Vol.83, pp.199-210

Hegazy, A.A., 2000, "Comparative study of the performances of four photovoltaic/thermal solar air collectors", *Energy Conversion and Management*, Vol. 41, No. 8, pp. 861-881

Holman, J.P., 1997, *Heat Transfer*, McGraw Hill, New York

Holman, J.P., 2001, *Experimental Methods for Engineers*, McGraw Hill, New York

Holtzman, G.A., Hill, R.W. and Ball, K.S., 2000, "Laminar natural convection in isosceles triangular enclosures heated from below and symmetrically cooled from above", *Journal of Heat Transfer, Transactions of the ASME*, Vol. 122, No. 3, pp. 485-491

Huang, B.J., Lin, T.H., Hung, W.C. and Sun, F.S., 2001, "Performance evaluation of solar photovoltaic/thermal systems", *Solar Energy*, Vol. 70, No. 5, pp. 443-448

Incropera, F.P. and DeWitt, D.P., 2002, *Introduction to heat transfer*, Wiley, New York

IEA PVPS (International Energy Agency Photovoltaic Power Systems Programme), 2005, "*Trends in Photovoltaic Applications - Survey report of selected IEA countries between 1992 and 2004*", Report IEA-PVPS T1-14:2005

IEA SHC (International Energy Agency Solar Heating and Cooling Programme), 2006, "*Solar Heat Worldwide – Markets and Contribution the Energy Supply 2004*"

ISO 9806-3, 1995, *Test methods for solar collectors: Thermal performance of unglazed liquid heating collectors*

Ji, J., Han, J., Chow, T.-T., Han, C., Lu, J. and He, W., 2006, Effect of flow channel dimensions on the performance of a box-frame photovoltaic/thermal collector, *Journal of Power and Energy, Proceedings of the Institution of Mechanical Engineers, Part A,* Vol. 220, No. A7, pp. 681-688

Kalogirou, S. Tripanagnostopoulos, Y. and Souliotis, M, 2005, "Performance of solar systems employing collectors with colored absorber", *Energy and Buildings*, Vol. 37, pp. 824-835

Kalogirou, S.A. and Tripanagnostopoulos, Y., 2007, "Industrial application of PV/T solar energy systems", *Applied Thermal Engineering*, Vol. 27, No. 8-9, pp. 1259-1270

Kang, M.C., Kang, Y.H., Lim, S.H., and Chun, W., 2006, "Numerical analysis on the thermal performance of a roof-integrated flat-plate solar collector assembly", *International Communications in Heat and Mass Transfer*, Vol. 33, pp. 976–984

Karyakin, Y.E., Martynenko, O.G., Sokovishin, Y.A. and Ustok, K.Z., 1985, "Numerical simulation of unsteady-state natural convection in triangular enclosures", *Heat Transfer - Soviet Research*, Vol. 17, No. 3, pp. 1-33

Kind, R.J. and Kitaljevich, D., 1985, "Wind induced heat losses from solar collector arrays on flat-roofed buildings", *Transactions of ASME, Journal of Solar Energy Engineering*, Vol. 107, pp. 335-341

Knowles, E. (Ed.), 2005, *The Oxford Dictionary of Quotations*, Oxford University Press, Oxford

Krauter, S.C.W., 2006, *Solar electric power generation: Photovoltaic energy systems*, Springer-Verlag, Heidelberg

Kribus, A., Kaftori, D., Mittelman, G., Hirshfeld, A., Flitsanov, Y., and Dayan, A., 2006, "A miniature concentrating photovoltaic and thermal system", *Energy Conversion and Management*, Vol. 47, No. 20, pp. 3582-3590

Medved, S., Arkar, C., and Cerne, B., 2003, "A large-panel unglazed roof-integrated liquid solar collector—energy and economic evaluation", *Solar Energy*, Vol. 75, pp. 455–467

Morrison, G.L. and Litvak, A., 1988, *Condensed Solar Radiation Data Base for Australia*, School of Mechanical and Manufacturing Engineering, University of New South Wales, FMT/1

Mosfegh, B. and Sandberg, M, 1998, "Flow and heat transfer in the air gap behind photovoltaic panels", *Renewable and Sustainable Energy Reviews*, Vol. 2, pp.287-301

Moukalled, F. and Acharya, S., 2001, "Natural Convection in a Trapezoidal Enclosure with Offset Baffles", *Journal of Thermophysics and Heat Transfer*, Vol. 15, No. 2, pp 212-218

National Institute of Water and Atmosphere (NIWA), 2007, *Climate Summaries*, www.niwascience.co.nz [cited 20/8/07]

National Renewable Energy Laboratory (NREL), 2008, *Solar Irradiance Spectrum: Air Mass 1.5*,
http://rredc.nrel.gov/solar/spectra/am1.5/ [cited 10/10/2008]

Othman, M.Y.H., Yatim, B., Sopian, K., and Bakar, M.N.A., 2005, "Performance analysis of a double-pass photovoltaic/thermal (PV/T) solar collector with CPC and fins", *Renewable Energy*, Vol. 30, No. 13, pp. 2005-2017

Probst, M.M., and Roecker, C., 2007, "Towards an improved architectural quality of building integrated solar thermal systems (BIST)", *Solar Energy*, Vol. 81, pp. 1104–1116

Poulikakos, D. and Bejan, A., 1983 (a), "The fluid dynamics of an attic space", *Journal of Fluid Mechanics*, Vol. 131, pp. 251-269

Poulikakos, D. and Bejan, A., 1983 (b), "Numerical study of transient high Rayleigh number convection in an attic-shaped porous layer", *Journal of Heat Transfer, Transactions of the ASME*, Vol. 105, No. 3, pp. 476-484

PV Catapault, 2005, *PVT ROADMAP A European guide for the development and market introduction of PV-Thermal technology*

Raffel, M., 1998, *Particle image velocimetry: a practical guide*, Springer, Berlin

Raman, V. and Tiwari, G.N., 2008, "Life cycle cost analysis of HPVT air collector under different Indian climatic conditions", *Energy Policy*, Vol 36, No. 2, pp 603-11

Rawlinson's, 2005, *Rawlinson's New Zealand construction handbook with cd-rom*, Rawlinson's, Auckland

Ridouane, E.H. and Campo, A., 2005, "Experimental-based correlations for the characterization of free convection of air inside isosceles triangular cavities with variable apex angles", *Experimental Heat Transfer*, Vol. 18, No. 2, pp. 81-86

Ridouane, E.H., Campo, A. and Hasnaoui, M., 2006, "Turbulent natural convection in an air-filled isosceles triangular enclosure", *International Journal of Heat and Fluid Flow*, Vol. 27, No. 3, pp. 476-489

Ridouane, E.H. and Campo, A., 2007, "Effects of attaching baffles onto the inclined walls of attic frames for purposes of energy conservation", *Heat Transfer Engineering*, Vol. 28, No. 2, pp.103-111

Rosell, J.I., Vallverdu, X., Lechon, M.A and Ibanez, M, 2005, "Design and simulation of a low concentrating photovoltaic/thermal system", *Energy Conversion and Management*, Vol. 46, No. 18-19, pp. 3034-3046

Santbergen, R. and van Zolingen, R.J.C., 2006, "Modeling the thermal absorption factor of photovoltaic/thermal combi-panels", *Energy Conversion and Management*, Vol. 47, pp. 3572–3581

Schuler, A., Roecker, C., Scartezzini, J.-L., Boudaden, J., Videnovic, I.R., Ho, R.S.-C. and Oelhafen, P., 2004, "On the feasibility of colored glazed thermal solar collectors based on thin film interference filters", *Solar Energy Materials & Solar Cells*, Vol. 84, pp. 241-254

Schuler, A., Boudaden, J., Oelhafen, P., De Chambrier, E., Roecker, C. and Scartezzini, J.-L., 2005 a, "Thin film multilayer design types for colored glazed thermal solar collectors", *Solar Energy Materials & Solar Cells*, Vol. 89, pp. 219-231

Schuler, A., Roecker, C., Boudaden, J., Oelhafen, P. and Scartezzini, J.-L., 2005 b, "Potential of quarterwave interference stacks for colored thermal solar collectors", *Solar Energy*, Vol. 79, pp. 122-130

Siegel, J and Howell, J., 2002, *Thermal Radiation Heat Transfer*, Taylor and Francis, New York

Solar Energy Laboratory (SEL), 2007, *TRNSYS 16 User Manuals*, Solar Energy Laboratories, Madison

SPF, 2007, *SPF Info*, www.solarenergy.ch [cited 20/8/07]

Swiss Federal Office of Energy, 2000, *New generation of Hybrid Solar PV/T collectors*, Final Report DIS 56360 / 16868

Statistics NZ, 2001, *2001 Census of Population and Dwellings*, Statistics New Zealand, Wellington

Tiedemann, T.F. and Maytrott, C.W., 1997, "Indoor testing using a large area solar simulator", *Proceedings of International Solar Energy Conference*, April 1997, pp. 297-304

Tiwari, A. and Sodha, M.S., 2007, "Parametric study of various configurations of hybrid PV/thermal air collector: Experimental validation of theoretical model", *Solar Energy Materials and Solar Cells*, Vol. 91, No. 1, pp. 17-28

Tonui, J.K. and Tripanagnostopoulos, Y., 2007a, "Improved PV/T solar collectors with heat extraction by forced or natural air circulation", *Renewable Energy*, Vol. 32, No. 4, pp. 623-637

Tonui, J.K. and Tripanagnostopoulos, Y., 2007b, "Air-cooled PV/T solar collectors with low cost performance improvements", *Solar Energy*, Vol. 81, No. 4, pp. 498-511

Tripanagnostopoulos, Y., Souliotis, M and Nousia, T., 2000, "Solar collectors with colored absorbers", *Solar Energy*, Vol. 28, No.4, pp.343-356

Tripanagnostopoulos, Y., Nousia, T., Souliotis, M. and Yianoulis, P., 2002, "Hybrid photovoltaic/thermal solar systems", *Solar Energy*, Vol. 72, No. 3, pp.217-234

Van der Werff, I., Amor, R. and Donn, M., 2003, *Standard data files for computer thermal simulation of solar low energy non-residential buildings*, Energy Research Group, School of Architecture, Victoria University, Wellington

van Helden, W.G.J., van Zolingen, R.J.C. and Zondag, H.A., 2004, "PV thermal systems: PV panels supplying renewable electricity and heat", *Progress in Photovoltaics: Research and Applications*, Vol. 12, pp. 415-426

Versteeg, H.K. and Malalasekera, W., 1995, *An introduction to computational fluid dynamics: the finite volume method*, Prentice Hall, Harlow, England

Vokas, G., Christandonis, N., and Skittides, F., 2006, "Hybrid photovoltaic-thermal systems for domestic heating and cooling-A theoretical approach", *Solar Energy*, Vol. 80, No. 5, pp. 607-615

Watmuff, J.H., Charters, W.W.S., and Proctor, D., 1977, "Solar and wind induced external coefficients for solar collectors", *Comples No. 2, 56*

Weiss, W and Stadler, I., 2001, "Façade integration – a new and promising opportunity for thermal solar collectors", *Proceedings of the Industry Workshop of the IEA Solar Heating and Cooling Programme*, Task 26, Delft

Zondag, H.A., 2008, "Flat-plate PV-Thermal collectors and systems: A review", *Renewable and Sustainable Energy Reviews*, Vol. 12, No. 4, pp. 891-959

Zondag, H.A., de Vries, D.W., van Helden, W.G.J., van Zolingen, R.J.C., and van Steenhoven, A.A., 2002, "The thermal and electrical yield of a PV-thermal collector", *Solar Energy*, Vol. 72, No. 2, pp.113-128

Zondag, H.A., de Vries, D.W., van Helden, W.G.J., van Zolingen, R.J.C. and van Steenhoven, A.A., 2003, "The yield of different combined PV-thermal collector designs", *Solar Energy*, Vol. 74, No. 3, pp. 253-269

Zondag, H.A., van Helden, W.G.J., Elswijk, M.J., and Bakker, M., 2004, "PV-thermal collector development – an overview of the lessons learnt", *Proceeding of the 19th European PV Solar Energy Conference and Exhibition*, June, 2004, Paris

Zondag, H.A., van Helden, W.G.J., Bakker, M., and Elswijk, M.J., 2005, "A roadmap for the development and market introduction of PVT technology", Presented at *15th Symposium Thermische Solarenergie*, Bad Staffelstein, Germany, 27-29 April 2005

Appendix A: Uncertainty Analysis

A.1 Uncertainty in BIPVT and Solar Collector Testing

All thermocouples used in the solar testing were 3mm T-type MIMS thermocouples. The thermocouples were calibrated to a secondary standard against a platinum resistance thermometer, with an accuracy of ±0.05K, using a temperature controlled circulating water bath and a five point calibration for temperatures in the range 0°C to 100°C. The thermocouple temperatures were monitored using a Picolog TC-08 eight channel thermocouple DAQ system connected to a computer via the USB interface and manually recorded. The standard deviation for the thermocouples was found to be less than 0.2K. Considering the accuracy of the platinum resistance thermometer and that of the thermocouples, the uncertainty of the temperature sensors was conservatively taken to be ±0.3K.

The flow of water through the collector was set at a constant rate and monitored throughout the testing periods by manually measuring the time taken for a known mass to pass through the collector. The standard deviation for this was found to be approximately 3% of the measurement, conservatively taken to be 5% of the reading.

The pyranometer used in the testing was a Middleton Solar EQ08-E First Class Pyranometer (Calibration Certificate Number C2830) with a certainty of ±3% of the reading.

To determine the uncertainty in the collector testing, the method proposed by Kline and McClintock as cited by Holman (2001) was used, where the calculated result of the measurements (R) is a function of the independent variables used in its calculation ($x_1, x_2, x_3,\ldots, x_n$). In general terms this can be expressed as shown in Equation 48.

$$R = R(x_1, x_2, x_3, ..., x_n) \tag{48}$$

For a series of measurements in which it is assumed that the uncertainty of each measurement has the same odds of occurring, the uncertainty of the result (w_R) is a function of the uncertainty of the independent variables ($w_1, w_2, w_3,\ldots, w_n$) as shown in Equation 49.

$$w_R = \sqrt{\left(\frac{\partial R}{\partial x_1} w_1\right)^2 + \left(\frac{\partial R}{\partial x_2} w_2\right)^2 + ... + \left(\frac{\partial R}{\partial x_n} w_n\right)^2} \tag{49}$$

When determining the uncertainty in collector efficiency, the collector efficiency (η) is a function of the mass flowrate (m), inlet temperature (T_i), outlet temperature (T_o), solar radiation ($G"$), collector area ($A_{collector}$) and fluid specific heat (C_p) as shown in Equation 50.

$$\eta = \frac{mC_p(T_o - T_i)}{AG"} \tag{50}$$

Therefore the uncertainty in determining the collector efficiency, assuming uncertainty in the collector area and specific heat are zero, is given by Equation 51.

$$w_\eta = \sqrt{\left(\frac{\partial \eta}{\partial m} w_m\right)^2 + \left(\frac{\partial \eta}{\partial T_o} w_{T_o}\right)^2 + \left(\frac{\partial \eta}{\partial T_i} w_{T_i}\right)^2 + \left(\frac{\partial \eta}{\partial G''} w_{G''}\right)^2} \tag{51}$$

Where:

$$\frac{\partial \eta}{\partial m} = \frac{C_p (T_o - T_i)}{AG''}$$

$$\frac{\partial \eta}{\partial T_o} = \frac{mC_p}{AG''}$$

$$\frac{\partial \eta}{\partial T_i} = \frac{-mC_p}{AG''}$$

$$\frac{\partial \eta}{\partial G''} = \frac{mC_p (T_o - T_i)}{AG''^2}$$

By substituting the values of the measurements and the associated uncertainty for testing of the glazed BIPVT the uncertainty in thermal efficiency is approximately ±10%, and for the unglazed BIPVT the uncertainty is approximately ±7%.

A.2 Uncertainty in Natural Convection Measurements

As with the BIPVT and solar collector testing, T-type thermocouples were used in the determination of the natural convective heat transfer coefficients in the model

attic enclosure. The thermocouples were calibrated to a secondary standard against a platinum resistance thermometer, with an accuracy of ±0.05K, using a temperature controlled circulating water bath and a five point calibration for temperatures in the range 0°C to 100°C. The thermocouple temperatures were monitored using a Picolog TC-08 eight channel thermocouple DAQ system connected to a computer via the USB interface and manually recorded. The standard deviation for the thermocouples was found to be less than 0.2K. Considering the accuracy of the platinum resistance thermometer and that of the thermocouples, the uncertainty of the temperature sensors was conservatively taken to be ±0.3K.

Therefore, when calculating the heat losses by conduction, the uncertainty is a function of the hot side temperature (T_h), the cold side temperature (T_c), the wall area (A), the wall thickness (L) and the insulation conductivity (k). However, the uncertainty in the final three parameters is unlikely to be as large as that of the temperatures and so the uncertainty in the conduction heat loss becomes a function of the hot and cold temperatures as shown in Equation 52.

$$w_{Q_{cond}} = \sqrt{\left(\frac{\partial Q}{\partial T_h} w_{T_h}\right)^2 + \left(\frac{\partial Q}{\partial T_c} w_{T_c}\right)^2} \tag{52}$$

Now taking a worst case scenario, in which the hot and cold side temperatures are both equal at 20°C the uncertainty in the determination of the conduction heat loss, is as shown:

$$w_{Q_{cond}} = \sqrt{\left(\frac{0.3}{20}\right)^2 + \left(\frac{0.3}{20}\right)^2}$$

This results in a very conservative maximum uncertainty for all conduction heat losses of ±2%. Furthermore, it should be noted that as the hot wall temperature increases the uncertainty begins to reduce.

In addition to the uncertainty of the calculated conduction heat losses, there is also an uncertainty associated with the neglecting of radiation. This was discussed in the analysis of the experiment, where it was found that radiation resulted in less than 5% of the heat transfer. Therefore, in determining the uncertainty in the convection heat transfer, it is estimated that the uncertainty of the radiation term is ±5%. Finally, the uncertainty of the electrical power meter is ±2%.

Therefore, having determined the uncertainty associated with the conduction, radiation and electrical heat loads. The uncertainty in determining the heat transfer by convection is given by Equation 53.

$$w_{Q_{convection}} = \sqrt{w_{Q_e}{}^2 + w_{Q_{end,cond}}{}^2 + w_{Q_{back,cond}}{}^2 + w_{Q_{base,cond}}{}^2 + w_{Q_{rad}}{}^2} \quad (53)$$

By substituting the uncertainty values into this, it is found that the uncertainty in the convection heat transfer is approximately ±6%.

Subsequently it is possible to determine the uncertainty associated with the derivation of the natural convection heat transfer coefficient (h_c) which is a function of the convective heat transfer ($Q_{convection}$), heater area (A_h), the heater temperature (T_h) and the cold side temperature (T_c) as shown in Equation 54.

$$h_c = \frac{Q_{convection}}{A_h(T_h - Tc)} \tag{54}$$

Assuming that the uncertainty associated with the area is negligible; the uncertainty of the heat transfer coefficient becomes a relationship of the temperatures and heat transfer as shown in Equation 55.

$$w_{h_c} = \sqrt{\left(\frac{\partial h_c}{\partial Q_{convection}} w_{Q_{convection}}\right)^2 + \left(\frac{\partial h_c}{\partial T_h} w_{T_h}\right)^2 + \left(\frac{\partial h_c}{\partial T_c} w_{T_c}\right)^2} \tag{55}$$

This results in an uncertainty of approximately ±6% in the heat transfer coefficient (as the uncertainty of the temperature terms are small relative to the convection term).

Similarly, the error associated with the experimental Nusselt number is also ±6% assuming the characteristic height of the enclosure and the conductivity of air is also negligible.

Appendix B: Performance of Coloured Solar Collectors

B.1 Introduction

When examining solar collectors one could be excused for believing that they can have them "painted any colour … so long as it is black", as Henry Ford famously stated about the Model T Ford (Knowles, 2005). Until relatively recently, the idea of not using either a black, or other selective surface, coating appears to have avoided attention in the literature. The irony of significant amounts of research money and time being invested into developing high performance selective and black surfaces is that it misses the fact that, according to Weiss and Stadler (2001), 85% of architects would prefer solar collectors in colours other than black, irrespective of the effect it may have on the system performance.

Tripanagnostopoulos et al. (2000) were perhaps the first researchers to seriously address the issue of coloured absorbers for solar collectors. In their study they examined the performance of unglazed and uninsulated, unglazed and insulated and glazed and insulated solar collectors that were black, blue and brown in colour. They showed that the efficiency of the collectors was actually quite similar despite their external appearance. Further they proposed the use of reflectors as a means of augmenting the performance of their collectors. In a follow-up study by Kalogirou et al. (2005), it was found that although coloured absorbers required higher levels of auxiliary heating, in a large domestic water heating application, the thermal output was only 18% lower than collectors with a selective surface.

In another recent study Medved et al. (2004) demonstrated the use of a brown unglazed solar collector for swimming pool heating. Although the influence of colour was not an objective of their study, they note that their collector could achieve efficiencies of approximately 74% if it were optimised.

As an alternative to using a coloured absorber, Schuler et al. (2004, 2005 a and b) examined the use of coloured glazing as a means of changing the appearance of solar thermal collectors. In these studies thin film interference filters and multilayer optical stacks are presented as a means of achieving a coloured appearance from the glazing placed over the standard selective surface absorbers. The downside however, as the authors mention, is that there is still significant development needed to prove these glazings, both in terms of manufacturability and operational life.

Therefore, in light of the lack of data relating to the performance of coloured solar collectors the aim of this study was to examine how colour influenced the efficiency of solar thermal collectors.

B.2 Collector Design

Unlike many commercially available collectors, and those of Tripanagnostopoulos et al. (2000), the collectors in this study were not constructed from finned copper tubes Instead the collectors were fabricated from two colour coated mild steel sheets that were folded to form a rectangular cross section tube. Additionally

mineral wool insulation was placed behind the absorber sheet and a low-iron glass cover above the collector as shown in Figure 99.

Although the fabrication of finned copper tube style collectors is well understood, the unconventional design of the collector, and the desire for it to be made from relatively low-cost pre-coated steel, presented a number of challenges. The main challenge is due to the fact that the material is galvanised and coated in paint. As such the material cannot be welded without removing both these coatings. In order to circumvent this issue, it was decided to bond the secondary folded sheet to the coloured absorber with a high temperature Silicone adhesive.

Due to the batch production nature of the prototype, the secondary sheet was folded using a brake press, holes were drilled to allow fluid into the underside of the rectangular tube, nipples were soldered to the rear surface around these holes to allow a manifold to be attached, the ends were sealed and the top absorber sheet was bonded into place. Finally, a removable low-iron-glass cover was placed over the collector to prevent convection losses.

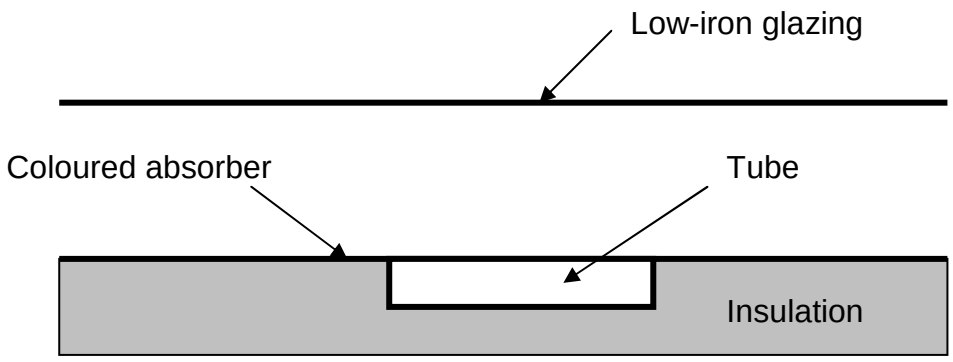

Figure 99: Partial cross-section of coloured collector

B.3 Measurement of Coloured Absorber Performance

When examining the performance of either glazed or unglazed coloured flat plate solar collectors, it is important to characterise their spectral absorption characteristics. From a theoretical perspective the thermal efficiency of a flat plate solar collector can be represented by a relationship between the collectors heat removal factor (F_r), the collector heat loss coefficient (U_L), the inlet (T_i) and ambient temperatures (T_a), solar radiation (G'') and the collector transmittance-absorptance product ($\tau\alpha$) as shown in Equation 56.

$$\eta = F_r(\tau\alpha) - F_r U_L\left(\frac{T_i - T_a}{G''}\right) \tag{56}$$

Of these parameters, the transmittance-absorptance product is the only one that is based solely on a physical property of the collector materials. The absorptance provides a measurement of the optical properties of the radiation absorbing surface, in this case the coloured absorber, while the transmission component measures the portion of the radiation transmitted by any glazing layer. Therefore, in order to understand the optical characteristics of the coloured collectors it was decided to determine their absorptance properties over the solar radiation spectrum.

To determine the absorption of the colour coated mild steel the diffuse reflectance (ρ) of a white, red, green, grey and black sample were measured at 20nm wavelength intervals between 300nm to 2500nm using a spectrophotometer and a 6° integrating sphere at Industrial Research Limited (Wellington, NZ). Based on

the reflectance measurements it is possible to determine the absorptance (α) component using Equation 57, as it can be assumed that there is negligible "transmittance" component in air (Duffie and Beckman, 2006).

$$\alpha = 1 - \rho \tag{57}$$

By integrating the absorptance derived from the measurements of the reflectance it was found that the black painted steel had relatively constant reflectance characteristics across the measured wavelengths of the Air Mass 1.5 (AM1.5) solar spectrum. However the other coloured samples, as would be expected, were more sensitive to wavelength. In particular the white sample absorbs less than 35% of the AM1.5 radiation. Interestingly, the red sample absorbed a larger portion of the shorter wavelengths (<1100nm) than the longer wavelength radiation, where it reflected a similar portion of the radiation to the white sample. This was to be expected, as the sample appears red because it will absorb all wavelengths other than those that correspond to the red portion of the visible spectrum.

Having determined the absorption characteristics of the absorber, to determine the transmittance-absorptance product of a glazed coloured collector it is necessary to substitute the measured spectral absorption characteristics and the low iron glass transmittance characteristics of Dietz (1954) into Equation 58.

$$\tau\alpha = \frac{\int_{\lambda_1}^{\lambda_2} \tau_\lambda \alpha_\lambda I_{\lambda,i} d\lambda}{\int_{\lambda_1}^{\lambda_2} I_{\lambda,i} d\lambda} \quad (58)$$

By integrating these values over the AM1.5 spectrum the transmittance-absorptance product for glazed solar collectors of the various colours can be found. Based on this method, the transmittance-absorptance values determined for each colour are given in Table 7.

Table 7: Transmittance-absorptance product of glazed coloured collectors

Colour	Transmittance-absorptance product
Black	0.87
Grey	0.81
Green	0.72
Red	0.60
White	0.32

B.4 Theoretical Coloured Collector Performance

Having determined the transmittance-absorptance product for the various coloured glazed collectors it is possible to determine their theoretical performance using a one-dimensional steady state thermal model based on the Hottel-Whillier-Bliss equations presented by Duffie and Beckman (2006).

Under these conditions the useful heat gain can be calculated using Equation 59.

$$Q = AF_R\left[(\tau\alpha).G'' - U_L(T_i - T_a)\right] \quad (59)$$

Where the useful heat gain (Q) is given by a relationship between the collector area (A), the heat removal efficiency factor (F_R), the transmittance-absorptance product of the coloured collector ($\tau\alpha$), the solar radiation ($G"$), the collector heat loss coefficient (U_L) and the temperature difference between the collector inlet temperature (T_i) and the ambient temperature (T_a).

The heat removal efficiency factor (F_R) can be derived from Equation 60, which accounts for the mass flow rate in the collector (m) and the specific heat of the collector fluid (C_p).

$$F_R = \frac{mC_P}{AU_L}\left[1 - e^{-\frac{AU_L F'}{mC_P}}\right] \tag{60}$$

To determine the heat removal efficiency factor it is necessary to calculate a value for the corrected fin efficiency (F'). This is done by first calculating the fin efficiency (F) using Equation 61. This determines the efficiency of the finned area between adjacent tubes and takes into account the influence of the tube pitch (W) and the tube width (d). Furthermore, the coefficient (M) accounts for the thermal conductivity of the absorber and is derived from Equation 62.

$$F = \frac{\tanh\left(M\,\frac{W-d}{2}\right)}{\left(M\,\frac{W-d}{2}\right)} \tag{61}$$

$$M = \sqrt{\frac{U_L}{k_{abs}L_{abs}}} \tag{62}$$

Therefore, the corrected fin efficiency (*F'*) can be calculated using Equation 63, noting that there is no bond resistance term as would be found in the analysis of a finned tube analysis, and where the overall heat loss coefficient (U_L) of the collector is the summation of the collector's edge, bottom and top losses. It is taken that the bottom loss coefficient is given by the inverse of the insulations R-value (i.e. K_b/L_b) and Equation 64 gives the edge losses, where *p* is the collector perimeter and *t* is the absorber thickness.

$$F' = \frac{\frac{1}{U_L}}{W\left[\frac{1}{U_L(d+(W-d)F}\right] + \frac{1}{\pi d h_{fluid}}} \tag{63}$$

$$U_{edge} = \frac{K_{edge} pt}{L_{edge} A_{collector}} \tag{64}$$

The top loss coefficient is a function of both radiation and wind and can be calculated using Klein's empirical equation (Equation 65) (Duffie and Beckman, 2006).

$$U_{top} = \left\{ \frac{N}{\frac{c}{T_{pm}}\left(\frac{T_{pm}-T_a}{N-f}\right)^e} + \frac{1}{h_w} \right\}^{-1} + \frac{\sigma\left(T_{pm}+T_a\right)\left(T_{pm}^2+T_a^2\right)}{\left(\varepsilon_p + 0.00591 N h_w\right)^{-1} + \frac{2N+f-1+0.133\varepsilon_p}{\varepsilon_g} - N} \tag{65}$$

Where:

$$c = (520 - 0.000051\beta^2) \qquad f = (1 + 0.089h_w - 0.1166h_w\varepsilon_p)(1 + 0.07866N)$$

$$e = 0.430(1 - \frac{100}{T_{pm}}) \qquad T_{pm} = T_{in} + \frac{Q / A_{collector}}{F_R U_L}(1 - F_R)$$

and β is the collector mounting, σ is the Stefan-Boltzmann constant, N is the number of covers or glazing layers, ε_g is the emittance of the glazing, ε_p is the emittance of the plate and h_w is the convection heat transfer due to the wind.

From these equations it is then possible to calculate the useful heat gain from the solar collector. By taking the ratio of the useful heat gain to the total radiation falling on the collector area (*Q/AG"*) we can subsequently determine the theoretical efficiency as given in Equation 56.

Therefore, by substituting the design parameters listed in Table 8 into the equations listed above, in combination with the measured transmittance-absorptance products for glazed collectors, it is possible to determine the theoretical thermal efficiency for the coloured collectors.

Table 8: Design parameters for coloured solar collectors

Parameter	Symbol	Value	Unit
Number of covers	N	1	
Emittance of plate	ε_p	0.95	
Emittance of cover	ε_c	0.88	
Number of tubes	n	2	
Collector Length	L	1.96	m
Collector Breadth	b	0.5	m
Collector Area	A	0.98	m^2
Absorber thickness	t	0.5	mm
Tube Hydraulic Diameter	d_h	9	mm
Tube Spacing	W	0.2	m
Tube Width	d	50	mm
Insulation Conductivity	k	0.045	W/mK
Back Insulation Thickness	L_b	0.1	m
Edge Insulation Thickness	L_{edge}	0.025	m
Absorber Conductivity	k_{abs}	50	W/mK
Mounting Angle	β	37	degrees

Subsequently the predicted thermal efficiency for each of the coloured collectors can be seen in Figure 100. As would be expected, the black collector has the highest predicted efficiency while the white collector has the lowest.

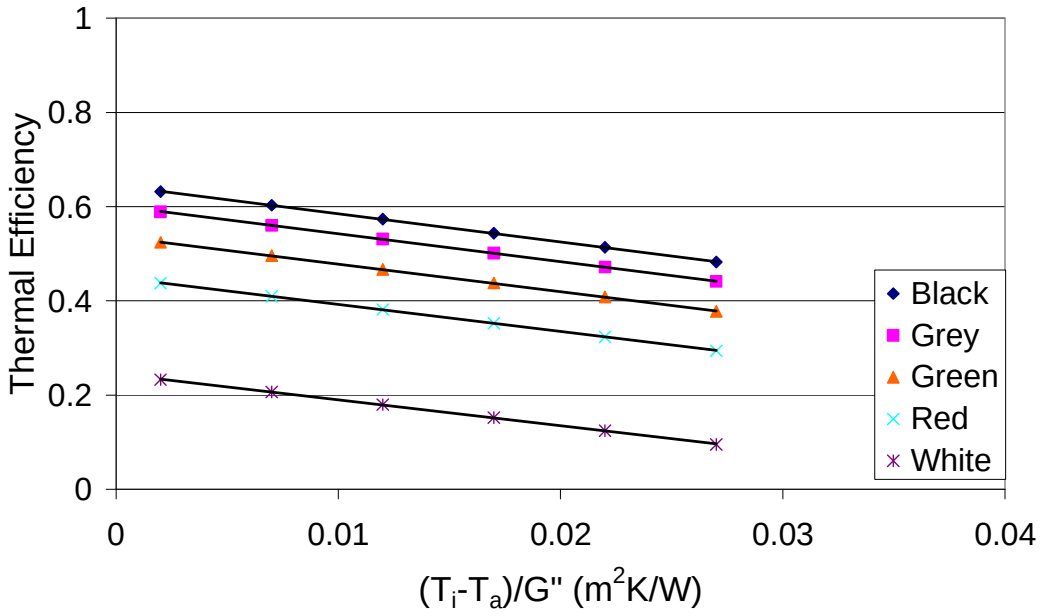

Figure 100: Theoretical efficiency of glazed coloured solar collectors

B.5 Experimental Method and Analysis

Although Figure 100 illustrates the potential performance of glazed colour collectors, good practice necessitates validating the model experimentally. As such two glazed prototype collectors were constructed for testing: one green and one grey. Although there are a number of potential methods for determining the thermal efficiency of solar water heaters, for this study a steady state outdoor thermal test setup similar to that recommended in AS/NZS 2535.1 (1999) was used, as shown in Figure 101.

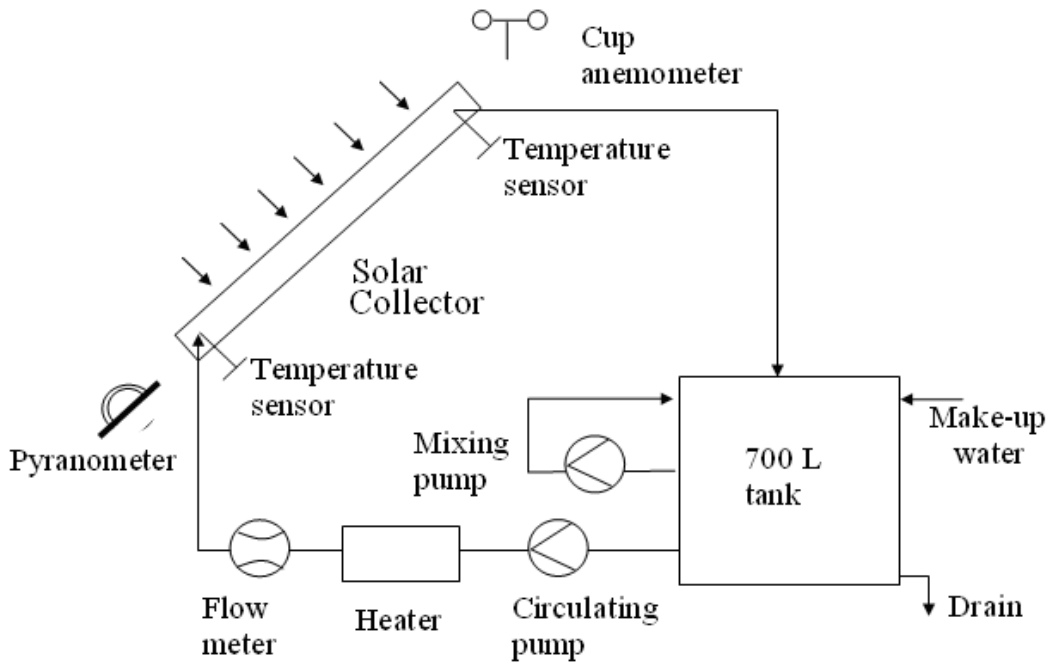

Figure 101: Collector test system

In order to test the prototype collectors, an unimpeded north facing test location was found on the University of Waikato library roof. The global solar radiation incident on the collectors' surface was measured using a calibrated WMO First Class pyranometer mounted inline with the collector at an angle equal to the local latitude (37 degrees).

Calibrated T-type thermocouples (±0.3K) were used to measure the inlet and outlet temperatures to the collector, and the ambient air temperature. A cup anemometer mounted adjacent to the test stand was used to monitor the wind speed. The flow rate through the collector was set at a constant rate and monitored throughout the testing periods by measuring the time taken for a known mass of water to pass through the collector.

Additionally, an instantaneous electric water heater with temperature control was mounted on the inlet side of the collector to provide a controllable inlet water temperature. The outlet from the collector was returned to a 700-litre water tank where it was well mixed to ensure that the heater did not encounter large instantaneous temperature variations.

A prerequisite to accurately determining the performance of the collector is to conduct a number of outdoor tests under a range of ambient conditions and allow it to reach steady state for each condition. Subsequently, when analysing the collectors, the instantaneous collector efficiency can be reached directly from the experimental results by taking the ratio of heat transfer in the collector to the product of the collector area and the global solar irradiance.

B.6 Experimental Performance of Coloured Collectors

From the experimental data collected during the testing it was possible to derive the efficiency equation of the both coloured collectors using a linear least squares regression analysis. The experimental data yields two equations that describe the grey and green collector efficiencies respectively, as shown in Equations 66 and 67.

$$\eta = 0.65 - 10.4\frac{T_i - T_a}{G''} \tag{66}$$

$$\eta = 0.63 - 14.6\frac{T_i - T_a}{G''} \tag{67}$$

Although this is the most common way of presenting the efficiency of the collector it can be better understood from an inspection of Figures 102 and 103, where the theoretically predicted efficiencies of the glazed coloured collectors are also shown.

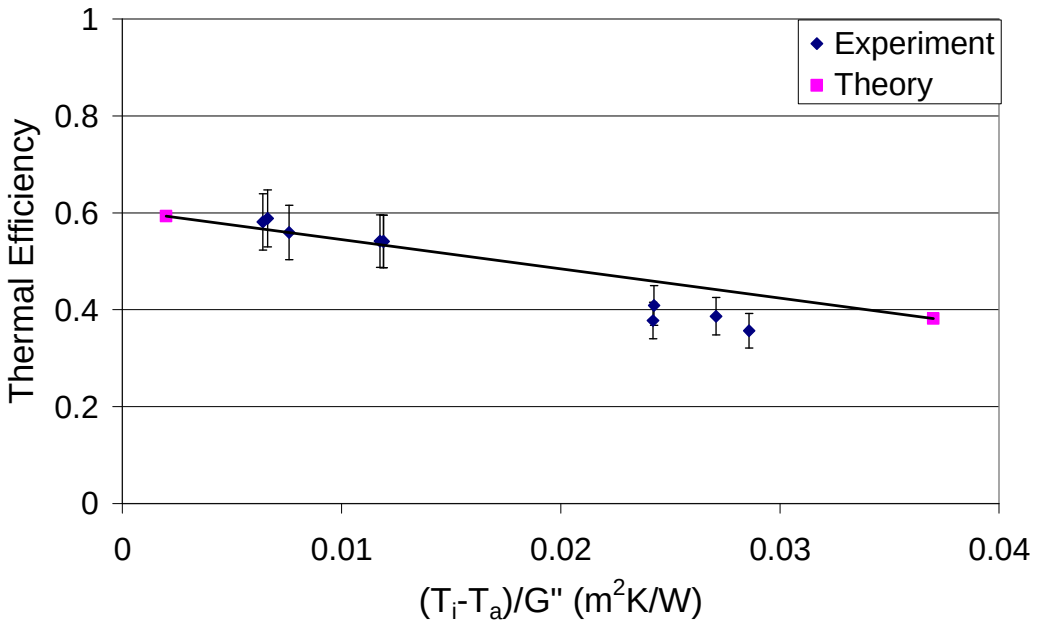

Figure 102: Experimental and theoretical efficiency of glazed grey solar collector

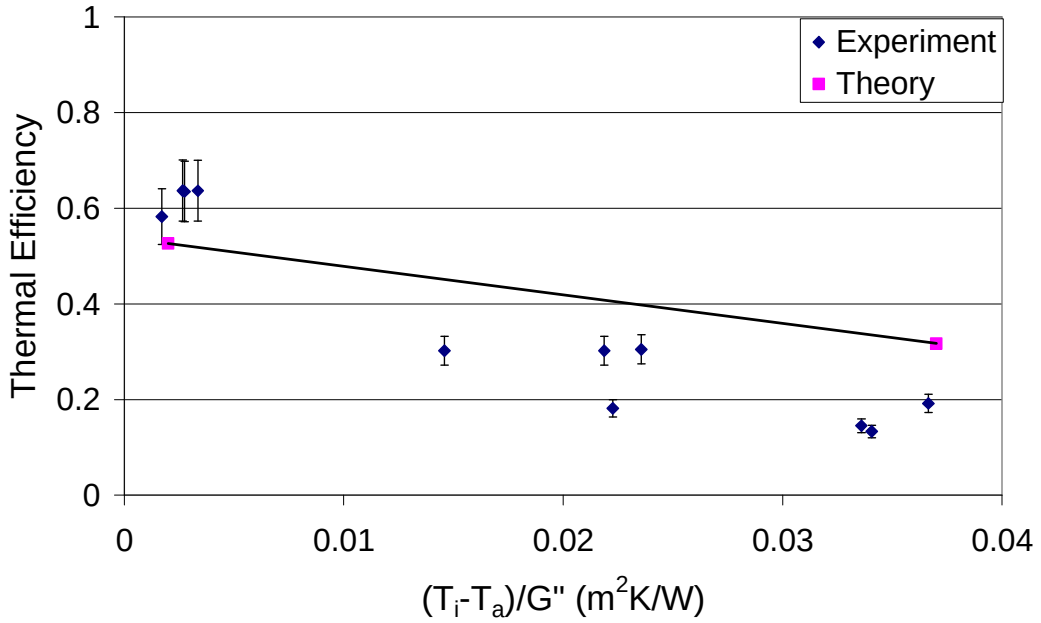

Figure 103: Experimental and theoretical efficiency of glazed green solar collector

From Figure 103, it can be seen that there is a discrepancy between the experimental and theoretical result for the green collector. This was due to unusually high wind speeds during the test leading to higher convective heat losses in the experiment than predicted by the model. However for the most part, the theoretical prediction corresponds fairly well with the experimental data. As such it is possible to optimise the collector using the measured values of the transmittance-absorptance product and the one-dimensional thermal model presented.

B.7 Annual Performance of Coloured Collectors

Having demonstrated and validated the design of the coloured solar collectors, it was decided to examine the fraction of a typical domestic water-heating load that could be provided by the various theoretical coloured collectors. Therefore, an F-

chart was constructed for the operation of the collectors in Auckland based on weather data taken from NIWA (2007). Although not as "in-depth" as a full annual transient analysis, such as could be performed by a program such as TRNSYS, the F-chart has been shown to provide good prediction of annual solar fractions (Duffie and Beckman, 2006).

For the calculation of the radiation it was assumed that the collector was oriented facing north and that the collector was inclined at an angle equal to latitude. Furthermore, the system was assumed to consist of 4m^2 of coloured collectors, coupled to a 170-litre storage tank providing the monthly heating loads shown in Figure 104.

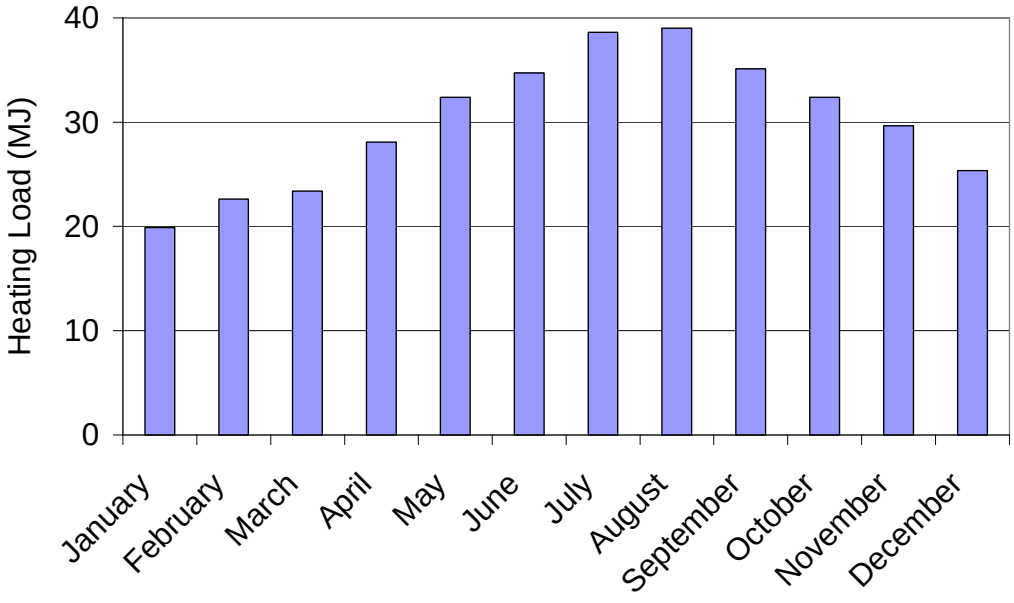

Figure 104: Monthly heating load for F-chart analysis

From the F-chart analysis it was found that, as expected, the black coloured collector had the highest annual solar fraction. However, it was also found that

although the efficiency of the coloured collectors was lower, they were still able to provide a reasonable fraction of the heating load, as shown in Figure 105.

It is interesting to note that even the white collector is able to provide approximately 25% of the heating load. As such there appears to be significant scope to vary solar collector colour and maintain a degree of solar heating.

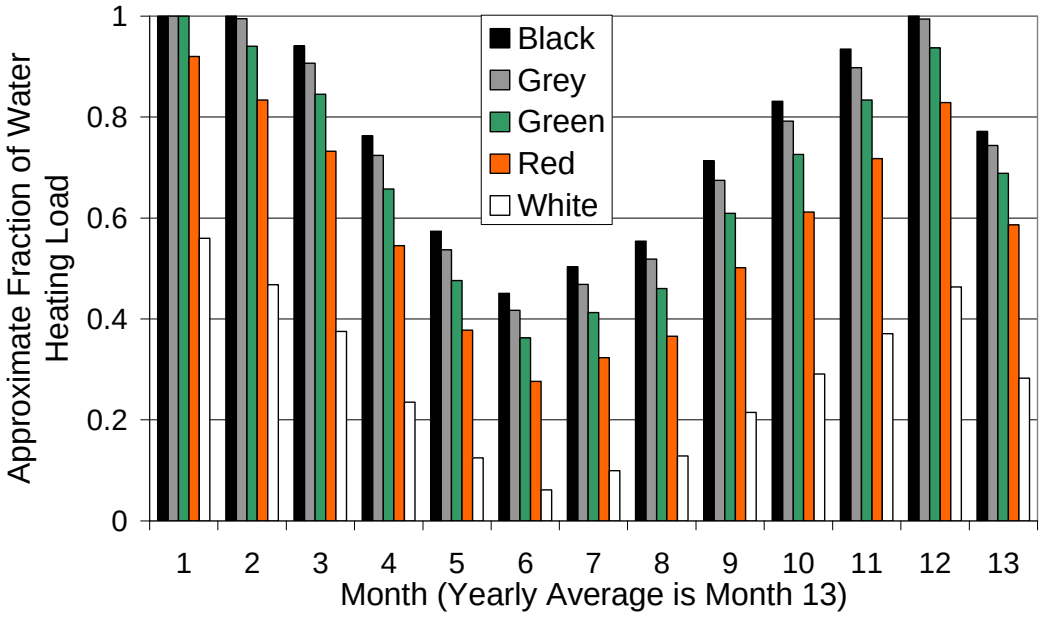

Figure 105: Approximate solar fraction provided by glazed coloured solar collectors

B.8 Conclusions and Discussion

Until recently the use of coloured solar collectors appeared to have been passed over in favour of improving black and selective surfaces. Over the course of this study it has been shown that the performance of coloured solar collectors can be accurately modelled using a combination of experimental and numerical

techniques. Furthermore, it has been shown that despite their lower efficiencies low-cost coloured mild steel collectors could potentially provide noticeable contributions to domestic water heating loads.

Finally, given the recent drive towards building integration of solar collectors (Weiss and Stadler, 2001) it would appear that the use of coloured solar collectors will start to be an area that receives more attention than it has to date.

Appendix C: Bending Stress in Absorber Sheet

C.1 Introduction

In essence the tube formed in the manufacture of the BIPVT collector can be considered as a rectangular pressure vessel subject to a uniform internal pressure. However, unlike a cylindrical pressure vessel, the membrane stresses in a rectangular pressure vessel are not uniform. There are a number of methods that can be applied to the determination of the stresses in a rectangular pressure vessel, including finite element analysis, superposition methods or the ASME Boiler and Pressure Vessel Code (Guo and Zeng, 1997).

Of the available methods however, Blach et al.' (1990) large deflection analysis has shown perhaps the best prediction of stress values in pressure vessels of rectangular cross section.

C.2 Method

In Blach et al.' study it is noted for deflections greater than half the thickness of the vessel wall that linear small deflection theory can not be satisfactorily applied as it under predicts the stress due to curvature in the walls.

To determine the stress in the vessel walls however, it is assumed that the stress at the centre of the tube surface (ie. in the top absorber plate) determines the design.

For example, assume the panel is 2m long (*a*) and the trough is 25mm wide (*b*) and made of steel 0.5mm thick with a maximum allowable combined bending and membrane stress (σ) of 180MPa.

Thus:

$$\frac{a}{b} = \frac{2000}{25} = 80$$

But this is outside the range of Figure 106, so to illustrate the point, assume *a/b*=2.

$$\frac{\sigma b^2}{Et^2} = \frac{180 \times 25^2}{200000 \times 0.5^2} = 2.25$$

From Figure 106 it can be seen that for *a/b*=2 and $\sigma b^2/Et^2$=2.25 that qb^4/Et^4~10 where *q* is the maximum working pressure in MPa.

$$\frac{qb^4}{Et^4} = 10 = \frac{q \times 25^4}{200000 \times 0.5^4}$$

Solving for *q* gives a maximum working pressure of 0.32MPa.

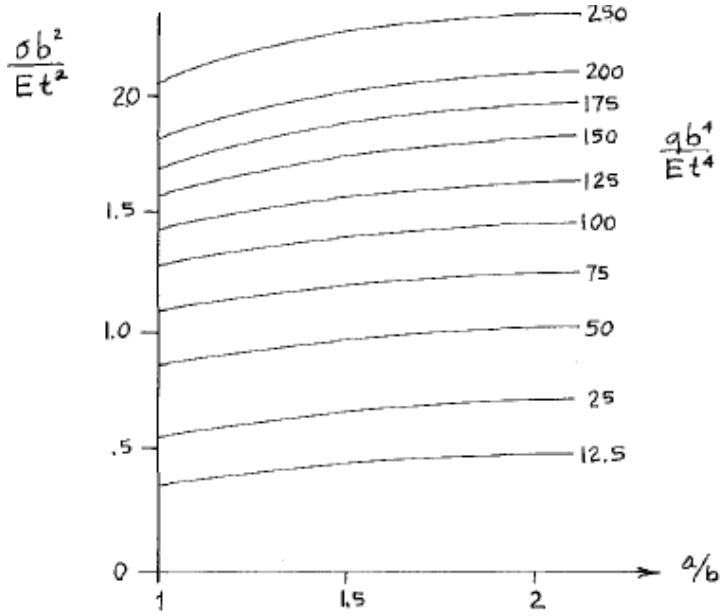

Figure 106: Total stress coefficients (adapted from Blach et al. 1990)

Consider the membrane stresses for a/b=2 and qb^4/Et^4=10. From Figure 107 it can be seen that for this condition $\sigma_m b^2/Et^2 \sim 4$.

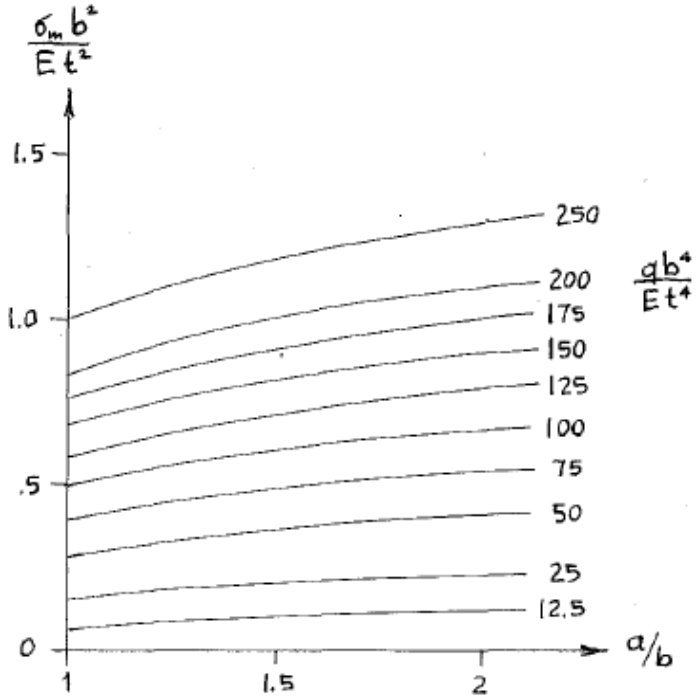

Figure 107: Membrane stress coefficients (adapted from Blach et al. 1990)

$$\frac{\sigma_m b^2}{Et^2} = 4 = \frac{\sigma_m \times 25^2}{200000 \times 0.5^2}$$

Solving for the membrane stress (σ_m) at the maximum operating pressure gives a value of 320MPa, therefore the pressure needs to be reduced to ensure the absorber plate does not deform. Therefore by setting the maximum design operating pressure at 100kPa the membrane stress decreases to 80MPa, or less than half the maximum stress.

However, assume the width of the trough is widened to 50mm while the other parameters are held the same and assuming *a/b*=2.

$$\frac{\sigma b^2}{Et^2} = \frac{180 \times 50^2}{200000 \times 0.5^2} = 9$$

From Figure 106 it can be seen that for *a/b*=2 and $\sigma b^2/Et^2$=9 that qb^4/Et^4=50 where *q* is the maximum working pressure in MPa.

$$\frac{qb^4}{Et^4} = 50 = \frac{q \times 50^4}{200000 \times 0.5^4}$$

Solving for q gives a maximum working pressure of 0.1MPa.

From Figure 107, it can be seen that for this condition $\sigma_m b^2/Et^2=4$. thus giving a membrane stress at the maximum operating pressure of 320MPa.

In order to use a wider trough width, the pressure would need to be decreased further. However, decreasing the maximum operating pressure for the BIPVT system makes it less flexible; principally because for large systems there will need to be long lengths of pipe used, thus giving higher pressure head losses. Potentially, if the operating pressure is reduced to satisfy the structural requirements, it may result in a condition where the head loss in the system exceeds the operating pressure and therefore allow no flow in the system.

C.3 Conclusion

In conclusion, without changing the material or the thickness of the material used in the BIPVT, the operating pressure should be reduced. However, because of the need to overcome pressure losses it is also necessary to reduce the trough width.

To satisfy the thermal requirements, multiple narrow troughs could be formed below the absorber sheet to increase the fin efficiency as suggested in the thermal modelling.

Appendix D: Development of a Typical Meteorological Year for Long Term Solar Energy Simulations in Hamilton

D.1 Introduction

Reliable engineering weather data is of significant importance when undertaking transient simulations of solar energy systems and energy use in the built environment. Furthermore, there are a significant number of simulation programs, such as BLAST and TRNSYS, which rely on this data to predict the performance of different energy systems.

In order to conduct these simulations there are a number of variations on "typical" weather data, such as ASHRAE's Weather Year for Energy Calculations (WYEC), Typical Meteorological Year Type 2 (TMY2) and the National Research Centre of Canada's Canadian Weather for Energy Calculations (CWEC), that are used in building and solar energy simulations (Crawley, 1998). However, this study concentrated on the development of a typical meteorological year (TMY) for Hamilton NZ that could be used in a range of simulation programs.

Currently, the availability of "typical" weather data for New Zealand locations is relatively restricted. Van der Werff *et al.* (2003) attempted to address this issue by developing a series of Test Reference Years (TRY) and "design days" for use across NZ, including Hamilton. They identified years which could be categorised as hot, cold or average as well as days satisfying similar parameters.

Crawley (1998) however, suggested that the disadvantage of TRY data is that it tends to result in mild years being used. Furthermore Crawley noted that TRY data does not contain measured values for solar radiation, but calculated values based on cloud type and coverage.

Crawley also noted that the TMY, developed by the National Climatic Data Centre (NCDC) and Sandia National Laboratories (SNL), tends to overcome the limitations of the TRY by using a series of "typical" months of data, rather than a single year, to represent a typical year.

Furthermore, the validity of TMY data for use in long term energy simulations for the Australasian region was demonstrated by Morrison and Litvak (1988). They developed TMY data for 22 locations across Australia and found that they were able to accurately predict the long term performance of solar water heating systems.

By population (Statistics NZ, 2001), Hamilton (37.5 S, 175 E) is New Zealand's fourth largest urban centre and forms the main service centre for the Waikato region. Furthermore, the Waikato and surrounds form the centre of production for the NZ dairy industry and, according to EECA (2006), the Waikato region uses approximately 10% of the nation's energy.

NIWA, cited by EECA (2004), found that the daily global radiation for Hamilton varies between 6.2 and 22MJ/m^2day, with an annual total of approximately

5100MJ/m^2. According to EECA (2001) this is comparable with a location such as Melbourne and significantly higher than a typical German location. As such, Hamilton presents a relatively good location for solar energy utilisation.

Given Hamilton's large population base, and the energy consumed in the surrounding Waikato Region, it is important that a better understanding of its meteorological conditions is established to aid in the design of solar and building energy systems.

D.2 Data Collection

To develop the TMY for Hamilton, approximately ten years of continuous hourly weather data was collected from an automated weather station located to the south of Hamilton for the period between January 1997 and June 2006.

Data was collected for four variables necessary in the formulation of the TMY: global solar radiation on a horizontal surface, ambient temperature, relative humidity and wind speed.

The reason, for selecting these parameters is that in energy simulations solar radiation levels determine the heat gain, the ambient temperature and wind speed determine heat loss by convection and relative humidity is important in determining latent energy and evaporation levels (for air conditioning systems).

D.3 Methodology

In order to produce the TMY for Hamilton, two methods of analysis were used. In the first method, the data was divided into 12 monthly sets, each containing the four meteorological parameters. To determine the most suitable months a short and long term mean were determined for each of the parameters.

The short term mean was developed by taking the mean of the hourly values of a particular parameter for the entire month of a particular year. The long term mean was determined by taking the mean of the monthly parameter values over the entire data set of ten years. Additionally, where a leap year occurred, the hourly values for February 29th were removed from the calculations so that each February was assumed to have only 28 days.

Subsequently, each of the parameters was qualitatively ranked in terms their perceived importance for energy simulations. Solar energy was taken as the main parameter followed by ambient temperature, relative humidity and wind speed.

Although wind speed tends to have a notable influence on heat loss, especially when examining solar collectors, the measurements were taken in a comparatively rural environment and so were believed not to be representative of those that would be experienced in Hamilton's suburban areas. Kind and Kitaljevich (1985) noted that there are significant variations between rural and urban wind velocity profiles.

Subsequently, the short term means were compared to the long term mean for the month. The month with the closest qualitative match between the mean values of the parameters was thus selected as the "typical" meteorological month for the TMY.

By this method it was found that for the two main parameters, solar radiation and temperature, the mean monthly values closest to the long term mean monthly value typically occurred in the same month, thus suggesting the selection of each month was appropriate.

Having determined each typical month, linear interpolation was performed to correct any significant differences between the parameter values from different months of different years. This operation only affected a maximum period of three hours in each month and as such should not significantly influence the long term output from any simulations.

To validate the TMY, a "mean" year consisting of the mean hourly values for each day was developed. Both the TMY and the mean year were then utilised in a performance simulation of a solar water heating system for pool heating, using the Canadian Renewable Energy Network's (2006) Enerpool Pro package. It should be noted that although a "mean" weather year was constructed such a year tends to remove natural meteorological variations, such as fast moving storm fronts, that would occur during a typical year. By utilising a TMY it allows the impact of these variations to be observed in simulation models.

In these simulations, the performance of a 100m^2 glazed solar collector array was analysed for both the TMY and also the mean year. In the simulations, the solar collector was assumed to have an efficiency given by Equation 68, where the efficiency (η) is a function of the inlet water temperature (T_i), the ambient temperature (T_a) and the global solar irradiance (G").

$$\eta = 0.75 - 5\frac{T_i - T_a}{G''} \tag{68}$$

The values in this equation were assumed to be representative of values for a glazed solar collector that may be used for swimming pool heating applications.

In the simulations it was assumed that the collectors were mounted on a roof with an elevation of 37.5 degrees, equal to Hamilton's latitude. Additionally, simulations were conducted at elevations of 60 degrees and 14 degrees to determine the performance of the system when biased for mid-winter and mid-summer performance.

D.4 Results

Having selected the typical months for the TMY, as shown in Table 9, a comparison was made between the long term mean and the TMY for the four parameters.

Table 9: Months selected for TMY

Month	Year
January	1998
February	2002
March	1998
April	2004
May	2004
June	1998
July	2002
August	1998
September	1997
October	1997
November	2003
December	2003

In Figure 108 it can be seen that the relationship between the long term mean and the TMY values for the solar radiation is excellent, with the deviation in the values being negligible. This is appropriate, as there was a heavy emphasis placed on the selection of solar radiation that was close to the long term monthly mean.

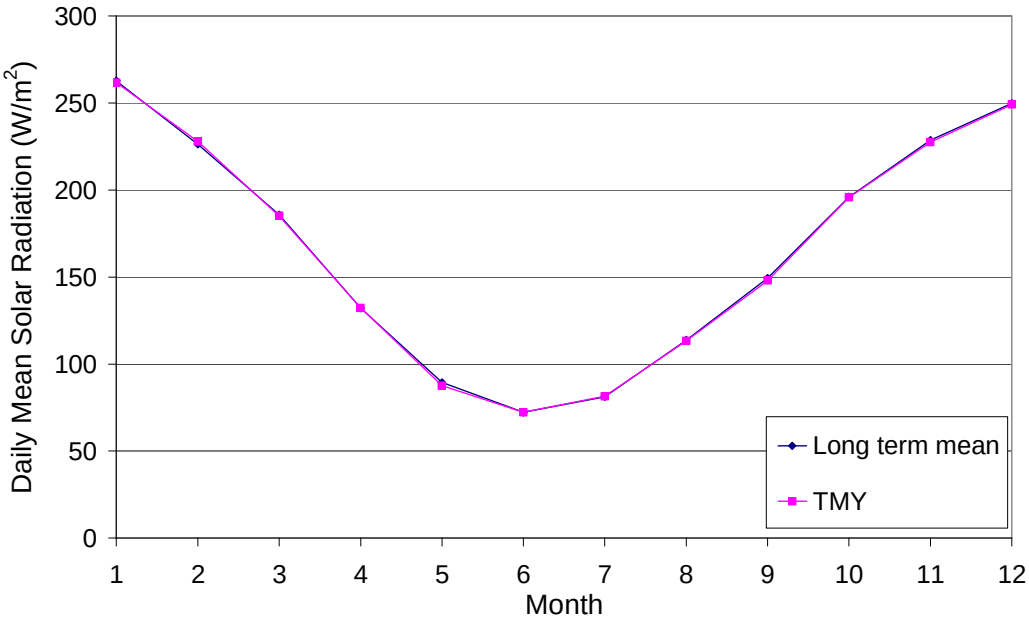

Figure 108: Solar radiation for TMY

Furthermore, the relationship between the ambient temperature (Figure 109), relative humidity (Figure 110) and wind speed (Figure 111), are reasonable. This suggests that the data selected for the TMY can represent the long term meteorological conditions of Hamilton.

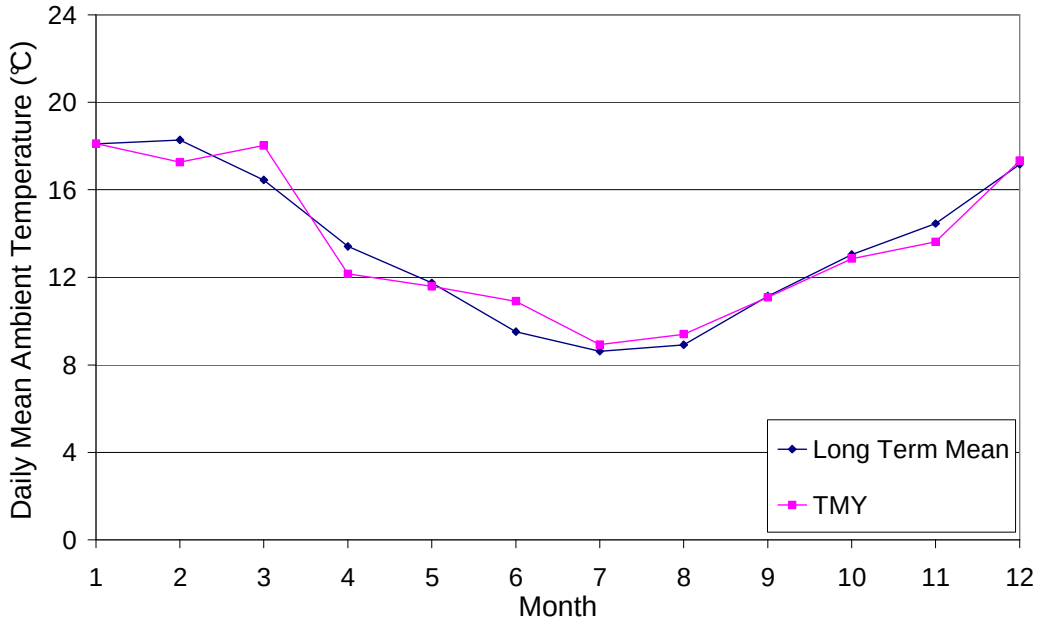

Figure 109: Ambient temperature for TMY

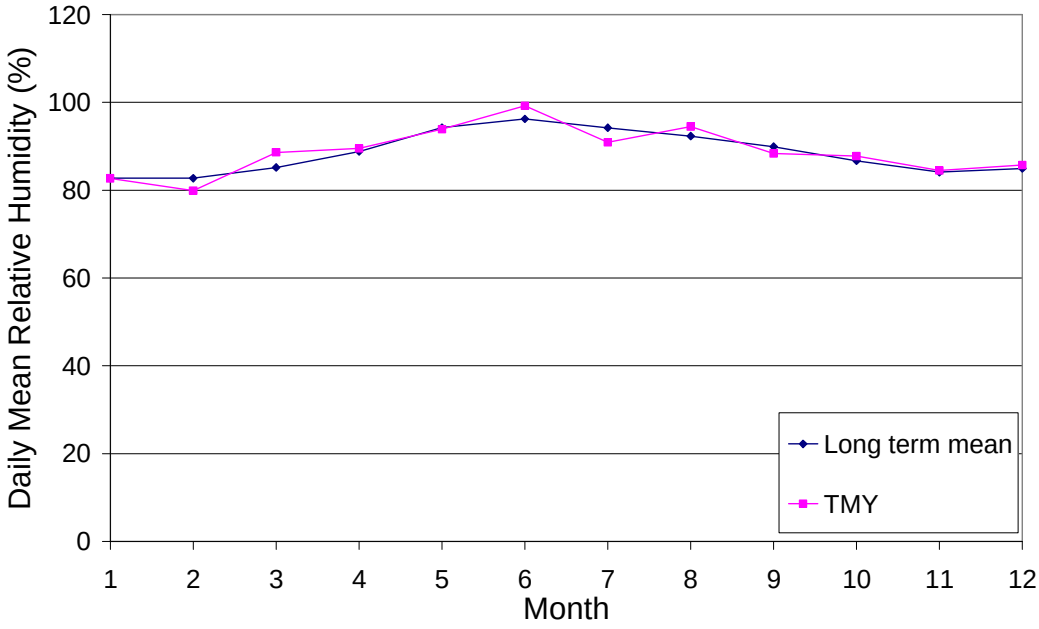

Figure 110: Relative humidity for TMY

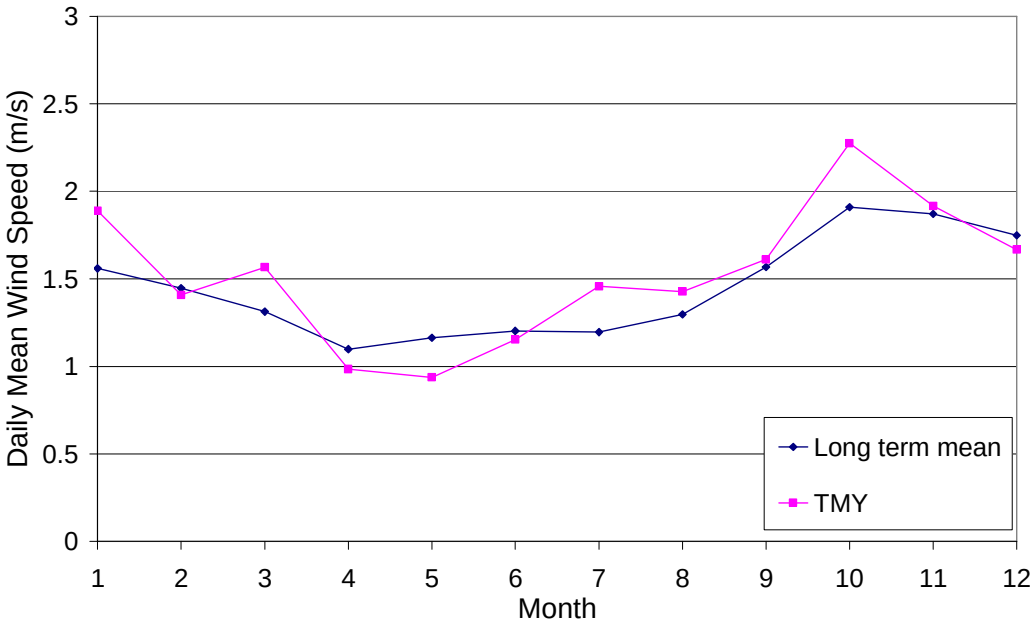

Figure 111: Wind speed for TMY

To validate the assumption, that the TMY could accurately represent the long term performance of a solar pool heating system, the output from a simulation using TMY data and a mean weather year were compared.

From the simulations that were conducted, it was found that the TMY was able to predict the performance of the solar pool heating system to within 2% of the mean weather year annual total. In addition, it was found that the monthly values were predicted to within 3%.

In Figure 112 it can be seen that, for a collector oriented at 37.5 degrees, that the difference in collected energy between the mean year and the TMY does not vary significantly. As such, the TMY can be used in performing accurate long term simulations of solar energy and building energy systems.

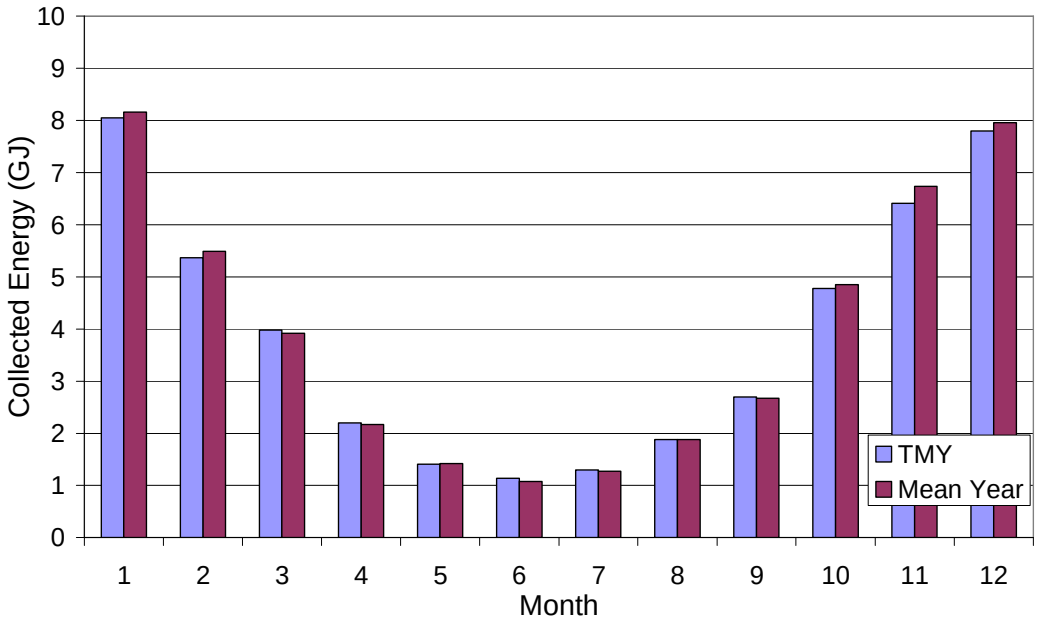

Figure 112: Collected energy for TMY and mean weather year

In addition it was found that the energy collected by the collectors could be improved by biasing the collectors at 14 and 60 degrees for either summer or winter performance. In Figure 113 it can be seen that at lower elevations the performance is much better over summer. However, during winter the collector with the highest elevation performs the best. Furthermore, at an elevation of 14 degrees it was found that the annual energy collected was the maximum of the three values simulated. However, at an elevation of 37.5 degrees the collectors offered a compromise between summer and winter performance.

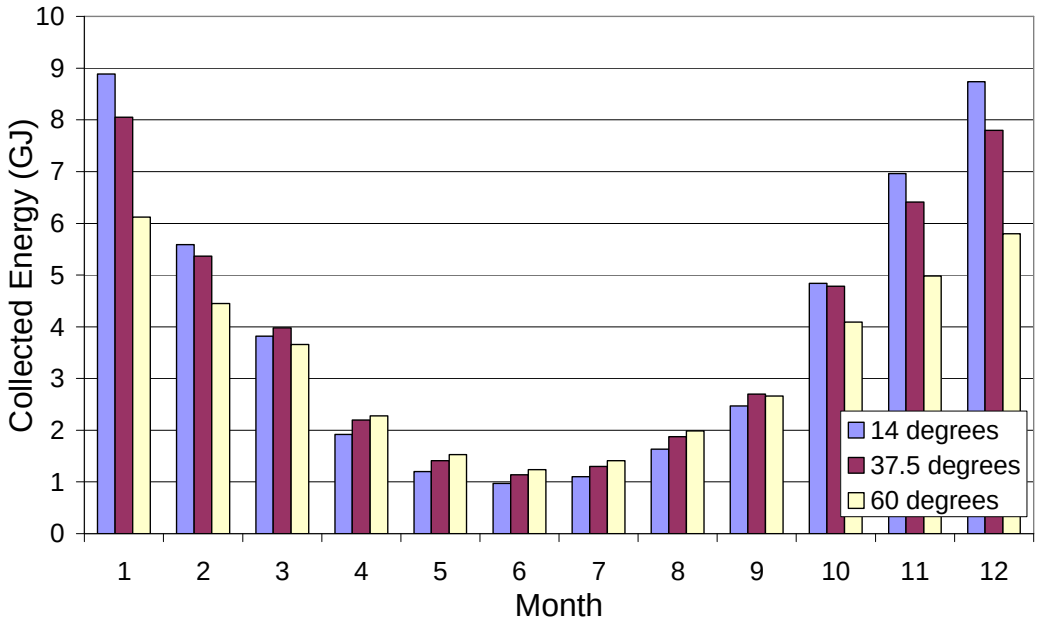

Figure 113: Collected energy for solar collectors at varying elevation angles

D.5 Discussion of TMY

As New Zealand's fourth most populous urban centre, there was a need to develop a typical meteorological year for Hamilton. Previously, Van der Werff *et al.* (2003) had identified "design days" for Hamilton; however these were felt to be inadequate to accurately predict the long term annual performance of solar and building energy use in simulation models.

As such, 10 years of meteorological data was collected for Hamilton. By taking the data for months which closely represented the long term mean weather patterns, a TMY was formulated. Using a computer simulation, it was found that the TMY was able to predict the output from a solar pool heating system, to within 2% of the long term mean. Additionally it was found that by orienting the

collectors at an angle equal to Hamilton's latitude a good yearly performance could be obtained from the solar heating system.

Based on the data presented, Hamilton is well suited to the use of solar energy and the development of a TMY allows accurate predictions of solar and building energy use to be made in the future.

Appendix E: Modelling a Building Integrated Photovoltaic Thermal (BIPVT) Solar Collector with Natural Convection

E.1 Introduction

In Chapter 6 of this thesis, the idea of coupling the thermal efficiency model of the BIPVT collector is combined with the correlation for natural convection in an attic space. Rather than repeat the modelling from Chapter 3 in Chapter 6, to show how natural convection is fitted with the model, the modified model is presented here. This is the method presented by, and taken directly from, Anderson et al. (2009).

E.2 Methodology

In order to analyse the thermal and electrical performance of the BIPVT a one dimensional steady state thermal model was developed with the collector represented as a flat plate thermal collector. As such a modified form of the Hottel-Whillier-Bliss equations presented by Duffie and Beckman (2006) was used.

Under these conditions the useful heat gain can be calculated using Equation 69.

$$Q = AF_R\left[(\tau\alpha)_{PV}.G - U_L(T_i - T_a)\right] \tag{69}$$

In this equation the useful heat gain (Q) is represented by a function of the collector area (A), the heat removal efficiency factor (F_R), the transmittance-

absorptance product of the photovoltaic cells ($\tau\alpha_{PV}$), the solar radiation (G), the collector heat loss coefficient (U_L), and the temperature difference between the cooling medium inlet temperature(T_i) and the ambient temperature(T_a).

Furthermore, the heat removal efficiency factor (F_R) can be calculated using Equation 70, which also accounts for the mass flow rate in the collector (m) and the specific heat of the collector cooling medium (C_p).

$$F_R = \frac{mC_P}{AU_L}\left[1 - e^{-\frac{AU_L F'}{mC_P}}\right] \tag{70}$$

In order to obtain the heat removal efficiency factor however, it is necessary to calculate a value for the corrected fin efficiency (F'). This is done by first calculating the fin efficiency (F) using Equation 71.

$$F = \frac{\tanh\left(M\frac{W-d}{2}\right)}{\left(M\frac{W-d}{2}\right)} \tag{71}$$

This equation determines the efficiency of the finned area between adjacent tubes by taking into account the influence of the tube pitch (W) and the tube width (d) of the rectangular cross-section tubes formed in the fabrication of the BIPVT. As such all calculations related to flow in the tubes were based on the tubes hydraulic diameter (d_h).

The coefficient (*M*) is a term which accounts for the thermal conductivity of the absorber and PV cell and is represented by Equation 72 (Vokas et al. 2006).

$$M = \sqrt{\frac{U_L}{k_{abs}L_{abs} + k_{PV}L_{PV}}} \tag{72}$$

As such, the corrected fin efficiency (*F'*) can be calculated using Equation 73.

$$F' = \frac{\frac{1}{U_L}}{W\left[\frac{1}{U_L(d+(W-d)F}\right] + \frac{1}{Wh_{PVA}} + \frac{1}{\pi dh_{fluid}}} \tag{73}$$

In Equation 73, h_{PVA} is a "quasi" heat transfer coefficient to account for the bond resistance between the PV cell and the absorber (Zondag et al., 2002) and h_{fluid} is the forced convection heat transfer coefficient inside the cooling passage determined from the Dittus-Boulter equation. Furthermore, the overall heat loss coefficient (U_L) of the collector represents the summation of the collector edge (Equation 74, where *p* is the collector perimeter and *t* is the absorber thickness), top and rear surface losses. In this equation it was assumed that the top loss coefficient, due to wind, could be calculated using Klein's empirical equation (Equation 75) as given by Duffie and Beckman (2006).

$$U_{edge} = \frac{K_{edge}pt}{L_{edge}A_{collector}} \tag{74}$$

$$U_{top} = \left\{ \frac{N}{\frac{c}{T_{pm}}\left(\frac{T_{pm}-T_a}{N-f}\right)^e + \frac{1}{h_w}} \right\}^{-1} + \frac{\sigma\left(T_{pm}+T_a\right)\left(T_{pm}^2+T_a^2\right)}{\left(\varepsilon_p + 0.00591Nh_w\right)^{-1} + \frac{2N+f-1+0.133\varepsilon_p}{\varepsilon_g} - N} \tag{75}$$

Where:

$$c = (520 - 0.000051\beta^2) \qquad f = (1 + 0.089h_w - 0.1166h_w\varepsilon_p)(1 + 0.07866N)$$

$$e = 0.430(1 - \frac{100}{T_{pm}}) \qquad T_{pm} = T_i + \frac{Q/A_{collector}}{F_R U_L}\left(1 - F_R\right)$$

β is the collector mounting, σ is the Stefan-Boltzmann constant, N is the number of covers or glazing layers, ε_g the emittance of the cover or glazing, ε_p the emittance of the plate and h_w is the convection heat transfer due to the wind and is discussed later in this work.

However, if we consider the case of an unglazed collector, in which there is no cover, Equation 75 can not be applied. Instead it is necessary to calculate the top loss coefficient (U_{top}) by taking the summation of the individual contributions of radiation, natural and forced convection.

Under such conditions, the heat loss due to radiation can be expressed as a radiation heat transfer coefficient in terms of the sky temperature (T_s), the mean collector plate temperature (T_{pm}) and the plate emissivity (ε_p) as shown in Equation 76 (Eicker, 2003).

$$h_r = \sigma\varepsilon_p(T_{pm}^2 + T_s^2)(T_{pm} + T_s) \tag{76}$$

where the sky temperature is represented by the modified Swinbank equation of Fuentes (1987) as a function of the ambient temperature as shown in Equation 77.

$$T_s = 0.037536T_a^{1.5} + 0.32T_a \tag{77}$$

Furthermore, the losses due to natural and forced convection must also be taken into account. The forced convection heat transfer coefficient (h_w) can be calculated using Watmuff et al.' (1977) correlation in terms of wind velocity (v), as shown in Equation 78, while the natural convection loss (h_{nat}) can be represented by a function of the temperature difference between the mean collector plate temperature (T_{pm}) and the ambient temperature (T_a) as shown in Equation 79 (Eicker, 2003).

$$h_w = 2.8 + 3.0v \tag{78}$$

$$h_{nat} = 1.78(T_{pm} - T_a)^{1/3} \tag{79}$$

Using this method it is possible to determine an overall convection heat transfer coefficient (h_c) by combining both forced and natural convection heat transfer as shown in Equation 80 (Eicker, 2003). Subsequently by taking the summation of the convection and radiation losses, it is possible to determine the overall top loss heat transfer coefficient (U_{top}) for the unglazed collector.

$$h_c = \sqrt[3]{h_w^3 + h_{nat}^3} \tag{80}$$

Typically, when analysing solar thermal and standalone PVT collector systems, the rear surface heat loss coefficient is given by the inverse of the insulation R-value (ie. k_b/L_b); however it should be recognised that, ideally, the BIPVT will be integrated *into* the building rather than merely *onto* the building. As such, if the collector is integrated into the roof of a building then the calculation of the heat loss through the bottom or rear surface is less straight forward.

Given that the collector would be integrated into a roof it is feasible that it may be installed on a building using a "cold roof" insulation system. In such an installation the building would be insulated at ceiling level, therefore the use of insulation at the rear surface of the BIPVT would represent a second layer of insulation thereby adding to the cost of the system. In this mode of operation, it was recognised that the BIPVT would be installed above the air filled attic and that air had a similar thermal conductivity to typical insulation materials therefore presenting the possibility of using the air in this space as an insulating layer. Therefore the correlation for free convection in a triangular enclosure, or a pitched roof attic space, developed by Ridouane and Campo (2005) (Equation 81) was used to determine the heat loss from the rear surface of the BIPVT.

$$Nu = 0.286\, A^{-0.286} Gr^{1/4} \tag{81}$$

Where A is the aspect ratio of the attic or enclosure and is the ratio of the vertical height (H) and the horizontal width. The Grashof number (Gr) was taken to be

given by Equation 82 with properties based on the average of the BIPVT mean temperature and the ambient temperature:

$$Gr = \frac{g\beta(T_{pm} - T_a)H^3}{\upsilon^2} \tag{82}$$

Based on this, it is possible to calculate the heat transfer coefficient due to natural convection along the rear of the BIPVT collector and subsequently the overall heat loss coefficient for Equation 73.

Additionally, it is possible to analyse the thermal performance of the BIPVT collector by the inclusion of a packing factor. In practical terms, it is not always possible to have complete coverage of a panel with photovoltaic cells. As such Equation 69 can be modified to account for this packing factor (*S*) and the transmittance-absorptance product of the collector material ($\tau\alpha_T$) on to which the PV cells are laminated, as shown in Equation 83.

$$Q = S\left[AF_R\left[\tau\alpha_{PV}.G - U_L(T_I - T_a)\right]\right] + (1-S)\left[AF_R\left[\tau\alpha_T.G - U_L(T_I - T_a)\right]\right] \tag{83}$$

From these equations it is then possible to calculate the useful heat gain by the solar collector and the mean temperature of the BIPVT (T_{pm}). The electrical efficiency can be calculated based on the difference between the mean temperature of the BIPVT and the Nominal Operating Cell Temperature (NOCT), which is typically taken as 298K. For this study it was assumed that the cell had an efficiency of 15% (typical of a crystalline silicon PV cell) at NOCT, and that

the temperature dependent efficiency could be represented by Equation 84; where it was also assumed a 0.5%/°C decrease in electrical efficiency would occur (Green, 1998).

$$\eta_{electrical} = 0.15(1 - 0.005(T_{pm} - NOCT)) \tag{84}$$

Furthermore, by rearranging Equation 69 or 83, we can develop an equation for determining the thermal efficiency of the BIPVT, based on the transmittance-absorptance product of the BIPVT accounting for the packing factor. This equation is then expressed in the form shown in Equation 85.

$$\eta_{thermal} = F_R((S \times \tau\alpha_{PV}) + (1 - S) \times \tau\alpha_T) - F_R U_L \frac{T_i - T_a}{G} \tag{85}$$

By combining the elements of this design model and methodology it is therefore possible to predict the performance of a BIPVT style collector.